UNIVERSITEIT VAN PRETORIA
UNIVERSITY OF PRETORIA
YUNIBESITHI YA PRETORIA

Faculty of Health Sciences

School of Medicine

Department of Anatomy

Anatomical investigation of the interthalamic adhesion

Research dissertation for the degree MSc Macro-anatomy

Author: Miss Nicole van Heerden[1]

Student number: 16027168

Address: BMS building, Prinshof campus

Cell: (+27) 81 270 3692

E-mail 1: u16027168@tuks.co.za

E-mail 2: nicole.vanheerden04@gmail.com

Supervisor: Dr G. Venter[1]

Co-supervisors: Dr L. Prigge[1] and Dr H. Taute[1]

[1]Department of Anatomy, Faculty of Health Sciences, University of Pretoria

Date: 2023

CONTENTS

LIST OF TABLES

LIST OF FIGURES

LIST OF APPENDICES

TABLE OF ABBREVIATIONS

Abbreviation	**Abbreviation in full**
AC	Anterior commissure
ACPC	Intercommissural plane formed by line between anterior commissure and posterior commissure
BMS	Basic Medical Sciences
CSF	Cerebrospinal fluid
CV	Cresyl violet
dH_2O	Distilled water
DSM-V	Diagnostic and Statistical Manual of Mental Disorders, fifth edition
DTI	Diffusion tensor imaging
ECM	Extracellular matrix
EtOH	Ethanol
FM	Interventricular foramen (of Monro)
H&E	Haematoxylin and eosin
IA	Interthalamic adhesion
ICC	Intraclass correlation
IHA	Interhypothalamic adhesion
IHC	Immunohistochemical
KB	Kluver-Barrera
LFB	Luxol fast blue

Abbreviation	Abbreviation in full
M	Molar, unit of molarity, one mole per litre
mM	Millimolar, smaller unit of molarity, one millimole per litre
MRI	Magnetic resonance imaging
MRM	Magnetic resonance microscopy
MV10B	Methyl violet 10B
NRF	National Research Foundation
PA	Junction between the roof of the cerebral aqueduct and the third ventricle
PC	Posterior commissure
PVR	Periventricular region
RER	Rough endoplasmic reticulum
RESCOM	Research Committee
SBAH	Steve Biko Academic Hospital
SM	Stria medullaris
µm	Micrometre, unit of measurement equivalent to 0.001 mm
UP	University of Pretoria

PRE-STUDY DECLARATIONS

BUDGET

All costs necessary to complete this postgraduate study was covered by the postgraduate student and supervisor's research funds. Additional funding from sources such as the UP Postgraduate Bursary, Research Committee (RESCOM) and National Research Foundation (NRF) was not required for the completion of the study but were considered to cover any possible expenses as well as the cost of presenting findings at local and international conferences.

AUTHORSHIP

Co-authorship will be given only if significant contribution was made to the study submitted for publication, otherwise person(s) will be acknowledged for their assistance.

ACKNOWLEDGEMENTS

The completion of this research and dissertation took the combined effort and support from a group of people I will continuously remain grateful for. Firstly, I would never have been able to pursue a postgraduate education without the support of my parents, as well as their understanding when I needed more time (and money) than originally planned. If they did not consider my education important, it may have felt beyond my abilities and means to even try to complete it.

To Dr Venter, I will always appreciate the strong foundation she helped lay for me from honours until now. I have learned the most from her example. Without her patience and guidance, I would not have been able to learn as much as I did from my experience. Her critical thinking and attention to detail have helped me improve and strive to do better.

To Dr Prigge, who went from an intimidating examiner to a comforting supervisor, I am grateful for gentle understanding and kind words of encouragement when least expected.

To Dr Taute, I am grateful for the guidance in a new and daunting venture into histology, without which I would not have been able to complete a large component of this study.

To Prof Oberholzer, I am grateful for the final guidance in the review of my histology section in Dr Taute's absence.

Most importantly, with whom this study would not have existed without, I am grateful to the body donors and their families for their precious donation to my research and education at the University of Pretoria, as well as the technical staff who take great care of the dissection laboratories and human remains.

I am grateful for the help of various staff members along the way, such as Dr Serem for her practical guidance in the histology labs, Carolyn for her assistance with histological staining methods, and Jade for her assistance with data collection, inter-observer statistics and comforting presence in the laboratories.

Finally, I am grateful to my precious friends who encouraged me in more moments than I can count and mentored me through tales of their own experiences. Without them I may have given up, and much too early at that.

I have come to know that academics is far more than mere words on paper. I am grateful for my master's experience, with not only lessons in research, but in life itself.

EXECUTIVE SUMMARY

Due to the lack of literature investigating the function of the interthalamic adhesion (IA), uncertainty surrounds its significance and clinical importance within the brain. However, existing literature has been able to show a physical anatomical correlation with neurological disorders, such as schizophrenia. Only recently have studies provided limited insight into the role of the IA in the neural network of the brain, thus opening new avenues of investigation that will further our understanding of the neuroanatomy and the associated clinical implications.

The aim of this study was to conduct a descriptive, observational cross-sectional investigation of the IA in a sample of the South African population. This anatomical investigation included reports on the prevalence, location, shape, size and area of the IA and further correlated these factors with age and sexual dimorphism. In addition, this study included a histological investigation of the neuron arrangement within the IA to observe a possible implication of cell architecture for IA function.

This study used a sample of human brains dissected from bodies donated to the Faculty of Health Sciences at the University of Pretoria. Digital photography of midsagittal brain sections and scientific image-processing software (ImageJ) was used to generate the necessary measurements.

The data collected in this study was compared to known literature on the IA, noting the differences and similarities. The significance of the results was reported on.

This study provided an anatomical foundation on which to conduct further functional investigation in research of the IA within the human brain and provided a novel look into the histology of the IA and surrounding periventricular region (PVR).

Keywords: cytoarchitecture; massa intermedia; neuroanatomy; periventricular; thalamus

INTRODUCTION

The human brain is a complex structure and, like all structures in the body, it is prone to injury and illness, specifically neurological disorders. These disorders can span a wide spectrum of severity and signs and symptoms, which are diagnosed by an international standard published by the American Psychiatric Association, known as the fifth edition of the Diagnostic and Statistical Manual of Mental Disorders (DSM-V). The DSM-V is used widely in both clinical and research settings and draws from the evolving knowledge of the brain structure and function in academic literature (Black and Grant, 2014).

Understanding the mechanism of neurological disorders and injury in order to formulate appropriate treatment options for patients relies heavily on the understanding of the typical anatomy of the neurological structures involved, and the deviation from this typical anatomy (Vorstenbosch *et al.*, 2015; Habbal, 2017). The intent behind anatomical investigation of the brain in research is to map a network as functionally and geographically accurately as possible. This knowledge forms the basis for subsequent research and innovation of methodologies (i.e., the progression of scanning technologies such as magnetic resonance imaging (MRI) and diffusion tensor imaging (DTI)) and similarly assists with improving patient diagnosis and care (Kumar *et al.*, 2016; Roddy *et al.*, 2018).

Moreover, multiple DSM-V criteria need to be observed in order to reliably diagnose a disorder, therefore some patients with the same disorder may experience a different combination of symptoms (Black and Grant, 2014). This makes it likely that multiple variables are responsible for a condition to develop. This reiterates the importance of understanding the anatomy and function of each neurological structure and its interaction with other neurological and non-neurological structures such as hormones.

Anatomical literature improves by studying the most frequently observed tendency, as well as the variation within the human body. Each human being is unique, which is made especially true by the human brain. Some features of the brain may appear more significant than others, in terms of cognitive functioning, behavioural change or basic life, but each part is interconnected some way or another by a network consisting of almost one hundred billion neurons (Garman, 2011; Galakhova *et al.*, 2022).

The interthalamic adhesion (IA), as referred to in *Terminologia Anatomica* (Terminology, 1998), also referred to as massa intermedia, *adhesio interthalamica*, middle commissure, is a midline grey matter structure in the brain, extending from and joining the left and right hemispheric masses of the thalami. Thus, it forms a bridge between the two hemispheres of the brain. These connecting structures are typically described as commissures and consist of white matter fibres. Only recently have white matter tracts been visualised within the grey matter of the IA (Kochanski *et al.*, 2018). With so little confirmed information, it is still debateable whether it is appropriate to consider this structure (IA) as a commissure or not.

Brief mention towards a "thalamic commissure" was made in the 1990s, as a structure within the IA that interconnects the various midline nuclei of the thalami (Heick, 1996). However, subsequent research studies have opposed the term "commissure" in association with the IA (Severino *et al.*, 2016) except for recent studies by Borghei and co-workers in 2021 and Kochanski and co-workers in 2018. Interestingly, Borghei and co-workers reported significant findings in support of the IA as a commissure and probable "midline white matter conduit" similar to the anterior and posterior commissures (AC and PC, respectively). This is due to the identification of an extensive network of connectivity between regions of grey matter, such as the hippocampus and amygdala, by probabilistic tractography (Borghei *et al.*, 2021).

Previously, Kochanski and co-workers (2018) similarly used tractography to identify the decussation of white matter stria medullaris (SM) fibres within the IA in seven of their ten specimens with an IA. These SM fibres originated in either cerebral hemisphere to travel to the contralateral and ipsilateral lateral habenula, thus forming part of a limbic pathway. The left SM fibres tended to cross, whereas the right SM fibres tended to stay in the ipsilateral hemisphere. Interestingly, in two specimens without an IA, included as a control for the sample, the SM fibres crossed hemispheres via the PC (Kochanski *et al.*, 2018). The results in the aforementioned 2018 and 2021 studies conducted by Kochanski and co-workers and Borghei and co-workers, respectively, provided evidence for the justification of the IA as a middle commissure.

In 1993, Park and co-workers described the IA as a "grey commissure", but this was contradicted in a 2022 study by Parra and co-workers. These authors reported no evidence of a grey commissure in the IA due to their findings not meeting the condition that "neuronal somas must prevail" (Parra *et al.*, 2022). It is the opinion of the author, that it must be noted that the modality of data collection for this 2022 study was limited to histological examination with haematoxylin and eosin (H&E) staining, whereas the 2018 and 2021 studies that included evidence of a commissure provided this evidence through means of tractography. Differing methodologies can produce different results, but don't necessarily result in a different conclusion. Therefore, in most cases, results from varying methods should be compared rather than used as a sole means of explanation. For instance, an H&E stain alone will not produce enough data with which to draw a conclusion about neuronal bodies within tissue and will need to be substantiated by including specialised stains for neuronal bodies in the research methodology.

It is clear from the incongruent findings in the known literature that further peer-reviewed research is required to accurately describe the anatomy of the IA. The potential role of the IA as a white or "grey" commissure, whether comprised of white or grey matter tract fibres respectively, can have significant implications for understanding its functioning within the brain and associated thalamic pathways. This will further our understanding of neurological disorders with specific disruption in these pathways.

It has been established that academic literature pertaining to the IA is relatively scarce, therefore little information exists with regards to its function within the brain. Only recently, in the preceding decade, can an increase on this subject be seen. In addition, there is a general lack of specialised brain tissue regions included in histological study samples. The histological composition of the IA within known literature is not clearly described despite histological depictions of other structures in the brain, resulting in a void of information (Garman, 2011).

To understand the anatomy of tissue, especially of neurological structures such as the brain, it is crucial to study the development, function and clinical abnormalities of the tissue by means of determining its cytoarchitecture (Grisan *et al.*, 2018). Comparative study of the cytoarchitecture of neuroanatomy between species reveals insight into the evolutionary changes leading to, for example, the increased cognitive ability in primates and humans and cytoarchitectonic traits unique to certain species (DeFelipe, 2011).

The IA is a midline structure between the two thalami; therefore, it is most likely to be comprised of midline thalamic nuclei (Morel *et al.*, 1997; Puškaš *et al.*, 2005). The degree to which these nuclei present varies depending on the location of the IA within the third ventricle. Compared to other mammals, the human IA is much smaller and may be absent, is more variable in size and consists of fewer nuclei (Nopoulos *et al.*, 2001). In evolutionary terms,

comparative anatomy within and between species tends to report on the regression and conservation of traits. Structures that are sometimes dubbed “redundant” or disadvantageous for survival and species continuation tend to decrease in size or be removed from or “silenced” within the genetic pool during natural selection. Conversely, anatomical structures may develop and grow larger or more complex in certain animal populations, for instance, as seen in the development of the mammalian neocortex and the increased size and complexity of the brain from early hominins to modern-day Homo sapiens (DeFelipe, 2011). These are known as phylogenetic trends. There is not yet a “single all-purpose” method with which the scale of phylogenetics can be measured, therefore researchers analyse biological traits such as the rate of morphological evolution and the rate of diversification, regression and conservation of traits (Graham *et al.*, 2018). The evolution of complexity leading to the distinguishable power of cognitive functioning in human brains is hypothesised to be driven by cortical expansion, larger neurons, more complex dendritic connections and more efficient neural transmissions via synapses (Galakhova *et al.*, 2022). It would be beneficial to analyse these parameters in relation to the IA, and to understand the species-specific relevance of the difference in IA morphology between humans and other mammals.

According to the authors’ knowledge there have only been two studies in known academic literature, Kochanski and co-workers in 2018 and Borghei and co-workers in 2021, identifying the fibres that travel through the IA. These studies open a significant line of enquiry into the role of the IA within the neural network as it was previously thought that the IA held no significant connection to pathways in the brain. In the aforementioned study, these fibres were tractographically visualised with diffusion tensor imaging (DTI) and identified as stria medullaris (SM) fibres within the limbic system - a system responsible for emotion and behaviour (Kochanski *et al.*, 2018). The limbic system plays a major role in a human’s quality

of life and interaction with their environment. Midline nuclei in the thalamus, most likely found in the IA as well, have strong limbic area connections (Morel *et al.*, 1997).

A white matter tract within the epithalamus, comprised of the SM fibres, arches over the IA to terminate in the medial and lateral habenulas (Mihailoff and Haines, 2018). Compared to other species, this area of SM fibres within the habenula is larger in humans (Roddy *et al.*, 2018). In the latter of the two aforementioned studies, by Borghei and co-workers and recently published in 2021, the authors used probabilistic tractography to identify extensive connectivity between the IA and various regions of grey matter in the brain (Borghei *et al.*, 2021). Further investigation in this regard may lead us to discovering the function of the IA or its role in a larger system.

LITERATURE REVIEW

MACROSCOPIC ANATOMY

The IA is a midline grey matter structure within the third ventricle, connecting the two thalami of the brain (Katz and Chandar, 2014; Grow, 2018), as seen in Figure 1(b). Figure 1(a) shows what a brain looks like without an IA. The IA is comprised of parenchymal tissue that interconnects neuron- and axon-rich regions of the medial thalami (Whitehead *et al.*, 2015). If present, it forms during the 13th and 14th weeks of gestation as a fusion of the medial boundaries of the two thalami (Meisenzahl *et al.*, 2000).

Figure 1 Sagittal, coronal and axial MRI scans of a brain with the IA absent (a) and present (b; indicated by yellow arrow) (Trzesniak et al., 2016).

The IA is prevalent in approximately 70-80% of normal human brains, with a higher prevalence in females than in males (Nopoulos *et al.*, 2001). However, prevalence has been shown to be higher in MRI studies than in cadaveric studies, raising the average percentage of prevalence in a population to 87%, with still a higher incidence in females than in males (Wong *et al.*, 2021). It has been reported that the prevalence is statistically significantly lower in patients with neurological disorders, such as schizophrenia (Takahashi *et al.*, 2008; Trzesniak *et al.*, 2011, 2016).

Further sexual dimorphism of the anatomical features of the IA appears in size and length. The anterior-posterior length in a midsagittal section is greater in females than in males (Sen *et al.*, 2005). Similar to prevalence, IA length has been reported to be significantly less in patients with neurological disorders, including schizophrenia, bipolar disorder, and major depressive disorder (Takahashi et al., 2008a, 2008c, 2009a, 2009b, 2010; Trzesniak et al., 2011, 2012, 2016).

The shape of the IA has previously been categorically described as either oval, circular, triangular, pear-shaped or irregular, with the most common shape being oval or circular (Davie and Baldwin, 1967; Park *et al.*, 1993).

The location of the IA is arbitrarily determined by four quadrants within the medial view of the third ventricle. These quadrants have been divided by a transverse line, differing slightly in prior literature, which is bisected by another perpendicular line. Firstly, Davie and Baldwin (1967) determined the transverse line, which they named the FM-PA line, by connecting the posterior margin of the interventricular foramen (of Monro) (FM) and a junction between the roof of the cerebral aqueduct and the third ventricle (PA) (Davie and Baldwin, 1967), as seen in Figure 2.

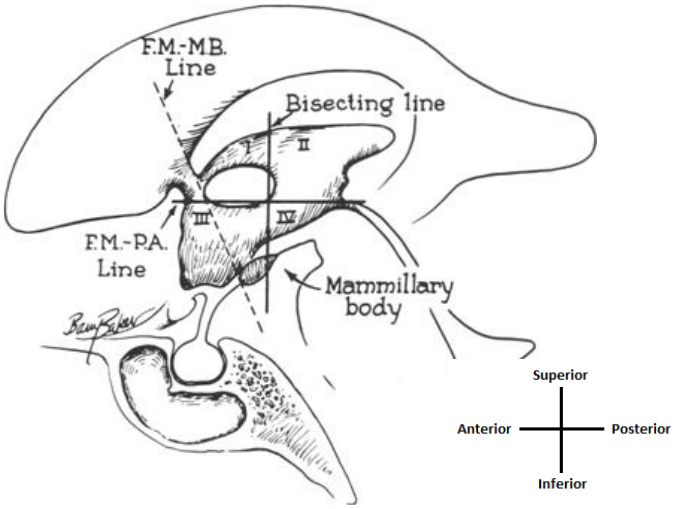

Figure 2 Division of the third ventricle in the study by Davie and Baldwin (1967), where FM is the foramen of Monro, MB is the mammillary body and PA is the junction between the roof of the cerebral aqueduct and the third ventricle.

Secondly, Malobabić and co-workers (1987) connected the AC and PC instead, to form the transverse ACPC line and subsequently dividing the third ventricle into superior and inferior sections (Malobabić *et al.*, 1987). This ACPC line was then bisected by a perpendicular vertical line to form anterior and posterior quadrants, as seen in Figure 3. This perpendicular line may pass through the IA itself or near the mammillary body posteriorly, as seen in Figures 2 and 3, but there is no specific anatomical structure used as reference to draw this line. This same method was used by Pavlović and co-workers in their study of Serbian brains (Pavlović *et al.*, 2020).

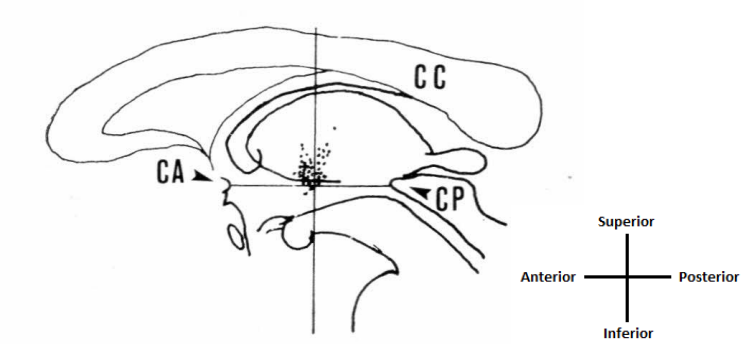

Figure 3 Division of the third ventricle in the study by Malobabić and co-workers (1987), where CC is the corpus callosum, CA is the anterior commissure, CP is the posterior commissure, and the black dots represent the locations of the IAs reported in the study.

Thirdly, Park and co-workers (1993) created a transverse line between the AC and the pineal body which was then perpendicularly bisected to form the quadrants within the third ventricle (Park *et al.*, 1993), as seen in Figure 4. The perpendicular line is drawn with no specific reference to an anatomical structure but must pass through the middle of the transverse line to divide it in half.

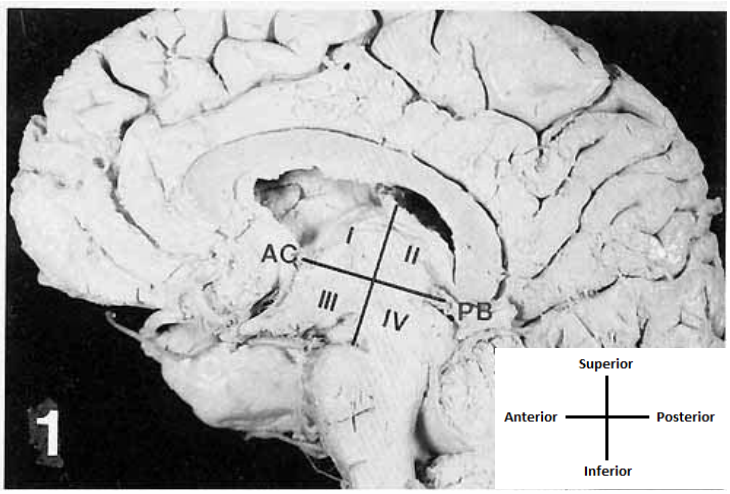

Figure 4 Division of the third ventricle in the study by Park and co-workers (1993), where the AC is the anterior commissure and PB is the pineal body.

Irrespective of the differing landmarks to form the transverse lines, the IA was most commonly located within the first and second, or superior, quadrants and at the centre of the third ventricle for all four of the aforementioned studies (Davie and Baldwin, 1967; Malobabić *et al.*, 1987; Park *et al.*, 1993; Pavlović *et al.*, 2020).

Despite a recent increase in the study of the IAs anatomical features, in correlation with certain neurological disorders, there is still little knowledge regarding the function of the IA and possible significant clinical implications. Certain morphological features of the IA, such as its size, duplication, and location, may have an influence on surgical planning and the onset of hydrocephalus (Cheng *et al.*, 2010; Nayak and Soumya, 2010).

It has been noted that an enlarged IA or the case of a double IA may be relevant during radiographical diagnoses of potential tumours and their removal (Nayak and Soumya, 2010), as an increased awareness and understanding of this structure may prevent its misdiagnosis as a tumour. Tubbs and co-workers report on the misdiagnosis of a double IA in a patient with hydrocephalus as a midline cyst due to the IAs' stretched and dilated appearance (Tubbs *et al.*, 2004). For these reasons the IA has become an important landmark for neuroradiology and neurosurgery during planning and execution of endoscopic and microscopic surgeries of the third ventricle (Baydin *et al.*, 2016).

Cases of a double IA in the literature are rare but have been reported in a few patients (Malobabić *et al.*, 1987; Tubbs *et al.*, 2004; Whitehead, 2015; Baydin *et al.*, 2016; Yasaka *et al.*, 2019; Pavlović *et al.*, 2020). Of these six studies only three had biological profile details for the patients with a double IA, all three of which were female. These instances included a 56 year old patient with different shaped and sized IAs (Pavlović *et al.*, 2020), a 14 month old

patient with Dandy-Walker variant syndrome (Tubbs *et al.*, 2004), and a dysmorphic 14 month old patient with an undiagnosed but presumed genetic disorder (Whitehead, 2015). Due to the nature of the patient in their reported incidence Tubbs and co-workers infer that it is possible that a double IA may occur in patients with additional congenital defects (Tubbs *et al.*, 2004). However, the scarcity of reports of a double IA in literature will make this hypothesis difficult to explore.

The varying location of the IA within the third ventricle may influence cerebrospinal fluid (CSF) flow dynamics within this ventricle. CSF flows naturally through the ventricular system from the lateral ventricles to the third ventricle through the left and right interventricular foramina, also known as the FM (Felten *et al.*, 2016). The CSF then travels through the cerebral aqueduct, also known as the cerebral aqueduct (of Sylvius), to the fourth ventricle situated between the pons and medulla oblongata anteriorly and the cerebellum posteriorly. Here, the CSF will enter the subarachnoid space either laterally, through the lateral apertures of the fourth ventricle (foramina of Luschka), or through the median aperture (foramen of Magendie), to be reabsorbed into the dural venous sinus system (Meunier *et al.*, 2020). Movement of CSF through the ventricular system and reabsorption into the blood circulation is dependent on "hydrostatic and osmotic pressure" gradients. The location of the IA can influence intracranial pressure within the third ventricle and affect the flow dynamics of CSF. This can have potential implications in the development of hydrocephalus, which is caused by an increase in intracranial pressure (Cheng *et al.*, 2010).

Obstruction caused by the IA in the ventricular system, either proximally if located nearer to the interventricular foramen or distally if located nearer to the aqueduct of Sylvius, may lead to poor flow and decreased reabsorption of the CSF. Hydrocephalus is just one of the possible

abnormalities caused by a disruption to or dysregulation in CSF homeostasis. This can lead to further complications, such as the incidence of intraventricular haemorrhages or the formation of tumours (Khasawneh *et al.*, 2018).

Apart from hydrocephalus, the absence and/or variant anatomy of the IA has been linked to various other neurological disorders such as schizophrenia, yet further research is required to understand the role this structure plays in the development or progression of these pathologies and to make inferences regarding its function within the brain.

MICROSCOPIC ANATOMY

Information regarding structural organisation of the IA is broken down into the organisation of the midline thalamic nuclei. There is little literature noting the internal anatomy of the IA, with only one study on the circular organisation of neurons within this region (Puškaš *et al.*, 2005) and an additional study on the identification of the decussation of stria medullaris fibres in the IA (Kochanski *et al.*, 2018).

There is controversy in the literature regarding the organisation of neurons within the IA, therefore further research in this area will allow a reliable consensus to be reached. So far, the most informative results were provided by Puškaš and co-workers (2005). The authors reported that all six specimens in their sample, sliced into frontal sections, showed a circular arrangement of neurons in both the IA and periventricular (PVR) regions, as seen in Figure 5. These arrangements were formed by an average of 7.29 neurons, of which fusiform neurons numbered the most (Puškaš *et al.*, 2005). The authors concluded that their findings suggest that the IA plays an active role in the brain. In contrast, the IA has been previously viewed as an insignificant structure due to its unknown functionality in humans (Puškaš *et al.*, 2014;

Damle *et al.*, 2017), even being described as a vestigial remnant in the brain (Borghei *et al.*, 2021).

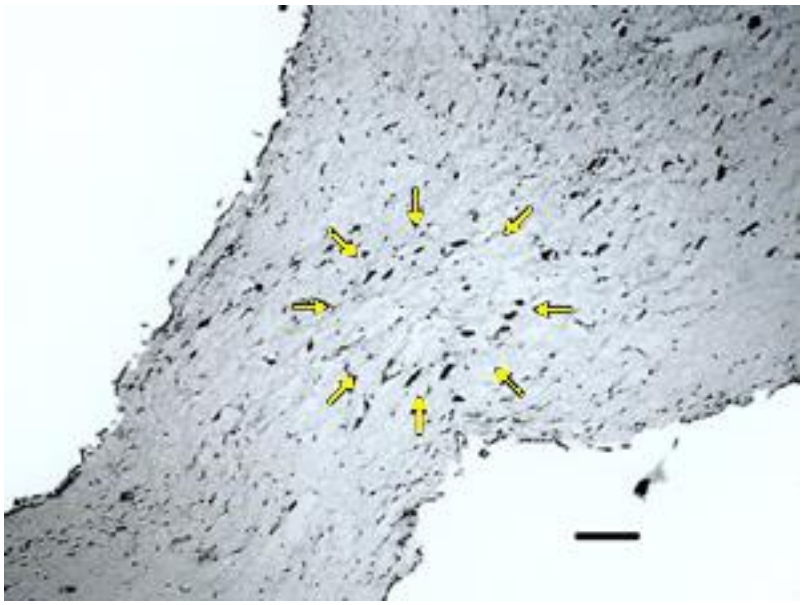

Figure 5 Circular arrangement of neurons in frontal section of IA (Puškaš et al., 2005), where neurons are indicated by yellow arrows. Stained with the Kluver-Barrera method. Bar represents scale of 100 μm.

According to Blumenfeld (2010), the IA is not considered a commissure although it does form a bridge between the two cerebral hemispheres. This is due to commissures being a type of white matter tract (Blumenfeld, 2010) which consists of axon fibre bundles sheathed in myelin, whereas the IA is a projection from the thalami comprised of grey matter which consists of axon fibre bundles lacking in myelin. Furthermore, according to our existing knowledge of relevant literature, the IA has not been found to actively perform a significant function, such as relaying information between the brain hemispheres as a commissure does. However, recent studies by Kochanski and co-workers (2018) and Borghei and co-workers (2021) have alluded to the IA's functional importance within the brain. In the study by Kochanski and

colleagues, stria medullaris fibres, which are comprised of white matter and form part of the limbic system, were mapped within the IA using diffusion tensor imaging (DTI) technology, as seen in Figure 6 (Kochanski *et al.*, 2018). These findings may have implications on the IA's classification as a commissure if further investigation reveals a significant composition of white matter with functional association in neural pathways.

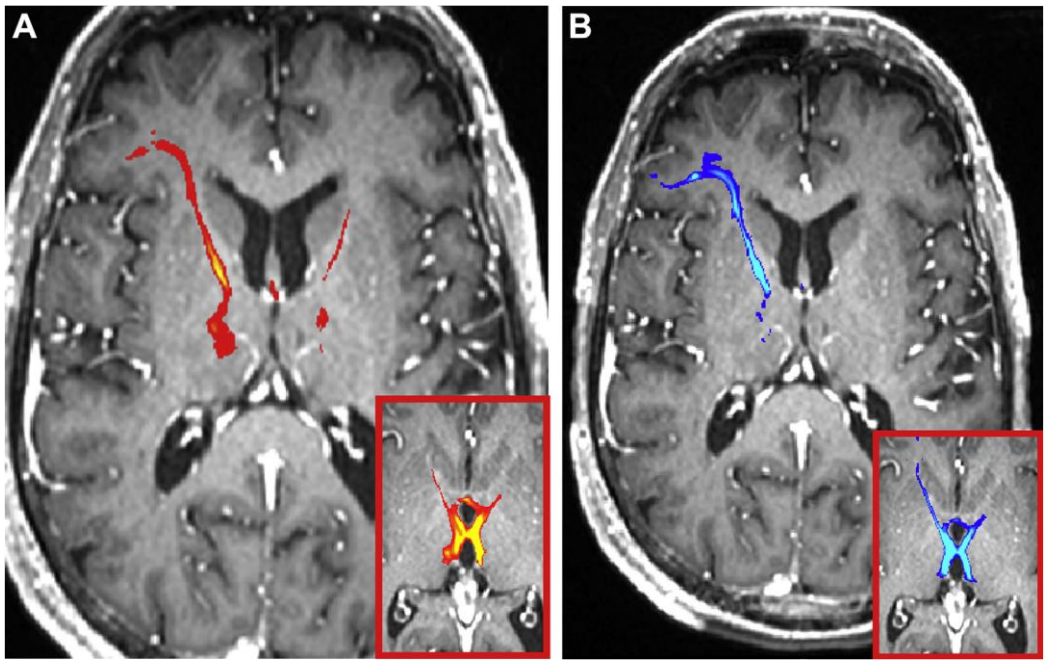

Figure 6 Probabilistic tractography of stria medullaris fibres crossing via the IA (Kochanski et al., 2018), where the left stria medullaris fibres are indicated in red and the right fibres in blue; decussation within the IA shown in block outlined in red.

In addition, Borghei and co-workers (2021) have recently dubbed the IA a grey commissure due to findings of an extensive network of pathways between the IA and other brain regions (Borghei *et al.*, 2021). These regions, from highest to lowest and based on a quantifiable connectivity measure, include the amygdala, hippocampus, entorhinal cortex, insula, lateral

orbitofrontal cortex, pericalcarine cortex, and medial orbitofrontal cortex. Other regions were reported in Borghei and co-workers' findings with lower measures of connectivity. An interhemispheric difference between the left and right hemispheres was significant in right-handed subjects only. Furthermore, a significantly higher measure of connectivity was found in females than in males in certain regions of the right and left hemispheres, such as the lingual region and cerebellum, respectively (Borghei *et al.*, 2021).

The limbic system plays a crucial role in a person's behaviour, being responsible for an individual's emotional response and memory. The stria medullaris forms the main pathway for afferent signals travelling through the thalamus to the lateral habenula (Blumenfeld, 2010), an anti-reward centre, in the epithalamus (Gold and Kadriu, 2019). An anti-reward centre, such as the lateral habenula, refers to this structure's function to potentiate "between-systems neuroadaptation" that gives rise to "negative affective states", for example, fear and depression, due to overstimulation of structures in the limbic pathway (Borsook *et al.*, 2016). Kochanski and co-workers (2018) reiterate that overstimulation of this pathway may result in "potentiation of learned helplessness, depression, and anxiety". The increased strength of nerve impulses to pathways resulting in the aforementioned behavioural states leads to increased conductive efficiency in these pathways. Their study reported the decussation of stria medullaris fibres in seven of their ten subjects with an IA, while the absence of the decussation seemed to correlate with a smaller IA size, although statistical significance was not reported (Kochanski *et al.*, 2018).

USE OF FIXED BRAIN SPECIMENS IN HISTOLOGICAL STUDIES

Anatomical studies of human sample populations are commonly comprised of cadaveric specimens. These specimens are often fixed with embalming fluid that consists of formalin, usually 10% of saturated formaldehyde solution but this percentage can be as high as 40% at some institutions (Gupta and Gauba, 2011; Kalanjati *et al.*, 2017). This process is used to temporarily halt or slow down the decomposition of the biological structures, allowing for these specimens to be used for academic and research purposes in medical programmes and studies. Although there are benefits to using cadaveric samples there are limitations as well, especially in research studies that are dependent on the true 'lifelike' elasticity and structure of specimens. Fixed cadavers are stiff and rigid due to embalming fluid that infiltrates the circulatory system and spreads widely throughout the body. Alternatively, acquiring fresh specimens can greatly reduce the sample size of a research project due to the expenses incurred in obtaining the fresh tissue, its availability and ethical restrictions of its use (Gupta and Gauba, 2011), depending on the country and institution of research. National power outages in South Africa, for example, negatively impact the preservation of bodies in freezers before they are embalmed. Moreover, there is increased pressure to complete the data collection on the fresh tissue in as short a time as possible, as decomposition of the biological material is not halted. These specimens are commonly frozen to be maintained for as long as possible, however this method of preservation can have negative implications on histological data collection due to the formation of ice crystals on a cellular level, causing morphological damage to the tissue (Pegg, 2010). This type of morphological change can lead to forced exclusion of data in research projects due to the destruction of cell integrity (Pegg, 2010). Therefore, histological samples should be obtained before the rest of the body is frozen.

Therefore, it has been investigated whether the use of fixed cadaveric material for neuro-histological studies remains viable and reliable for research purposes. Factors that were investigated in the literature included the time between clinical death and removal of the brain for fixation, known as the post-mortem interval (PMI) or delay (Shiurba *et al.*, 1998; Amunts *et al.*, 1999; Puškaš *et al.*, 2014), and the amount of time a specimen was fixed for before being histologically prepared and used as a histological sample. Tissue autolysis will take place during the PMI, therefore the longer the duration of this interval the greater the degradation that occurs and effect on immunohistochemical (IHC) staining (Shiurba *et al.*, 1998).

Preparation of human tissue includes cryopreservation and chemical fixation. Fixation methods are typically divided into perfusion and immersion fixation. Perfusion fixation is the common approach to prepare brain tissue in animal studies and refers to forcing the fixative solution through the vascular system, with the aid of cannulation, to circulate throughout the body and perfuse to the surrounding tissue (McFadden *et al.*, 2019). In contrast, immersion fixation is commonly used for the preparation and long-term storage of human brain tissue and refers to submersion in a chemical bath of fixatives that will diffuse into the brain tissue (McFadden *et al.*, 2019).

Studies reviewed by McFadden and co-workers have shown that perfusion fixation preserves tissue at a significantly higher quality than immersion fixation, however the latter method is a more common practice for the preservation and storage of human brain tissue due to the limitations of the former method (McFadden *et al.*, 2019). Blood vessels and tissue in general are often damaged before death, possibly leading to a failure or inadequate degree of perfusion, and the process of perfusion fixation requires a higher demand of expertise and

special equipment (McFadden *et al.*, 2019). In 2019, McFadden and co-workers conducted a systematic review of 35 studies that collectively reported on the perfusion fixation of 558 human brains. This review showed that perfusion fixation results in equal or greater subjective histology quality when compared to immersion fixation of relatively large volumes of brain tissue, in an equal or shorter amount of time. In human post-mortem brain tissue, it has been estimated that it can take 20 to 46 days for enough formaldehyde to diffuse to the innermost parts of a brain hemisphere and begin fixation (Dawe *et al.*, 2009). However, perfusion fixation has been reported to have some downsides, including the potential for tissue oedema or uneven fixation in the presence of cerebrovascular disease.

McFadden and co-workers (2019) reported that most studies in the sample literature showed preference for a shorter PMI, with the best IHC stain results at a PMI of less than 12 hours, yet satisfactory results up until 18 hours. However, McFadden and colleagues reported on a study noted a decrease in the quality of preservation of the cell constituents from as early as a PMI of five hours. In contrast, a different reported study included specimens with a PMI of up to 35 hours (McFadden *et al.*, 2019).

In 2013, Nlebedum and Ekele studied the effect of embalming fluid on the histological appearance of organs from embalmed specimens of the West African dwarf goat. Although this study sample did not include human or brain tissue, it conceptualised the viable use of embalmed/fixed tissue for histological research. This study suggests that tissue sections from embalmed cadavers with at least 4% formalin embalming fluid may be adequately fixed for histopathology. It is hypothesized that a high degree of vascularization in certain tissues (for example, the liver) may allow for better perfusion by embalming fluid, resulting in proper fixation (Nlebedum and Ekele, 2013).

Thus far, it has been uncertain whether the amount of time a cadaver specimen remains embalmed influences the histological studies thereof. In 2019, Alrafiah and Alshali tested a variety of histological staining methods on 10% formalin-fixed specimens of the frontal and temporal gyrus region of the brain. These specimens remained embalmed between one and twenty years before the study commenced. Histological examination of H&E-stained sections of the frontal and temporal grey matter and corpus callosum revealed normal appearances. Histological and IHC techniques yielded reproducible staining results when applied to human brain tissue stored in formalin for long periods of time, thus leading to the conclusion by the authors that they can be used as well-preserved biobank material to be utilised in neuropathology research and educational settings (Alrafiah and Alshali, 2019).

Histological studies will use certain methods of staining depending on the cellular structures that need to be identified. In a study by Shiurba and co-workers (1998), immunocytochemistry was tested on human brains fixed with formalin for less than a year. The investigators found that the prolonged storage of the specimens in formaldehyde caused progressive acidification of the tissue, leading to a decrease in immunoreactivity necessary for the data collection. However, this could be overcome with special treatment to still allow for antigen retrieval (Shiurba *et al.*, 1998). The investigators further tested Nissl staining on the fixed specimens, which can show the extent of autolysis caused by fixation by formalin. A final immunocytochemical test included Thioflavin-S counterstaining. This counterstain was shown to be useful for identifying amyloid deposits, a histopathological hallmark of Alzheimer's disease. This experiment shows how formalin-fixed brains can still be considered as valuable samples in histological studies, although may need additional treatments to overcome the limitations caused by long-term fixation (Shiurba *et al.*, 1998).

This formalin-fixed sample viability was further investigated by researchers Gupta and Gauba (2011) in a histological study of formalin-fixed cadaver tissue treated by H&E staining and observed with light microscopy. The sample consisted of cadavers embalmed with 40% formaldehyde 48 hours after death. The investigators analysed the tissue architecture by observing and scoring the arrangement of various cellular elements in relation to each other, the sharpness of the cellular outline, the size of the cell, intra-cellular details at the given magnification, size and position of the nucleus, staining properties of the nucleus, intra-nuclear features like nucleoli and the arrangement of chromatin, the state and staining of connective tissue, the absence of the intra-cellular spaces which indicated shrinkage, and lastly, the absence of the features which indicated cell death (Gupta and Gauba, 2011).

The investigators scored the fixed brain sample consisting of cerebral hemispheric tissue with a comparison score of nine, indicating an excellent match to a standard histological slide of the cerebral hemisphere. Further observation of the tissue showed clear areas around the bodies of some neurons, hypothesized by the investigators to be the result of the formation of artifacts during tissue processing which caused cell shrinkage.

Similarly to the abovementioned study, Kalanjati and co-workers (2017) investigated the possibility of analysing the morphology of the human cerebellar cortex from formalin-fixed cadavers, using H&E staining and light microscopy (Kalanjati *et al.*, 2017). Twelve adult male cerebella from cadaver anatomy preparations were embalmed, via the femoral artery, with 37% formalin fixative solution and stored for over a year. These specimens were cut and prepared for histological analyses of: (1) the total frequency of Purkinje cells, (2) the distance between the nuclei of two Purkinje cells, (3) the Purkinje cell density, which is equivalent to the quotient of the total distance divided by the frequency of Purkinje cells in a region, and

(4) the molecular layer thickness. The authors were able to report on all their objectives successfully despite the inclusion of fixed cadaveric brain specimens.

Another study specifically observed nervous system cellular structures with Fluoro-Jade and silver degeneration staining. These stains allow for the identification of cellular degeneration of neurons and can help quantify the extent of degeneration after fixation with formaldehyde (Garman, 2011). This study further observed that cell integrity was maintained by neurofilaments and microtubules.

In 2012, Dorathy and co-workers experimented with a simple, cost-effective rapid differential staining technique, known as the methyl violet (MV10B) stain, for identification of myelinated fibres and nerve cells. This study's sample consisted of neutral buffered formalin fixed human cadaver brains and spinal cords, from specimens embalmed within two hours after death. The authors found that the MV10B staining method does not require any differentiation, is highly cost effective, requires a low dye concentration, is simple and easy to perform, and delivers rapid and consistent results with adequate contrast between the myelinated fibres and nerve cells (Dorathy *et al.*, 2012).

In a comprehensive study, Paradiso and co-workers (2018) were able to report on the biochemical changes that occur in the donor tissue during four different fixation protocols, consisting of neutral-buffered formalin, with the addition of formic acid or glacial acetic acid. The investigators used a sample of five autoptic postnatal brains and sectioned the temporal lobe and hippocampus into one-centimetre-thick coronal macro-slices for fixation. The biochemical changes that the investigators were able to observe included a decrease in the pH level, which influences the exposure of target proteins and epitopes. For IHC methods, a delay on fixation, as well as the time of formalin fixation, can reduce the immunostaining

efficiency. Formalin degrades DNA and masks protein epitopes by forming covalent bonds between neighbouring proteins or nucleic acids, decreasing the rate of success of IHC. To unmask epitopes for antibody binding in formalin-fixed tissue, several enzymatic and heat-induced antigen retrieval methods have been introduced. In their H&E sample, the investigators observed a better preservation of the cell shape, a more compact parenchymal matrix and nucleolar and nuclear preservation with a formalin-formic fixation protocol. Four factors to consider in preservation of proteins for IHC in fixed tissue samples are the PMI, the specific fixation protocol and length, and antigen retrieval techniques (Paradiso *et al.*, 2018).

Table 1 below summarises useful conclusions drawn from the aforementioned studies investigating the viability of fixed brain tissue in research. Table 2 summarises useful observations made by the aforementioned studies when using specific stains to observe and identify cellular structures in a sample of fixed brain specimens.

Table 1 Viability of fixed brain tissue reported in literature

Study	Notes on fixed brain tissue viability	Viable
(Shiurba *et al.*, 1998)	There is progressive acidification of tissue and a decrease in cell immunoreactivity which requires special treatment for antigen retrieval	Yes
	Nissl substance is very sensitive to nucleases and reflects the extent of tissue autolysis at the time of formalin fixation	
(Gupta and Gauba, 2011)	Observation of cell shrinkage and artifacts due to tissue processing, however clear and well-preserved tissue organisation	Yes
(Garman, 2011)	Cell integrity was maintained by neurofilaments and microtubules	Yes
(Nlebedum and Ekele, 2013)	Suggests that tissue sections from embalmed cadavers with at least 4% formalin embalming fluid may be adequately fixed for histopathology	Yes
(McFadden *et al.*, 2019)	With perfusion fixation, the inner regions of the brain begin to degrade before they can be perfused with fixative solution	Yes
	A high percentage of alcohol fixative solution can lead to cell shrinkage	No
	A fixative solution containing glutaraldehyde can improve the preservation of tissue morphology for electron microscopy, but simultaneously lowers the success of IHC	Yes
	A fixative solution consisting of picric acid increases the success of IHC, but is more hazardous due to its explosive properties	No
	A fixative solution containing potassium dichromate improves fixation of lipids	Yes

Table 2 Summary of the use of specific stains in the study of the histology of fixed brain tissue

Stain	Note on stain used on fixed brain tissue
Thioflavin-S counterstaining	Useful for identifying amyloid deposits which are histopathological hallmarks of Alzheimer's disease (Shiurba *et al.*, 1998)
Fluoro-Jade stain + silver degeneration stains	Circumventricular organs are often mistaken for lesions; there are six in total (Garman, 2011)
	Nissl substance, which stains quite prominently in large-sized neurons but is usually not apparent in small-sized neurons at the light microscopic level, represents the rough endoplasmic reticulum (RER) (Garman, 2011)
	A variety of IHC markers exist for neurons. Some of these markers include synaptophysin, NeuN, neurofilament protein, neuron-specific enolase (NSE) (which is not entirely specific for neurons), and microtubule-associated protein 2 (MAP2) (Garman, 2011)
Immunostaining	Immunostaining with ionised calcium-binding adapter molecule 1 (Iba1) improves the visualisation of microglial dendritic processes (Garman, 2011)
MV10B stain	A simple, cost-effective, rapid differential staining technique for myelinated fibres and nerve cells (Dorathy *et al.*, 2012)
Thioflavin-S counterstaining	Useful for identifying amyloid deposits which are histopathological hallmarks of Alzheimer's disease (Shiurba *et al.*, 1998)

AIM OF STUDY

PROBLEM STATEMENT

Academic literature regarding the IA is scarce, with no known indication of its functional significance within the brain and direct implication in neurological pathways, as well as no clear representation of its cytoarchitecture.

AIMS AND OBJECTIVES

The aim is to conduct an anatomical investigation of the human IA in an adult South African sample to add to the academic literature regarding this subject on which to base further investigation regarding its function within the brain and clinical significance.

Objective one

The objectives for reporting on the prevalence and macroscopic anatomical characteristics of the IA and third ventricle are as follows:

a. Record prevalence, shape, and location of the IA in midsagittal sections of adult human brain specimens.
b. In ImageJ, record the anterior-posterior length, superior-inferior length, and midsagittal surface area of the IA.
c. In ImageJ, record the midsagittal surface area of the third ventricle.

Objective two

The objectives for reporting on the microscopic anatomical features of the IA and periventricular region are as follows:

a. Using light microscopy, observe and identify the structural arrangement of neurons in the IA and periventricular region of the thalamus in a histological section from the sagittal plane.
b. Using light microscopy, record the frequency of structural arrangements in each sample and the frequency of neurons in each structural arrangement, and classify neuron morphological type as either fusiform, oval, or multipolar.
c. Measure the diameters of the neuron structural arrangements (short axis and long axis) in μm.

METHODOLOGY

COMMITTEE APPROVAL

Research study approval was obtained from the Master's Research Committee and ethical clearance (clearance reference 3/2021) was obtained from the Research Ethics Committee of the University of Pretoria's Faculty of Health Sciences (see Appendix A for clearance letters obtained in the years 2021 and 2022). This study's ethical clearance pertains to the undertaking of an anatomically investigative study, that does not include any animals or living patients/volunteers, and the use of data collected from the brain specimens of donated bodies. Anatomical studies of donated bodies fall under the National Health Act, 61 of 2003. Dissections were conducted in the Department of Anatomy at the University of Pretoria's medical campus (Prinshof campus) and were completed in accordance with the ethical standards laid out in the 1964 Declaration of Helsinki and all subsequent revisions. Digital photographs were taken of all dissected specimens, with no personal identifiers visible. Specimens were processed in the histological labs for inspection under a light microscope.

STUDY DESIGN

This study included a descriptive, observational cross-sectional component of cadaveric brain samples. As the extent of this project was to investigate an anatomical structure in the brain and its prevalence and morphology in a specific human population, the study design is focused mainly on being qualitative and descriptive and data will be of both a quantitative and qualitative nature (Milligan and Chen, 2018).

The histological part of the study is specifically noted as an exploratory observational and qualitative component. As a pilot study, the focus was aimed towards hypothesis generation, as previous literature is minimal and requires more evidence to be able to support any significant theories. Therefore, the histological component of this study focused on hypothesis generation given the scarcity of prior known literature.

This study included simple methodology that can be conducted by an investigator with a background in human anatomy and training in human dissection, and most importantly, was ethically safe (Srikanth, 2013). As this study was only a cross-sectional study, causality of data was not investigated - this would require future investigation with functional MRI studies, as an example, which will be discussed later.

All the equipment necessary for this project is listed in Table 3 below.

Table 3 Study equipment

Item	Manufacturing details
Virchow brain sectioning knife	Miltex Instruments, Germany
Ruler with cm/mm scale	Not applicable
Digital camera	Nikon D3100, Tokyo, Japan
Desktop computer / laptop	Lenovo G50
ImageJ software	Version 1.8.0_172, developed by US National Institutes of Health (NIH), Maryland, USA
Drawing tablet	Wacom Intuos by Wacom Co. Ltd, Saitama, Japan
Microscopy oven	Term-O-Mat, Labotec Pty Ltd, Midrand, South Africa
Microtome	Leica RM 2255, Leica Biosystems, USA
Light microscope with camera	Axio Imager M2 with Axiocam 305, Zeiss, Germany

SAMPLE SIZE AND POPULATION

The following anatomical investigation and histological study has been done in continuation of a previous anatomical investigation of the IA in a South African population completed in 2019, as part of an Honours degree research project. Donated human material is the basis for most anatomical studies, and we are grateful to the University of Pretoria and its body donor

program, consisting of the donor families, for making this anatomical study possible. Unfortunately, due to the COVID-19 pandemic, the sample was smaller than previously anticipated. However, restrictions ensured that COVID-19 related deaths were excluded from the sample.

The sample size is summarised in Table 4 below.

Table 4 Sample size summary

Objectives	Short Description	Sample and Sample Size
Objective one	Reporting on the prevalence and macroscopic anatomical characteristics of the IA and third ventricle	83 formalin-fixed brain specimens
Objective two	Reporting on the microscopic anatomical features of the IA and periventricular region	34 H&E-stained and 34 CV-stained brain histological sections

The latter half of this study comprised of a histological sample processed from the fixed brain specimens. Fortunately, a larger histological sample than expected could be collected from the available specimens at UP. Therefore, the sample was formed from 34 tissue blocks cut from 21 formalin-fixed brain specimens. Of this sample, 14 consisted of specimens with an IA, whereas seven consisted of specimens without an IA. A power analysis based on the minimum

predicted sample size showed that a sample size of at least 10 would still be appropriate for research. Therefore, the final sample size in this study was sufficient to make the necessary observations of the cell architecture and neuronal organisation within the IA and periventricular (PVR) regions of the thalamus.

It is likely that different groups in the sample may be of differing sizes, such as an asymmetrical distribution of males and females in the overall population, due to the random nature of sample inclusion.

Specimens within the sample were included regardless of ancestry, height and weight of the donor, and excluded if significant damage to the regions of interest could be observed.

DATA COLLECTION

The original methodology to achieve the research objectives are summarised and presented in Figure 7 below.

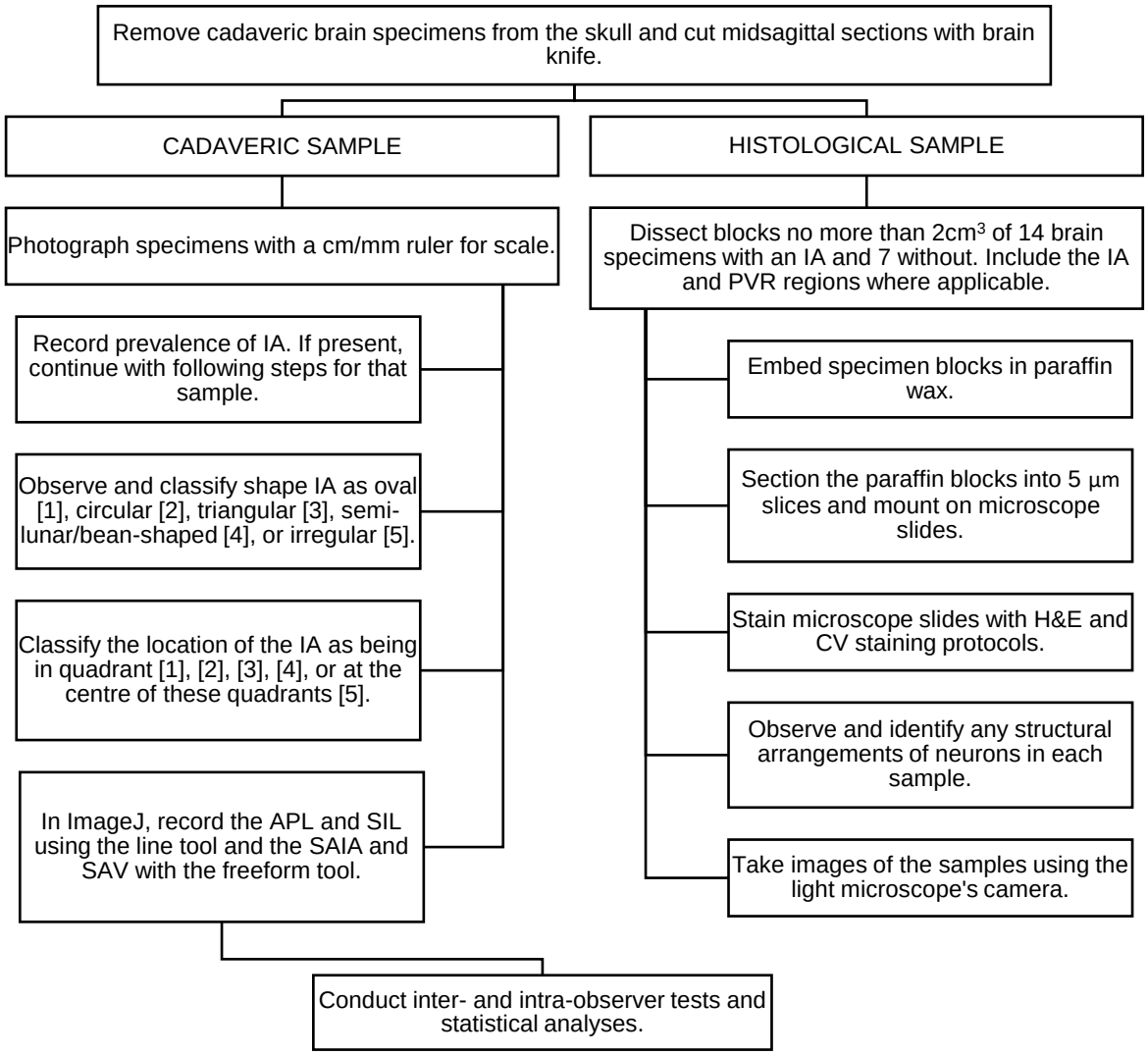

Figure 7 Data collection flow diagram, where IA is interthalamic adhesion, PVR is periventricular region, APL is anterior-posterior length, SIL is superior-inferior length, SAIA is surface area of the IA, SAV is surface area of the third ventricle, H&E is haematoxylin and eosin, and CV is cresyl violet.

Cadaveric Sample

For each sample, the brain was removed from the skull during undergraduate dissection modules by technical staff, following a horizontal craniotomy. Using the brain knife, a midsagittal cut was made to divide the brain into two approximately equal halves, providing

sections of the left and right midsagittal views. Care was taken when using the brain knife to make the section as precise as possible.

Samples were excluded if the specimens showed any clear physical signs of pathology or damage. The cerebral hemisphere, which appeared the most well preserved and with better defined structures, was included in the sample.

The chosen hemisphere was then placed with the lateral surface on a flat table, with the midsagittal view facing upwards, and the horizontal plane being based on an arbitrary line from the AC to the PC, the ACPC line. A cm/mm ruler was placed parallel to the horizontal plane of the section, inferior to the specimen and on the same flat surface. This acted as a scale for reference for the measurements when using ImageJ imaging software. A label for each specimen was added inferior to the ruler to identify each sample by its table number and cadaver number.

An image of each section was taken with a digital camera (Nikon D3100). The image was taken approximately 20cm away from the specimen, parallel to the flat surface and included the specimen, ruler, and label of the specimen. In order to maintain consistency with regard to the images, the images were always taken from above in a dissection hall with bright lighting and no camera settings were altered between the photos taken of the subsequent specimens.

All images were transferred onto a desktop computer/laptop where they were observed and analysed with ImageJ. Backup folders of these images were stored on the primary investigator's Google Drive until later moved to the University's Google drive.

The images were studied and the prevalence (categorical/discrete data) of the IA was recorded as either present (indicated by “1”) or absent (indicated by “0”) in a data collection sheet, available as Annexure B.

From this point, only images with an IA present were further observed and analysed.

The images were scrutinised next to identify the shape (categorical/discrete data) of the IA. The shape was classified as one of the following five categories, as seen in Figure 8 below:

- oval [Figure 8A],
- irregular [Figure 8B],
- semi-lunar [Figure 8C]/bean-shaped [Figure 8D],
- triangular [Figure 8E],
- circular [Figure 8F]

as collectively described by Davie and Baldwin (1967) and Park and co-workers (1993) and recorded in Annexure B. Semi-lunar or bean-shaped IA were placed into the same category due to the similarity in shape curvature which could make it difficult to distinguish between these two shapes distinctly.

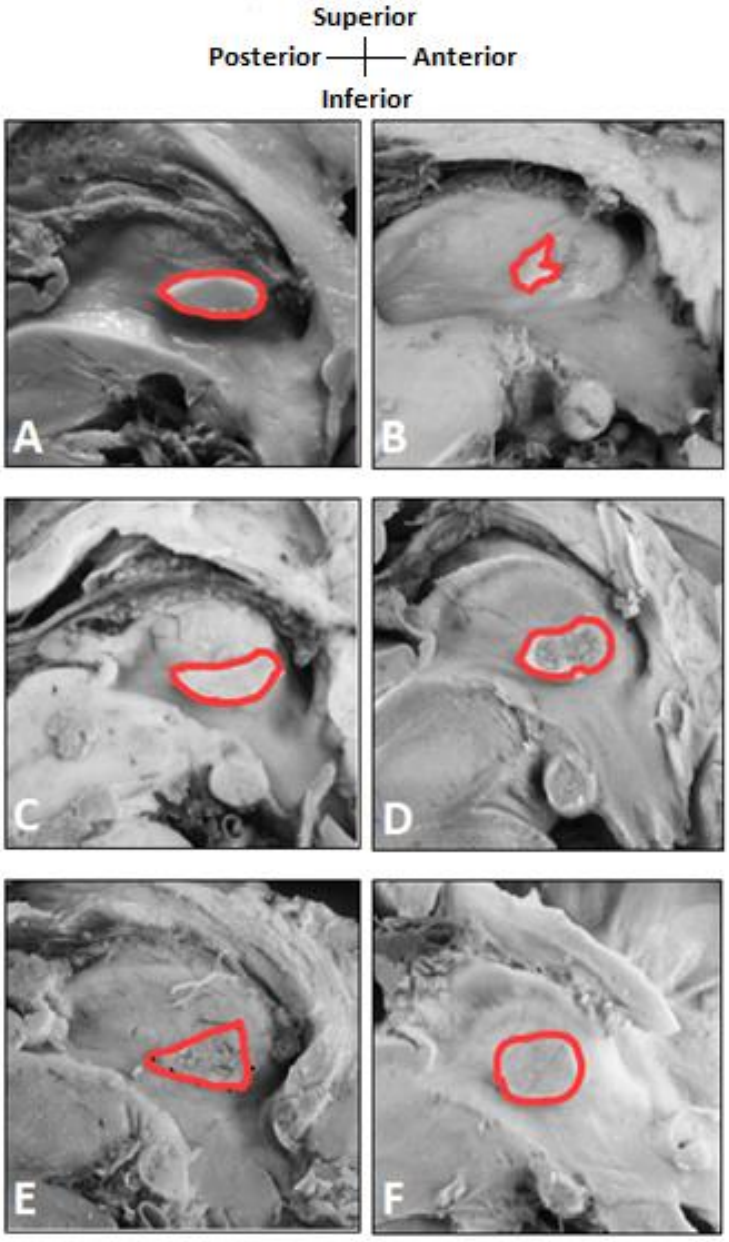

Figure 8 Shape categories (van Heerden, 2019).

The images were then opened in Microsoft Paint to create the arbitrary quadrants for identification of the location of the IA within the third ventricle, as seen in Figure 9. A horizontal line was drawn from the AC to the PC, forming the ACPC line. Due to the built-in grid in Microsoft Paint, a vertical line bisecting the ACPC line can be drawn reliably for each specimen. The number of grid blocks spanning the length of the ACPC line were counted and

halved to find the exact point at which the bisecting line will pass through the midpoint of the ACPC line and form a right angle (90°) with the ACPC line. The bisecting line begins at the upper limit of the third ventricle and ends at its lower limit in the vertical plane it is situated in. The location of the IA within the third ventricle could then be observed and recorded in Annexure B as being in one of the following five locations, as seen in Figure 9 below:

- the anterior-superior quadrant - indicated by a “1”
- the posterior-superior quadrant - indicated by a “2”
- the anterior-inferior quadrant - indicated by a “3”
- the posterior-inferior quadrant - indicated by a “4”
- the centre of these quadrants, indicated by a “5”.

If the IA was found to overlap in multiple quadrants, the location was determined based on the quadrant in which most of the IA mass was predominantly located.

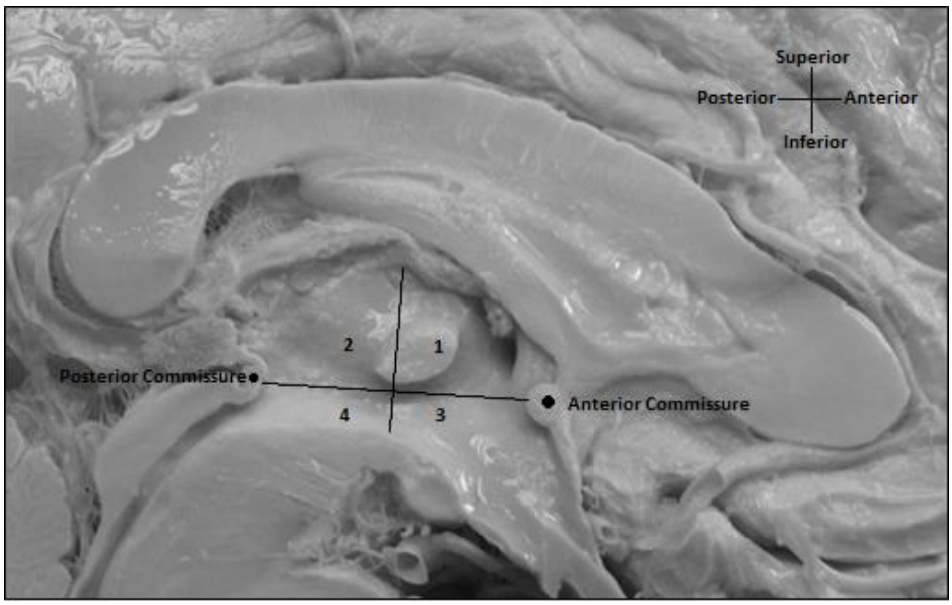

Figure 9 Location of the IA within the third ventricle (van Heerden, 2019), where 1 indicates the anterior-superior quadrant, 2 the posterior-superior quadrant, 3 the anterior-inferior quadrant and 4 the posterior-inferior quadrant.

These images, now with an arbitrary horizontal and vertical plane, were saved and used in the following steps.

The images were opened in ImageJ, a scientific image processing software application. For each image, the scale was calibrated (in mm) using the ruler in the image as a reference. The measurements of the IA and third ventricle (numerical/continuous data), as seen in Figure 10 below and recorded in Annexure B, are as follows:

- anterior-posterior length of IA (APL)
- superior-inferior length of IA (SIL)
- sagittal surface area of the IA (SAIA)
- sagittal surface area of the third ventricle (SAV).

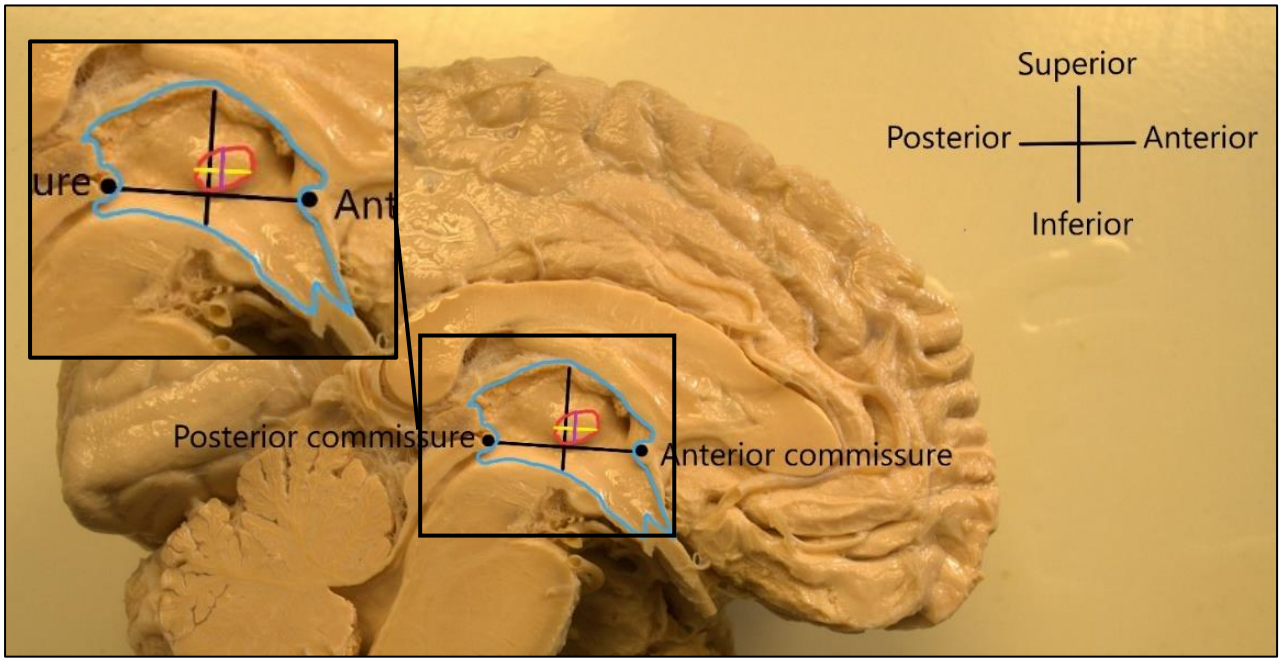

Figure 10 Measurements of the IA (van Heerden, 2019) indicated in yellow (APL), purple (SIL), red (SAIA) and blue (SAV).

Using the line tool in ImageJ, the APL was measured in millimetres (mm) from the most anterior limit of the IA to its most posterior limit, parallel to the ACPC line (indicated in yellow in Figure 10).

Using the line tool again, the SIL was measured in mm from the most superior limit of the IA to its most inferior limit, perpendicular to the ACPC line (indicated in purple in Figure 10).

A drawing tablet was connected to the computer to use the freeform tool in ImageJ with more control, thus providing more accurate results. The border of the IA was traced – the zoom tool was used to increase accuracy of outlining the border – and recorded in mm^2 as the SAIA (outline indicated in red in Figure 10). The border of the third ventricle was traced in the same manner and recorded in mm^2 as the SAV (outline indicated in blue in Figure 10). The border of the third ventricle was demarcated anteriorly by the AC and lamina terminalis, superiorly by the choroidal fissure and fornix, posteriorly by the habenular commissure, pineal gland, pineal and suprapineal recesses and the PC, and inferiorly from posterior to anterior, by following the opening to the aqueduct of Sylvius, the mammillary bodies, tuber cinereum, infundibulum of the pituitary gland and the optic chiasm.

Inter-observer and intra-observer data were collected for 10% of the sample by the primary investigator and a third-party, respectively, at a later stage. The inter-observer was trained by the primary investigator on the correct demarcation of the measurements and use of the tools to measure. This was to ensure the method of data collection was reliable and can be repeated to provide accurate results. Further statistical analyses were conducted on the data from the cadaveric specimens.

Histological Sample

Creating blocks from the specimens destroys the specimen in turn (regarding data collection for the first half of the study), therefore data collection was completed with this limitation in mind. The blocks were cut from the original sample of specimens after the first cadaveric half of the study's data was collected. From the collection within the Dissection Labs on the 3rd, 4th and 5th floors of the Basic Medical Sciences (BMS) building, the blocks were prepared for the second half of the study within the Histology Laboratory on the 6th floor of the BMS Building (transported in containers while submerged in formaldehyde).

All the materials necessary for the histological procedures are listed and described in Table 6.

Table 5 Histological materials

Item	Amount	Manufacturing details*
Phosphate buffer	0.1 M	Made in Histology lab*
Ethanol (EtOH)	Approx. 10ml per sample container, per fluid change	Ethanol Absolute 25L SAAR2233541ME, Merck
Xylene	Approx. 10ml per sample container, per fluid change	Xylenes, histological grade 534056-4L, Sigma
Haematoxylin	Approx. 100-200ml in staining container	Hematoxylin cryst 25g 104302.0025, Merck
Eosin	Approx. 100-200ml in staining container	Eosin Y Powder 25g 17372-87-1, MFCD00005040, Merck
Distilled water (dH_2O)	Approx. 500ml	UP Histology labs
Cresyl violet	0.1g	Merck & Co., Inc.
Entellan	-	Merck & Co., Inc.
Glass tubes	68 of medium size	White Scientific
Microscope slides	68 of 76x26x1mm size	Clearscan Frosted microscope slides
Microscope slide box	Two with space to hold 50 slides each	Homemade

** All reagents were obtained from Sigma-Aldrich, Johannesburg, South Africa, unless stated otherwise.*

Sagittal sections for the light microscopic component of the study were dissected to obtain samples from 14 brains with an IA and seven without. A total of 21 specimens were utilised in the histological sample population. Tissue blocks, no more than $2cm^3$, were dissected from the obtained samples for histological preparation. Samples with an IA included blocks of both the IA and PVR regions, except if the region was too small to embed. Samples without an IA only included the PVR region. This formed a sample of 34 tissue blocks in total, consisting of 10 blocks of the IA region, 20 blocks of the PVR region, and four blocks of a horizontal section including both the IA and PVR regions.

The histological preparation of the sample included embedding, sectioning, and staining processes prior to observation under the light microscope. Each of these processes are explained in the following section.

Embedding Protocol

The initial results after embedding the specimens appeared to be of low quality, thus the length of the original protocol was extended to improve the quality once viewed with a light microscope. This was achieved by multiplying the length of the standard embedding protocol by 1.8. Thus, the protocol depicted in the flow diagram (Figure 11) and described below is the optimised version used in this study.

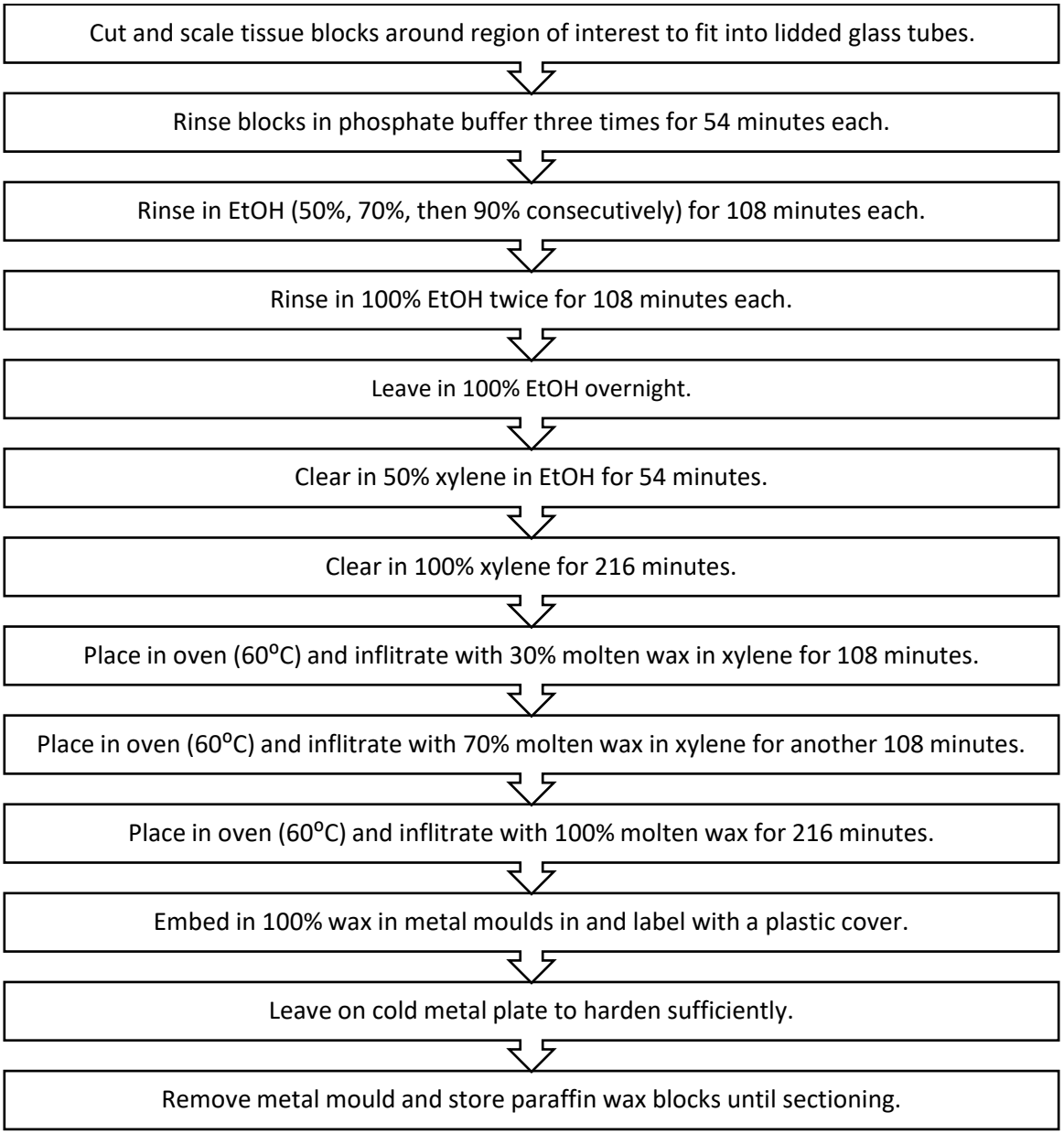

Figure 11 Flow diagram of embedding protocol.

The tissue blocks were cut and scaled to an appropriate size for embedding and placed in lidded glass tubes for the entire embedding process. The tubes were labelled by cadaver number and region (IA, PVR or horizontal) to identify the specimens later.

The tissue blocks were rinsed three times, for 54 minutes each, in 0.1 M phosphate buffer (81 mM $Na_2HPO_4.{}_2H_2O$, 19 mM $NaH_2PO4.H_2O$, pH 7.4) to remove formaldehyde from the fixed

specimens. The tissue blocks were dehydrated consecutively with multiple changes of EtOH (50%, 70%, 90%) for 108 minutes each, and then finally in 100% EtOH twice for 108 minutes each. The tissue blocks were then left in 100% EtOH overnight.

The next day, the blocks were cleared with 50% xylene in EtOH for 54 minutes, followed by 100% xylene for 216 minutes. The blocks were then placed in the oven (temperature set to 60^{o}C) to be infiltrated with 30% molten wax in xylene for 108 minutes, 70% molten wax in xylene for another 108 minutes, and finally with 100% molten wax for 216 minutes.

The tissue blocks were then embedded in 100% wax in metal moulds in preparation for sectioning and labelled with a plastic cover. The moulds were left to harden sufficiently on a cold plate, and the metal mould removed. If this step caused the wax block to detach from the plastic cover, the specimen had to be re-embedded in the mould until successfully moulded and attached to the plastic cover (the plastic cover is essential in inserting the block correctly on the microtome for sectioning).

Once the wax block was ready, it was trimmed with a microtome blade as close around the tissue specimen as possible. The microtome was then used to cut the block into 5 µm sections. These sections were transferred to a warm water bath to remove creases in the section and then placed onto a labelled microscope slide (and kept track of in the authors designated laboratory book). The microscope slides were left to dry in preparation for the staining protocols. A total of 68 slides, two sets of 34 slides each, were prepared for H&E staining of the first set and cresyl violet (CV) staining of the remaining set.

Haematoxylin and Eosin Staining Protocol

The first set of 34 slides was stained with H&E. The H&E staining protocol had already been optimised by the histology laboratory and did not require further adjustments, therefore the staining protocol that is depicted in the flow diagram (Figure 12) and described below is the standard protocol for H&E staining at the Department of Anatomy, University of Pretoria (Naidoo *et al.*, 2019).

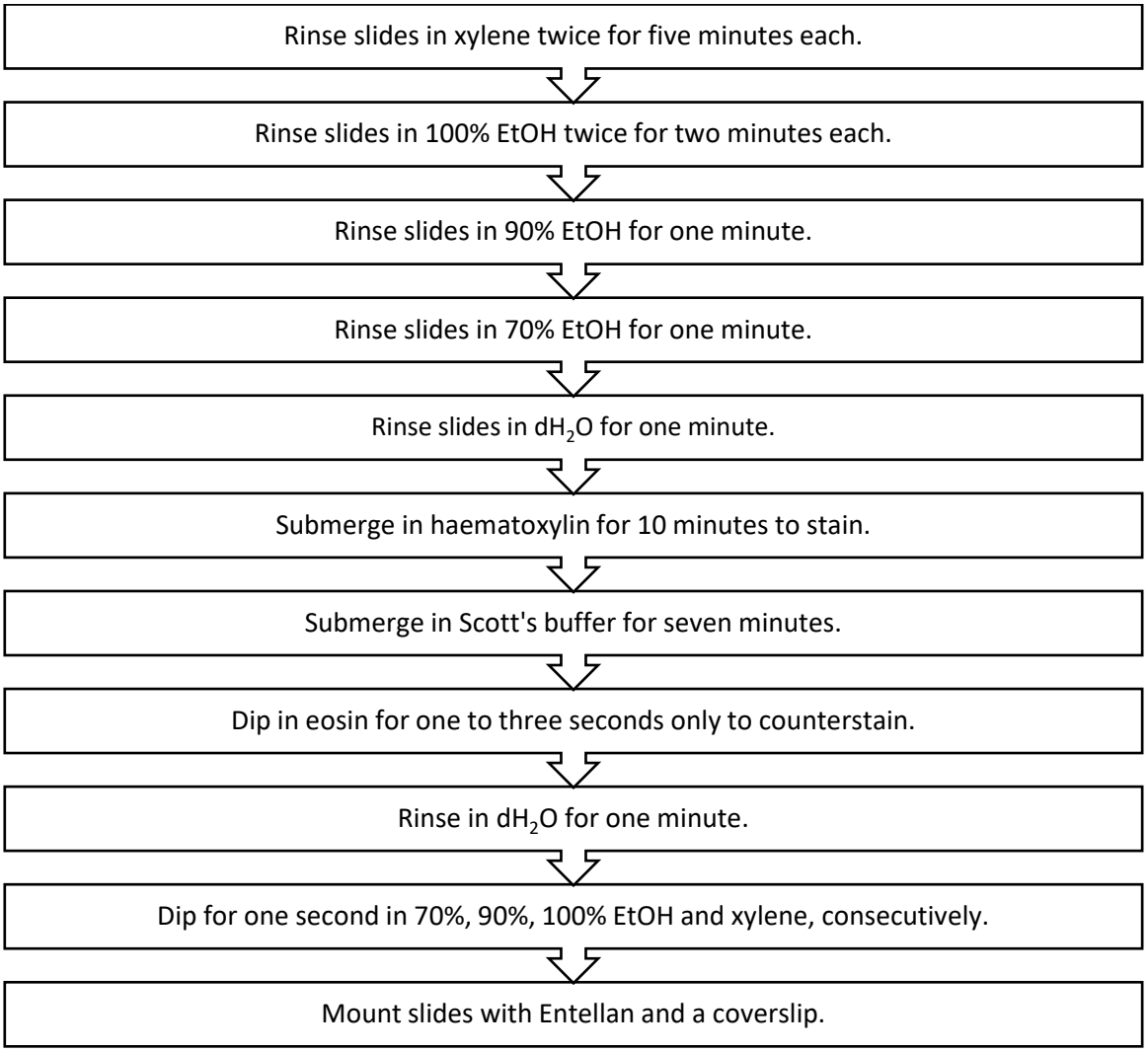

Figure 12 Flow diagram of H&E staining protocol.

The microscope slides underwent, in order, two rinses of xylene (five minutes each), two rinses of 100% EtOH (two minutes each), a one-minute rinse of 90% EtOH, a one-minute rinse of 70% EtOH, and a one-minute rinse in dH_2O. The slides were then stained with haematoxylin for 10 minutes, placed in Scott's buffer for seven minutes, and counterstained with eosin for one to three seconds only. The slides were then rinsed in dH_2O for one minute before being dipped consecutively in 70%, 90%, 100% EtOH and xylene. Each microscope slide was mounted with Entellan and a coverslip. Care was taken to ensure that bubbles were removed from under the coverslip.

Cresyl Violet Staining Protocol

The second set of 34 slides was stained with CV. The CV staining protocol required optimisation due to differing staining protocols available online (IGAKUKEN Neuropathology Database, no date; IHC WORLD, no date; The University of Queensland, no date; Neubacher, 2022). The protocol depicted in the flow diagram (Figure 13) and described below has been optimised to achieve the best staining results.

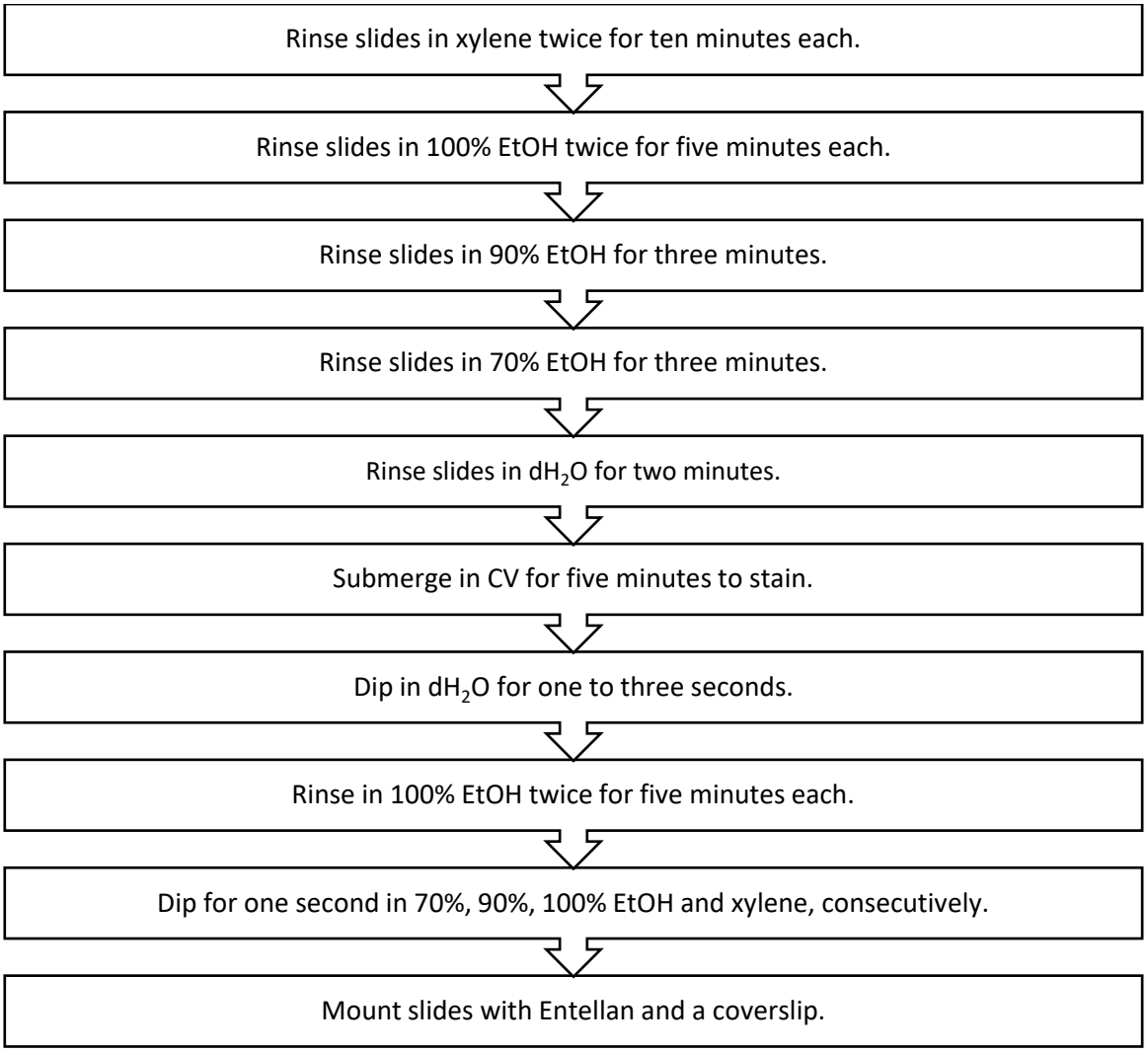

Figure 13 Flow diagram of CV staining protocol.

The microscope slides underwent, in order, two rinses of xylene (10 minutes each), two rinses of 100% EtOH (five minutes each), a three-minute rinse of 90% EtOH, a three-minute rinse of 70% EtOH, and a two-minute rinse in dH_2O. The slides were then stained with CV for five minutes and dipped in dH_2O for one to three seconds before differentiating in 95% EtOH for four minutes and 30 seconds. The slides underwent a further two rinses in 100% EtOH (five minutes each) and two rinses in xylene (five minutes each). Each microscope slide was mounted with Entellan and a coverslip. Care was taken to ensure that bubbles were removed from under the coverslip.

Light Microscopy

The slides were observed with a light microscope with a camera at 5X, 10X and 20X magnification. For H&E-stained slides, the cytoplasm stains pinkish due to the eosinophilic properties while the basophilic nuclei of the cells stain blue/purple. For the CV-stained slides, the cytoplasm stains a very light purple/clear, whereas the Nissl substance and nucleoli of the cells stain a dark blue/purple. Ideally, the H&E and CV stains will look like Figure 14A and 14B below, respectively.

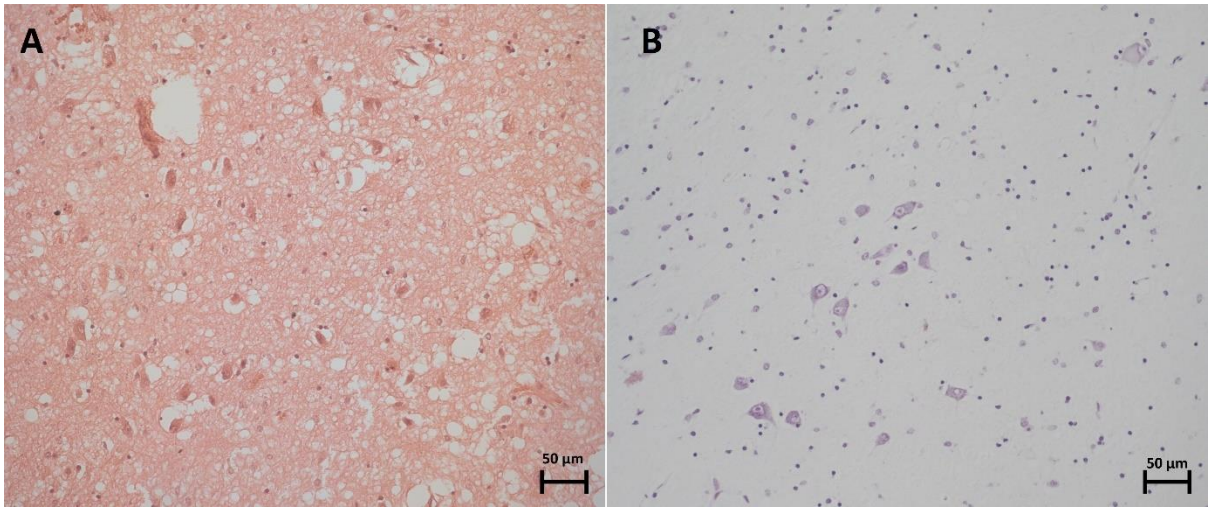

Figure 14 An ideal representation of an H&E stain (A) and a CV stain (B) at 20X magnification.

Data collection for this study had to be adapted due to results contrasting with the original hypothesis. Each sample was observed to identify any structural arrangements of cells, specifically the neurons (observational data). The morphological types of the neurons were observed and noted.

STATISTICAL ANALYSES

Statistical tests were performed on the cadaveric data only, as the quantitative component of this study. These tests and results were generated by making use of three different software programs:

- MS Excel spreadsheets,
- SPSS v21
- PAST v3, a free statistical programme.

Descriptive data was collected in the form of the frequency of prevalence and absence of the IA in the sample and within groups of the sample (male and female), and the frequency of classifications within groups of the sample (shape and location of the IA). Central tendencies were also recorded in the form of means and modes, and data dispersion in the form of ranges and standard deviations. These values were used in correlation testing for any statistically significant results.

Numerical data was first tested for normal distribution. Correlations where data was normally distributed used Pearson's correlation coefficient. Alternatively, for data that did not follow normal distribution, and if there was a monotonic relationship between the datasets, Spearman's correlation coefficient was used. However, if there was not a monotonic relationship between the datasets the data was analysed using Kendall's tau-b.

Results were generated with independent t-tests for categorical data against continuous numerical data, one-way ANOVA tests for categorical data with multiple levels against one group of continuous numerical data, Chi-square tests for categorical data against categorical data, and binary logistic regression for binary data against continuous numerical data. Results

were considered statistically significant if the p-value was less than 0.05 for a 95% confidence interval.

To test for reliability and repeatability of the study's methods, intraclass correlation (ICC) was performed with both an inter-observer and intra-observer. To remove bias and ensure integrity of results, the inter- and intra-class data was recorded a while after the initial data was recorded.

The ICC was based on a two-way mixed effect, absolute agreement, single rater model for continuous numerical data. An ICC value is considered poor as a score of reliability if it is less than 0.5, moderate if it is between 0.5 and 0.75, good if it is between 0.75 and 0.9, and excellent if it is greater than 0.9 (Koo and Li, 2016). In this study, the ICC was considered acceptable if the result was greater than or equal to 0.5. Categorical data is typically evaluated using Cohen's kappa, however for data with more than two categories, as is the case with the shape and location variables used in this study, a method to quantify the ICC does not exist (Chakraborty *et al.*, 2021).

DATA MANAGEMENT

All research sample data was captured electronically in an MS Excel spreadsheet on the primary investigator's computer, as seen in Annexure B for the cadaveric and microscopic components of the study. These datasheets, together with all the specimen photographs were shared with the supervisors, backed up to an external hard drive and UP Google Drive account (which is also shared with the supervisors). All study data compiled, including the results, were uploaded to the University of Pretoria's data management system, and will be kept for a minimum of 15 years from the end of this study until 2037, as required, and will be password protected.

Physical data, which consists of the blocks and slides in the latter half of the study, are stored for a minimum of 15 years from the start of the study until 2035 in identifiable slide boxes on shelves or within designated cabinets in the Histology Lab, room 6-31 of BMS, and the storeroom, room 6-27 of BMS, on Prinshof Campus, University of Pretoria.

The samples can be destroyed once the required minimum of 15 years for storage has passed and if space is required for new samples. The samples will be regarded as hazardous waste and removed and destroyed as such by a waste management company contracted by the University of Pretoria.

RESULTS

MORPHOLOGICAL FINDINGS

A total number of 83 brain specimens were collected, after exclusion due to significant damage to the region of interest, to determine the prevalence of an IA within the sample. The age of the sample ranged from 27 to 102 years, with an average age of 71.55 years and standard deviation of 16.23 years. Specimens were included in the sample regardless of their ancestry, height, and weight.

The IA was present in 57 specimens, accounting for 68.67% of the total sample, and absent in the remaining 26 specimens. Of those with an IA, 29 were male (63.04% of the male sample subgroup) and 28 were female (75.68% of the female sample subgroup).

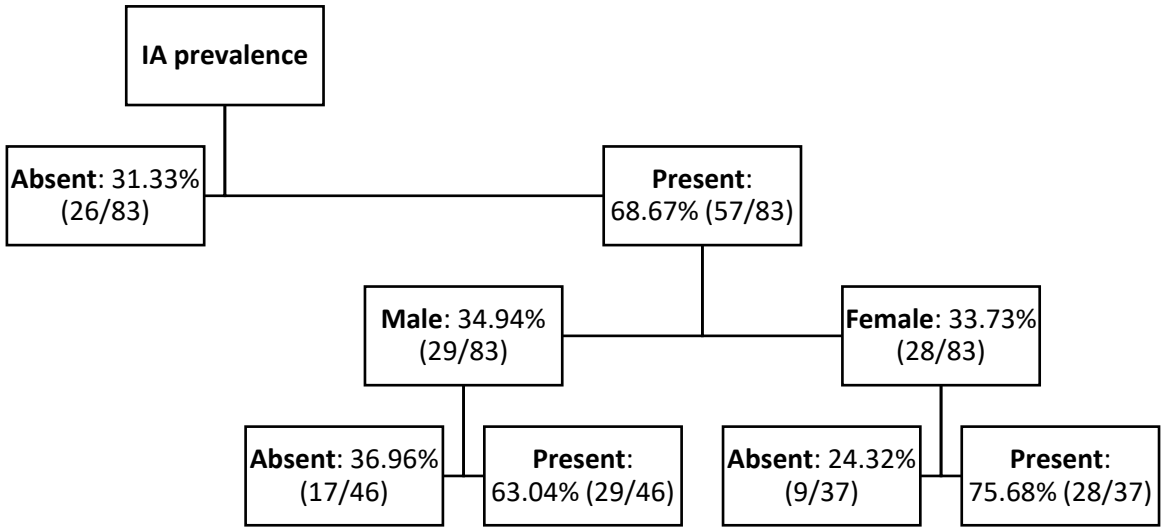

Figure 15 Illustration of IA prevalence in sample and sex subgroups.

Chi-square testing for association between sex and prevalence of an IA, as well as binary logistic regression between age and prevalence of an IA, showed no statistically significant

relationships between these variables. Therefore, no post-hoc testing was necessary as no specific association would be evident.

There was one instance of a double IA in a 72-year-old male specimen, accounting for 1.2% of the sample, as seen in Figure 16 below. Both IAs were a similar oval shape, but of differing size and location within the third ventricle.

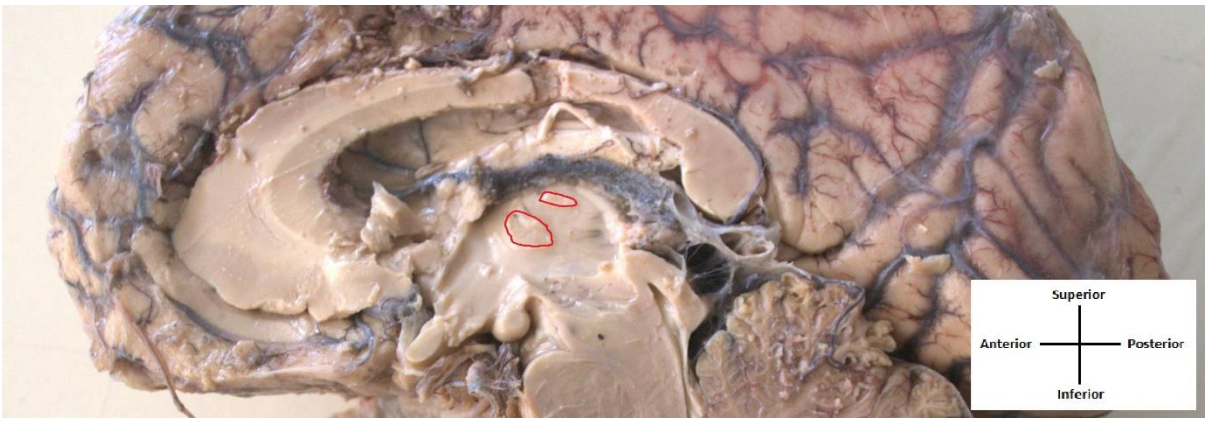

Figure 16 Double IA (outlined in red) in 72-year-old male brain specimen.

The remainder of the results focused only on the sample group where the IA was prevalent. The double IA was considered as two separate instances in the dataset, as both IAs contribute to the analysis of the anatomical morphology of the IA in this sample. Therefore, a total of 58 IAs were analysed in a sample group of 57 specimens with an IA.

The most common shape of the IA was oval (see Table 7), recorded in 28 specimens (48.3% of the sample group). This modality was followed by 11 semi-lunar/bean-shaped IAs (19%), nine triangular IAs (15.5%), five circular IAs (8.6%), and five irregularly shaped IAs (8.6%). No statistically significant difference between sex and shape of the IA was found, nor between

age and shape. A visual representation of these shapes can be seen in Figure 8 previously mentioned in the methodology. If the IA was found to overlap in multiple quadrants, the location was determined based on the quadrant in which most of the IA mass was predominantly located.

Table 6 Frequency of shape type in males and females

		Shape of the IA					Total
		Oval	**Circular**	**Triangular**	**Semi-lunar / bean-shaped**	**Irregular**	
Sex	**Female**	11	3	5	5	4	**28**
	Male	17	2	4	6	1	**30**
Total		**28**	**5**	**9**	**11**	**5**	**58**

The most common location of the IA within the third ventricle was the anterior-superior quadrant (see Table 8), as recorded in 51 instances (87.9% of the sample group) (see Figure 17). This was followed by six instances in the posterior-superior quadrant (10.3%), an example is shown in Figure 18 below. There was one instance in the anterior-inferior quadrant (1.7%) (see Figure 19), and no instances in the posterior-inferior quadrant or at the centre of the four quadrants. No statistically significant difference between sex and location of the IA within the third ventricle was found, nor between age and location.

Table 7 Frequency of location type in males and females

		Location within third ventricle					Total
		Quadrant 1	**Quadrant 2**	**Quadrant 3**	**Quadrant 4**	**Centre**	
Sex	**Female**	26	2	0	0	0	**28**
	Male	25	4	1	0	0	**30**
Total		**51**	**6**	**1**	**0**	**0**	**58**

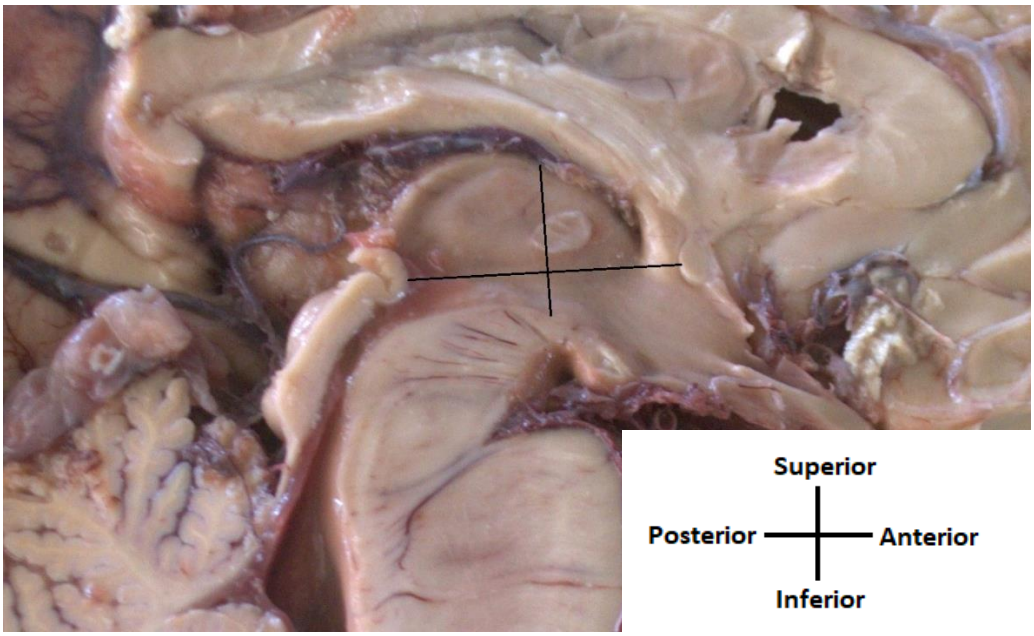

Figure 17 Sample where IA is located in anterior-superior quadrant.

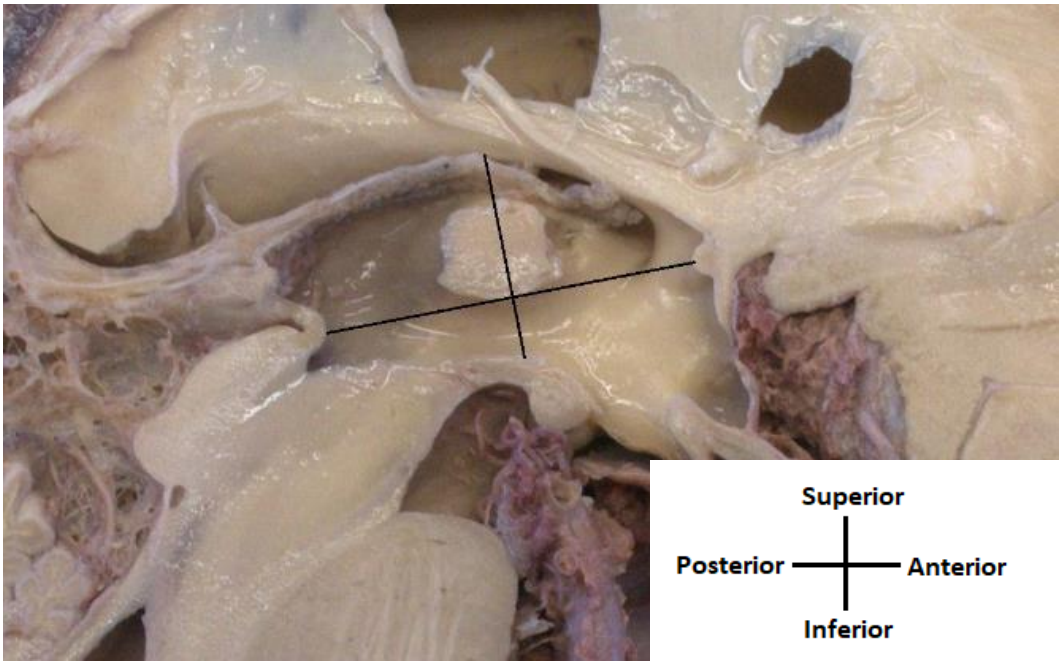

Figure 18 Sample where IA is located in the posterior-superior quadrant.

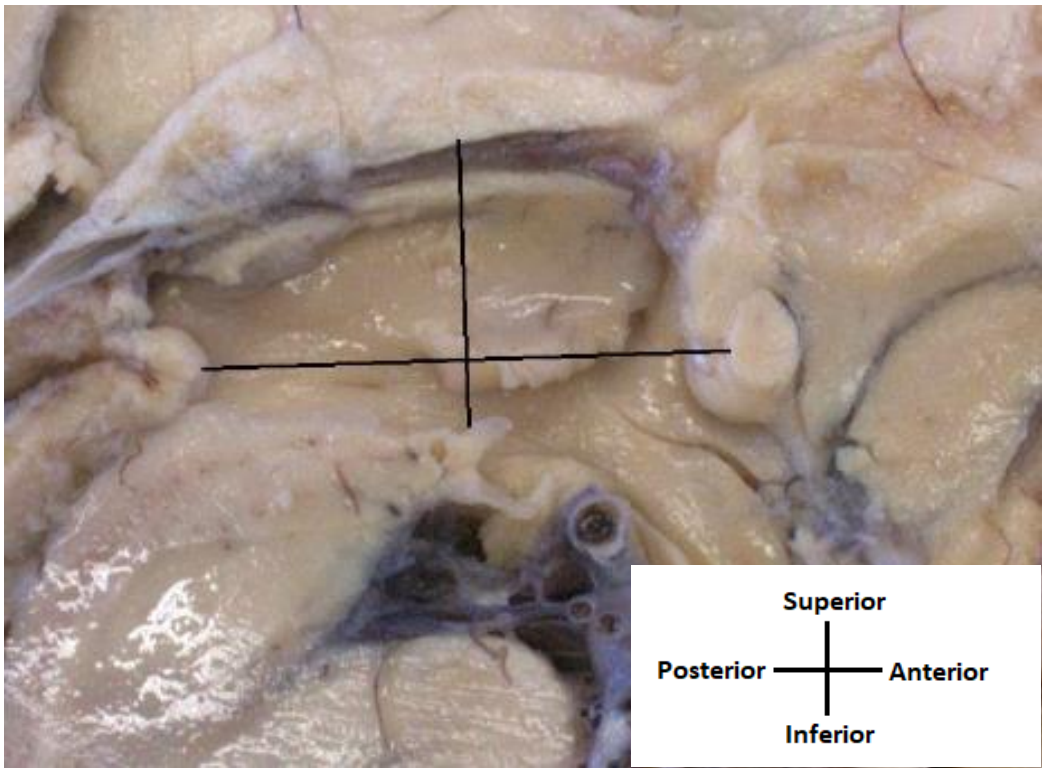

Figure 19 Sample where IA is located in the anterior-inferior quadrant.

As shown in Table 9, the average sizes for the APL, SIL, SAIA and SAV in a South African sample were 6.31 mm, 4.23 mm, 25.68 mm^2, and 548.90 mm^2, respectively. A visual representation of these measurements and the average values reported in the sample can be seen in Figure 20.

Table 8 Descriptive statistics of measurements

Measurement	Minimum	Maximum	Mean	Std. Deviation
APL (mm)	1.03	12.63	6.31	2.39
SIL (mm)	0.89	11.72	4.23	2.236
SAIA (mm^2)	1.21	113.23	25.68	21.65
SAV (mm^2)	292.45	782.26	548.90	114.89

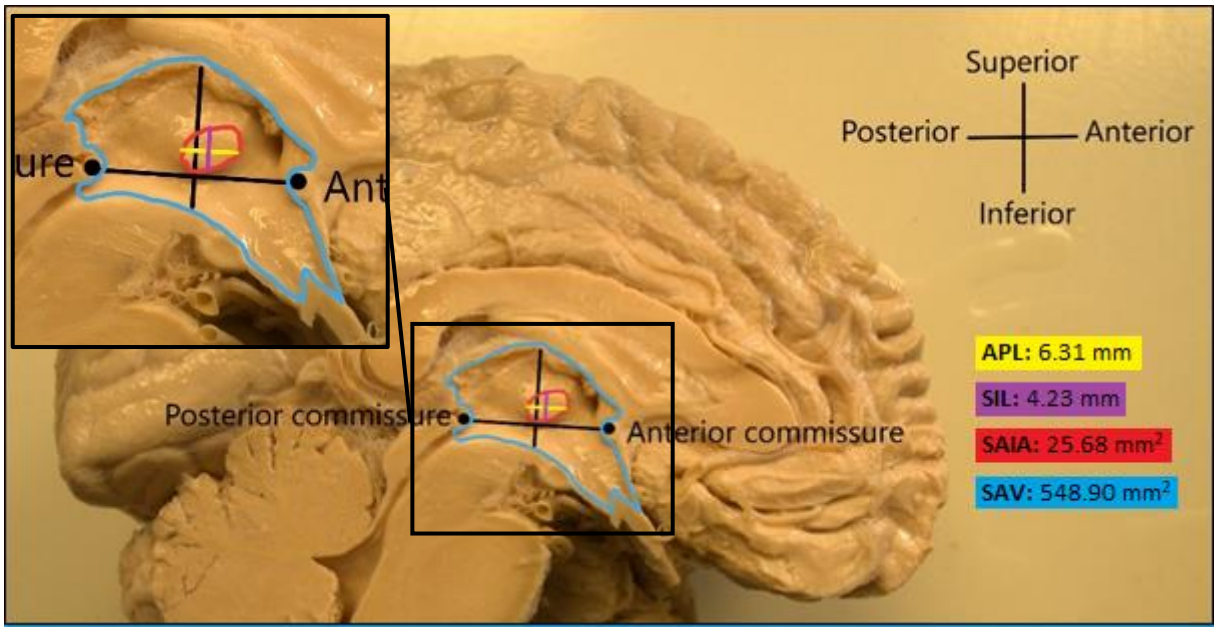

Figure 20 Representation of average measurements within the sample (van Heerden, 2019).

The dataset for measurements was tested for normal distribution using the Shapiro Wilk's test and showed that the APL and SAV measurements followed normal distribution, whereas the SIL and SAIA measurements did not, as seen in Figure 21 below.

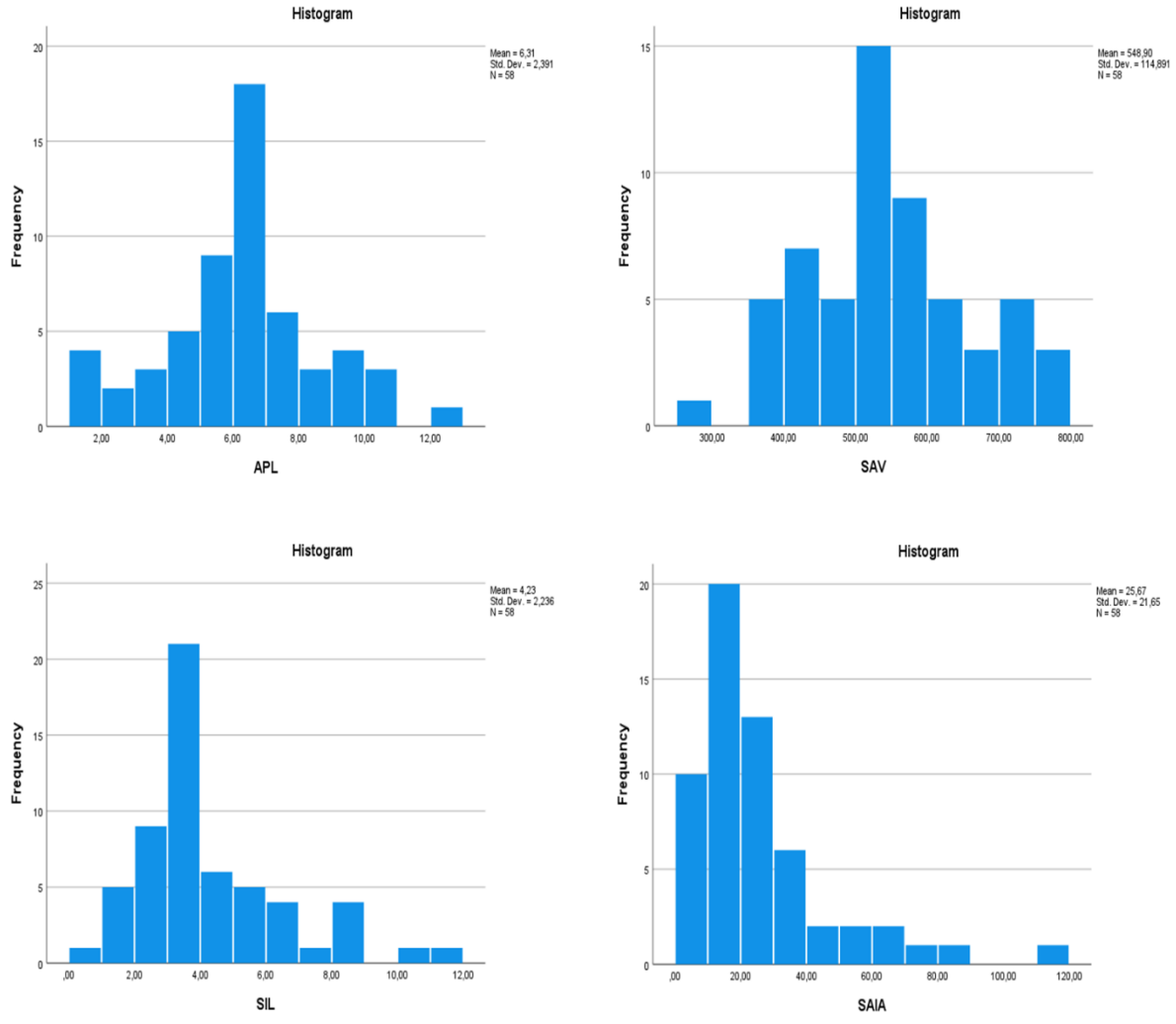

Figure 21 Histograms illustrating the distribution of data for the APL, SIL, SAIA and SAV measurements.

The scatterplots of the non-normal data plotted against the data for all other measurements was used to determine if the relationships were monotonic and can be seen in Figure 22 below.

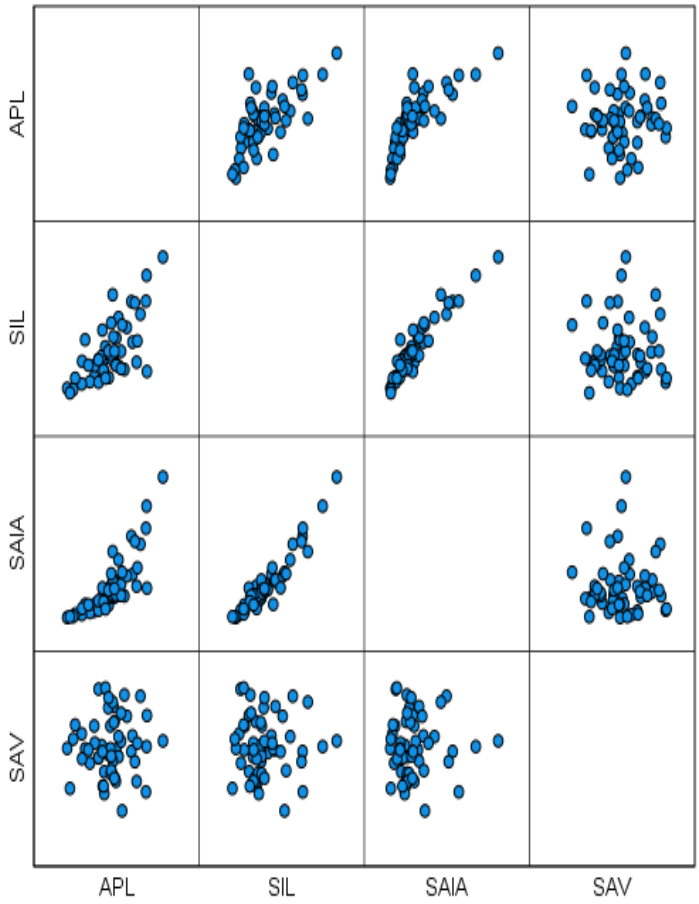

Figure 22 Scatterplots of the APL, SIL, SAIA and SAV measurements in relation to each other.

This outcome proved true and therefore, all assumptions for using the Spearman's correlation were met. The relationship between normally distributed data was analysed with Pearson's correlation coefficient, and the relationship between non-normally distributed data was analysed with Spearman's correlation coefficient.

Highly statistically significant correlations were found between the APL and the SIL (good, positive correlation of 0.586, p-value < 0.001), the APL and the SAIA (strong, positive

correlation of 0.851, p-value < 0.001), and the SIL and the SAIA (strong, positive correlation of 0.878, p-value < 0.001). These correlations are expected as they are in direct relation to each other.

The SAV measurement showed extremely weak correlations with all the other measurements, namely with the APL (correlation coefficient of 0.061, p-value = 0.648), SIL (correlation coefficient of -0.006, p-value = 0.965) and SAIA (correlation coefficient of 0.023, p-value = 0.867), with no statistically significant relationships.

No statistically significant relationships between the sex and any of the four measurements were found. Furthermore, there was no statistically significant relationship between age and any of the four measurements either.

HISTOLOGICAL FINDINGS

The expected histological observations were based on the findings from the 2005 study by Puskas and co-workers. In their study, the authors observed a circular organisation of neurons in the IA and PVR however, these results could not be replicated in our study. Therefore, the objectives in our study were adapted to record all significant observations that were possible, especially between the region of the IA and the PVR.

Due to the long-term fixation of the cadaveric material used to source the histological sample, a notable degree of damage to the sample tissue was observed. This did not alter the overall observation of the cells and their various morphological types for our purposes. A degree of vacuolation could be observed within our sample specimens, mostly adjacent to vessels or neurons but not within the neurons.

No specific structural arrangements of the neurons in either the IA or PVR were identifiable. Indeed, the cytoarchitecture appeared to be random except for a distinguishable range in the frequency and dispersion of certain cells upon simple observation.

The H&E staining resulted in a pink colouring of the cytoplasm of the cells, with darkly stained blue/purple nuclei. The most distinguishable components that were observed included arteries, veins, red blood cells, microglial cells, and pyramidal cells. The CV staining resulted in almost clear/transparent representation of the extracellular matrix (ECM) and darkly blue/purple-stained rough endoplasmic reticulum (RER), thus greatly improving the visualisation of the Nissl substance, the nuclear membrane, and the nucleoli of the cells.

Staining of the ECM is vastly different between the two stains and H&E was more effective in visualising any notable patterns in cellular arrangement within the ECM. As seen in Figure 23 below, the sample appeared to be more striated towards the left edge, as opposed to the smoother appearance towards the middle of the sample area.

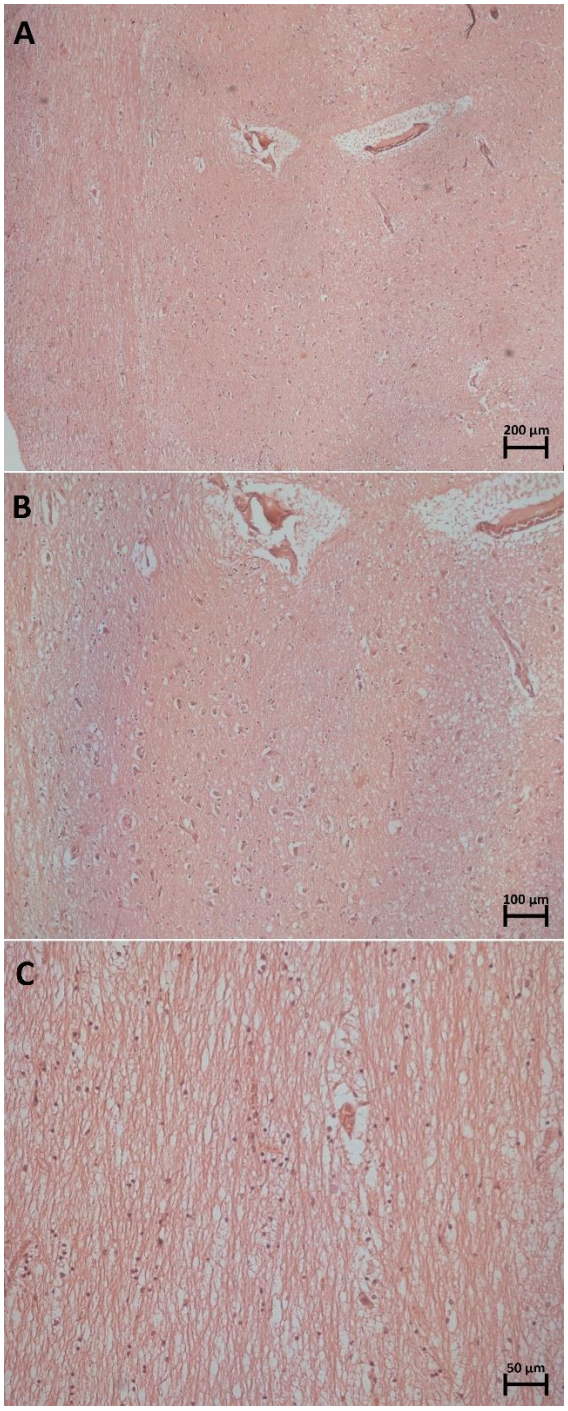

Figure 23 An H&E-stained sample at 5X (A), 10X (B), and 20X (C) magnifications.

Another sample showed intermittent striations in the ECM, as seen in Figure 24 below. This observation is not attributed to chatter, as is sometimes seen in slide sections due to damage from the microtome while being sliced.

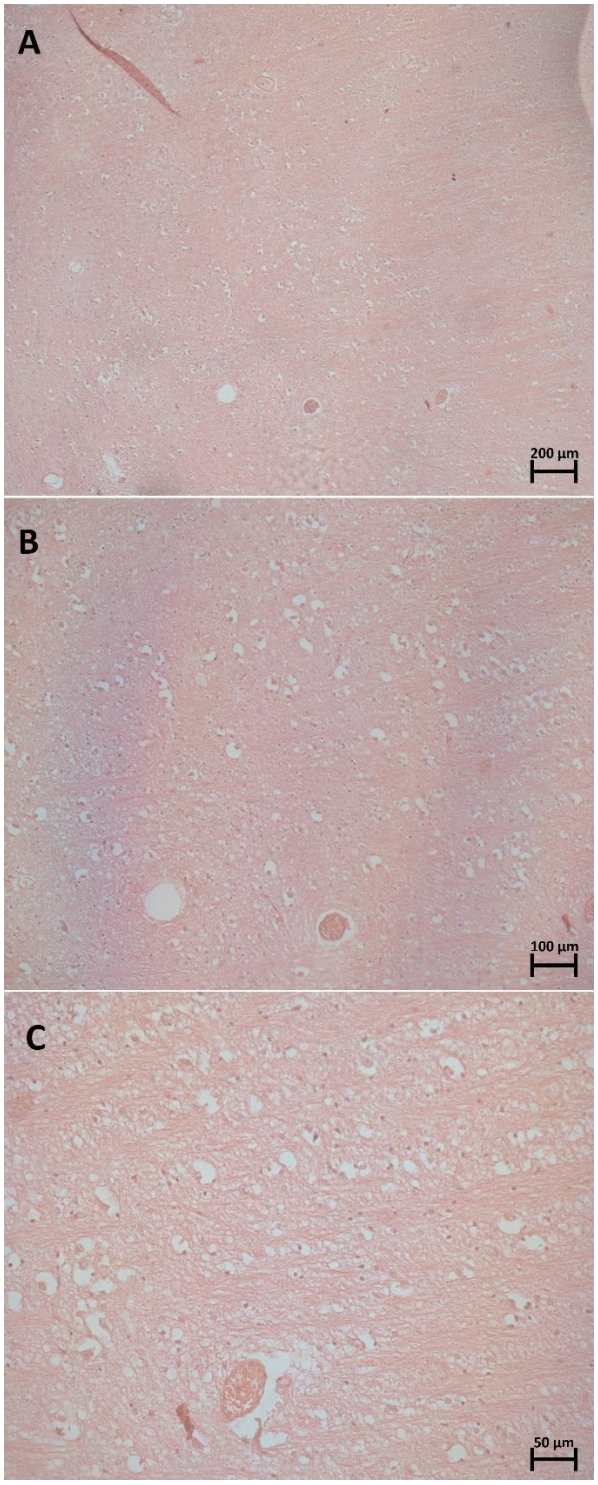

Figure 24 An H&E-stained sample at 5X (A), 10X (B), and 20X (C) magnifications.

Microglia were clearly the most abundant cell type. However, neurons were widespread throughout the specimens, but this could only be clearly observed with CV staining. With careful observation it is possible to slightly demarcate a few neuronal structures with the H&E staining (dark purple stains), but given the effort and high likelihood of failure, it is much better to rely on the CV staining for a more accurate observation of neuronal structures, as seen in Figure 25. The neurons are indicated by the darker blue/purple stains. The white spaces in the H&E stains are evidence of tissue vacuolation/damage. In order to identify myelin another stain would have needed to be used, such as luxol fast blue.

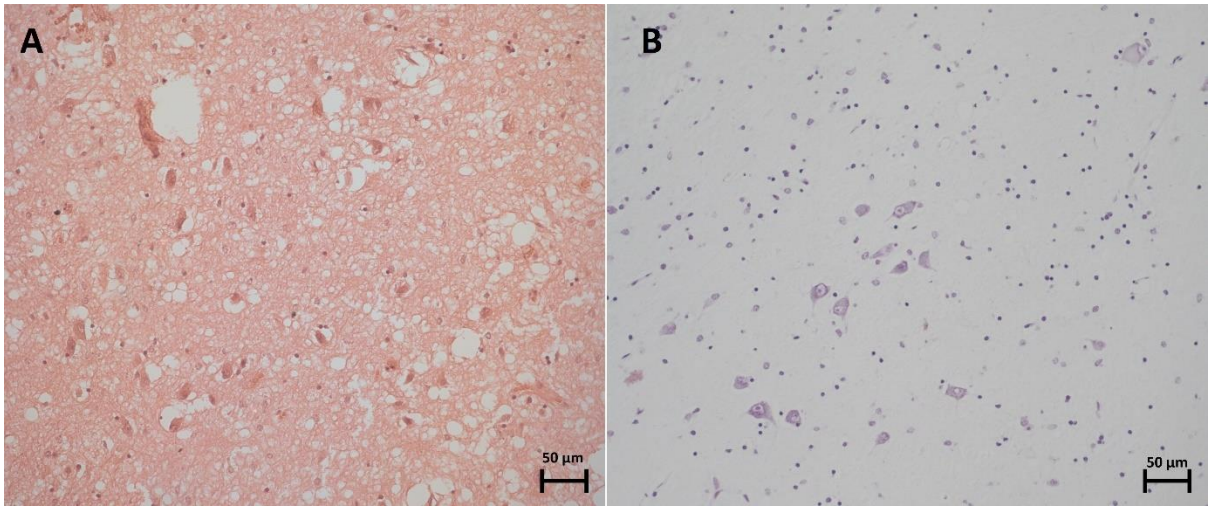

Figure 25 An H&E stain (A) versus a CV stain (B) of the same sample at 20X magnification.

There does not appear to be any pattern or structural organisation in the appearance of neurons within the regions of interest. There are, however, zones of higher frequency of neurons dispersed at random, as seen in Figures 26 and 27. Neurons, when viewed using light microscopy, are typically characterised by their large cell bodies, Nissl substance (darkly

stained with CV), and a clear nucleolus within its nucleus (Garman, 2011). In our sample, there appeared to be a monomorphic population of neurons.

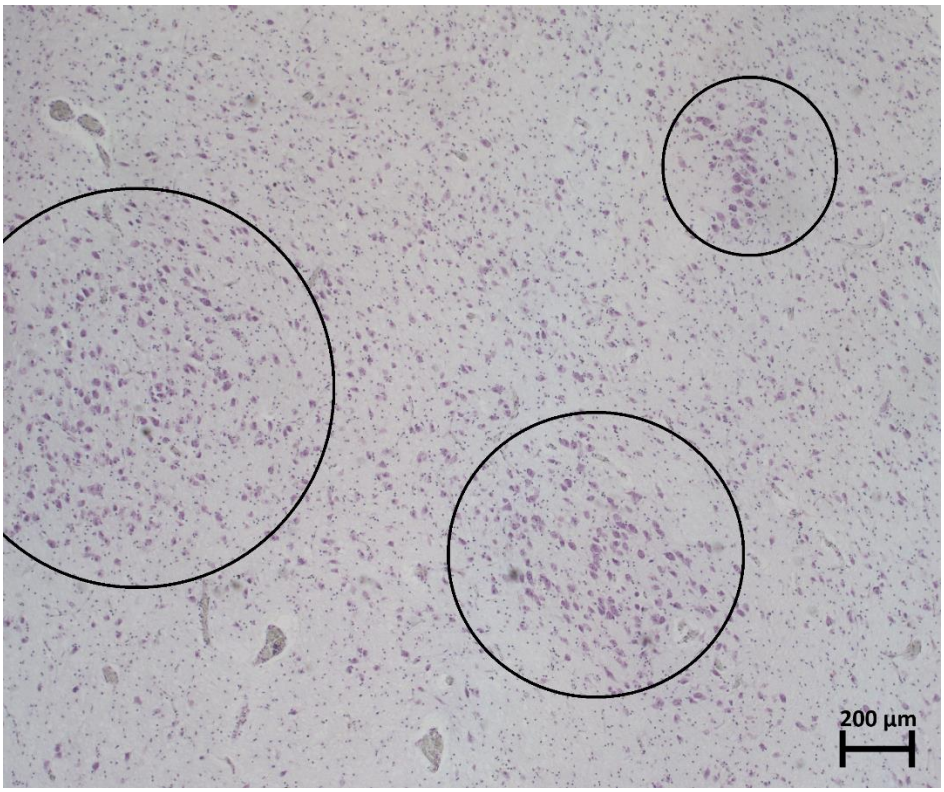

Figure 26 A CV-stained sample of the PVR at 10X magnification. The areas within the black circles show denser zones of neurons randomly dispersed through the tissue of the PVR.

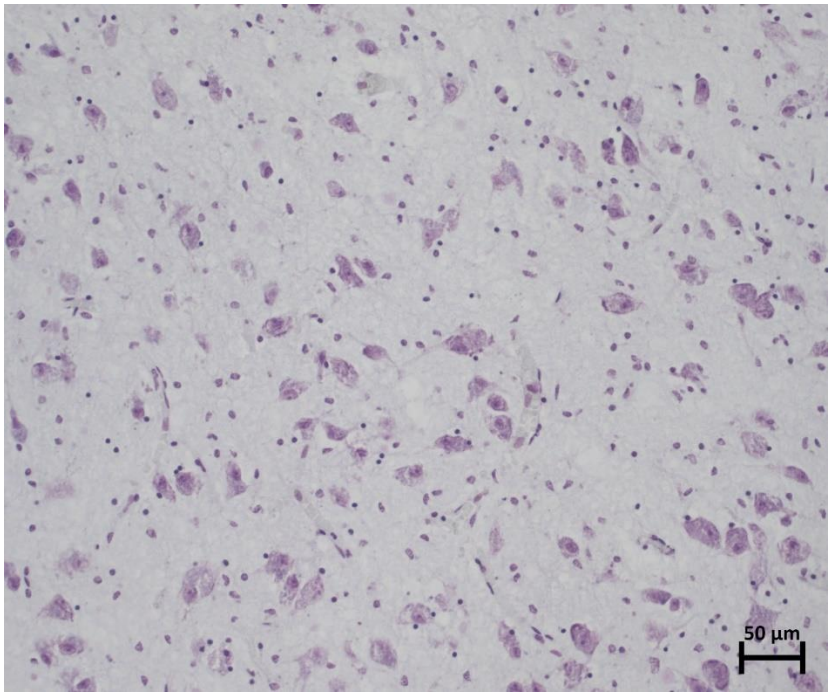

Figure 27 A CV-stained sample of the PVR at 20X magnification in a neuron-dense zone.

The images below show the appearance of blood vessels found within the region of interest. The veins (see Figure 28) are identified by their collapsed appearance due to a very thin or non-existent smooth muscle wall (tunica media). An artery (see Figure 29) can be distinguished by a thicker wall of smooth muscle. Because we know that these specimens were cut on a sagittal plane, we can deduce that these blood vessels are running horizontally and laterally through the thalamus. Arteries and veins are often found running alongside each other.

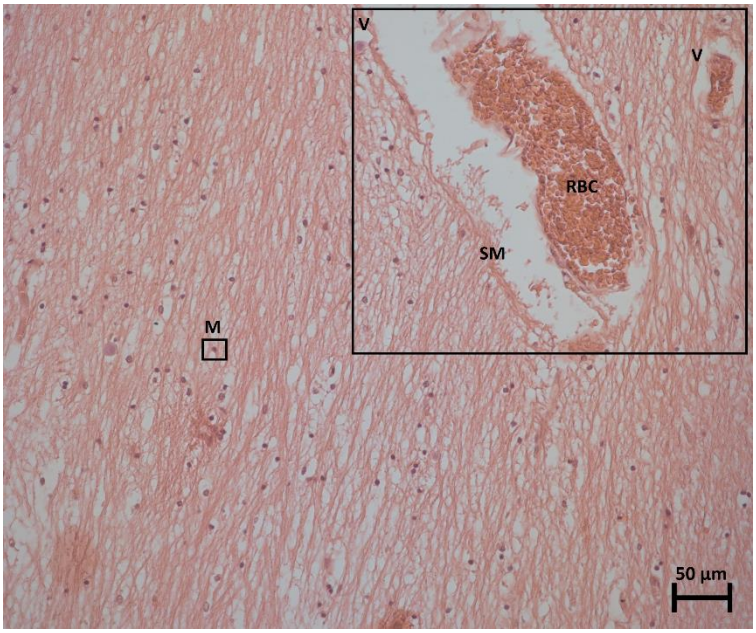

Figure 28 An H&E-stained sample of the PVR at 20X magnification depicting a larger and smaller vein (V) running alongside each other, where the thin smooth muscle (SM) wall can be seen surrounding the red blood cells (RBC), and dark, purple-stained microglial cells (M).

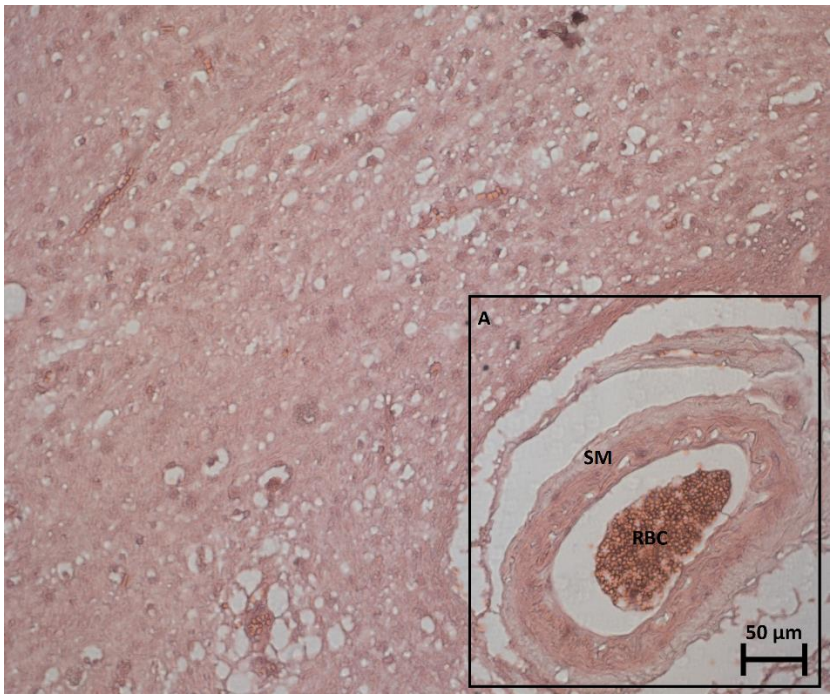

Figure 29 An H&E-stained sample of the PVR at 20X magnification depicting an artery (A), where the thick smooth muscle (SM) wall can be seen surrounding the red blood cells (RBC).

In some images of the histological samples, the appearance of a dense cellular layer of microglial cells on the edge of the tissue was noted. This was seen very clearly with the CV stain. In each instance there appears to be an outer dense layer at the edge and an inner neuronal layer, with a sparse tissue layer of microglial cells between them. These layers can be seen in Figures 30 and 31 below, of the same sample with H&E staining and CV staining, respectively.

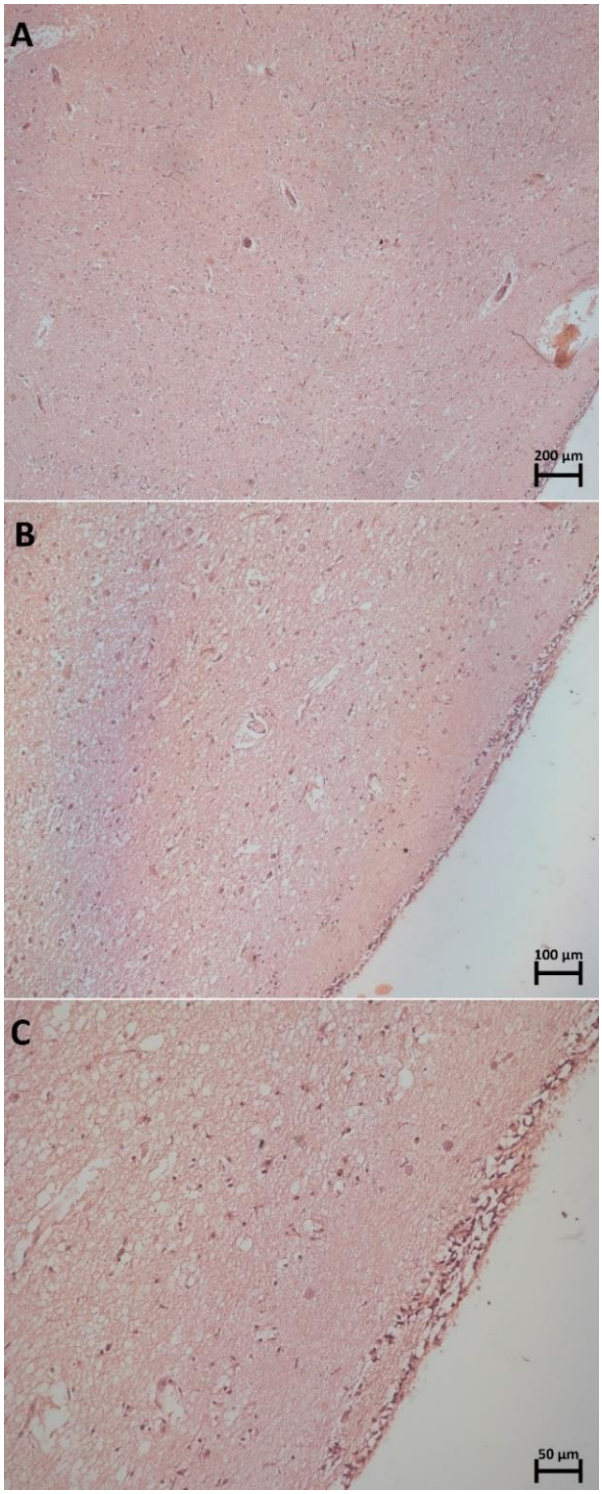

Figure 30 An H&E-stained sample of the PVR at 5X (A), 10X (B), and 20X (C) magnifications.

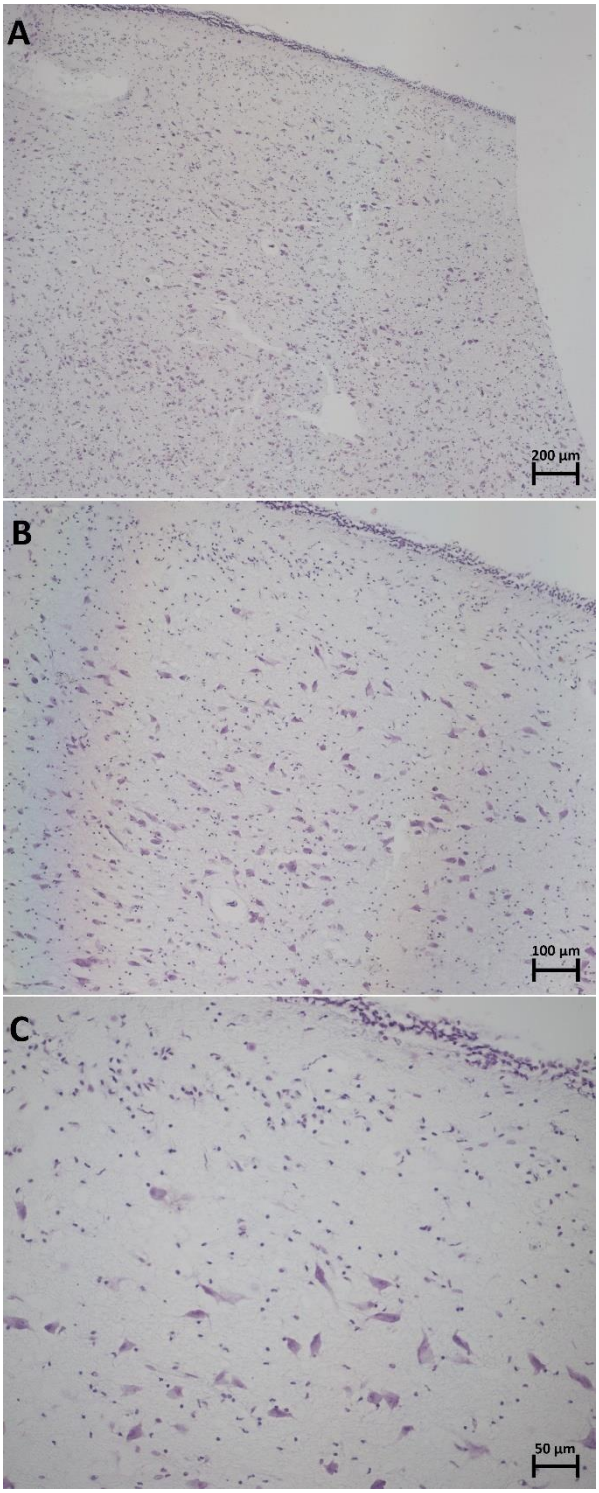

Figure 31 A CV-stained sample of the PVR at 5X (A), 10X (B), and 20X (C) magnifications.

Another sample showed a similar lining of densely packed cells, however a section of this lining suddenly appears convoluted, as seen in Figure 32 below.

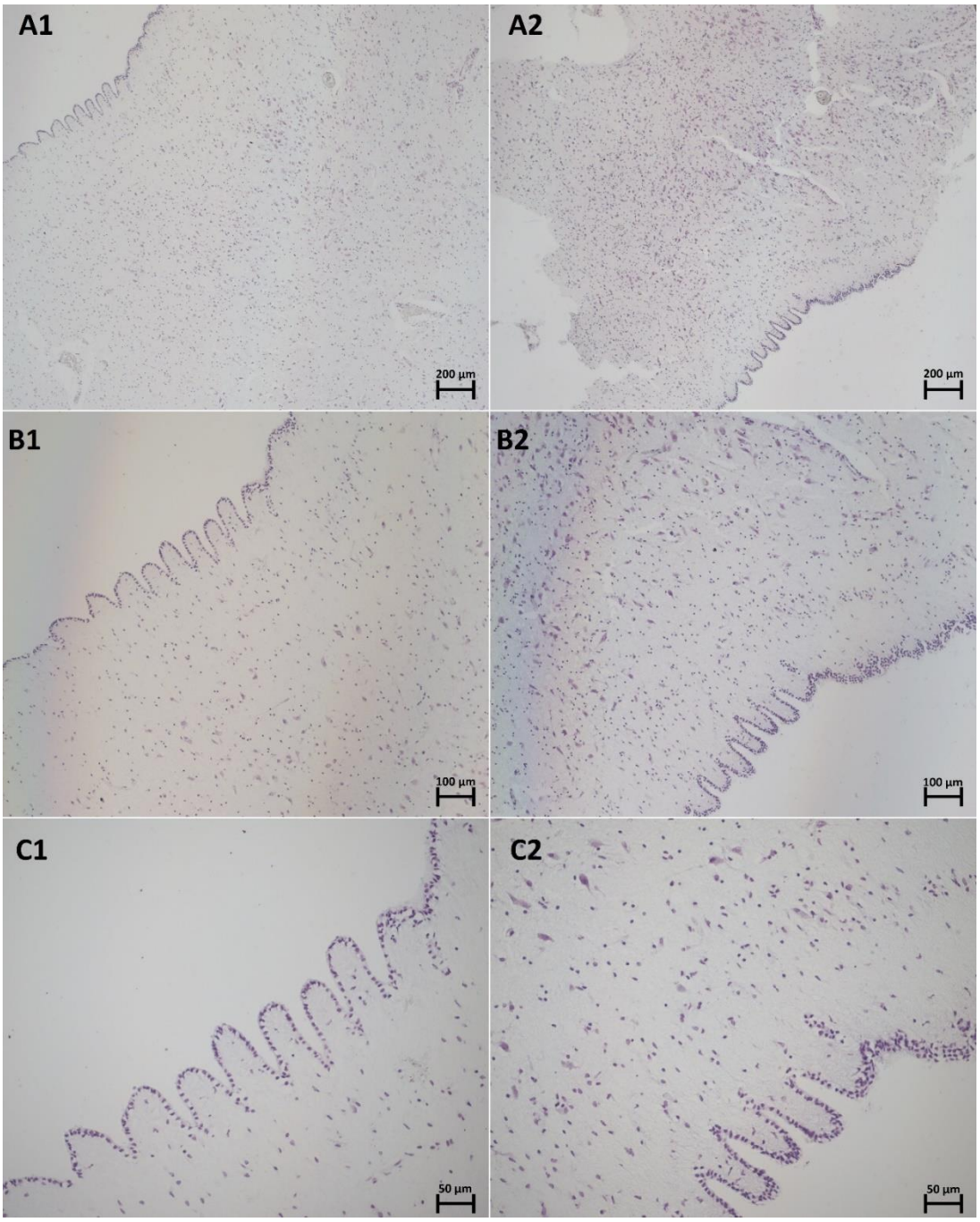

Figure 32 A CV-stained sample of the PVR at 5X (A), 10X (B), and 20X (C) magnifications. In the same sample, A1-C1 appears to have a single layered lining, whereas area A2-C2 appears to have 2-3 layers in the convoluted lining.

The images of the samples were used to compare the IA and PVR regions within the same specimen with an IA and to compare the PVR between specimens with and without an IA. Images of horizontal sections were compared to the sagittal sections to note any difference to cytoarchitecture depending on the orientation of the tissue.

In all instances, no apparent significant differences could be reported, as shown in the images for comparison below (see Figures 33 to 40).

In Figure 33, a comparison of the IA and PVR in the same sample with H&E staining reveals significantly more damage in the PVR than the IA region. The IA region seems to show a higher density of glial cells.

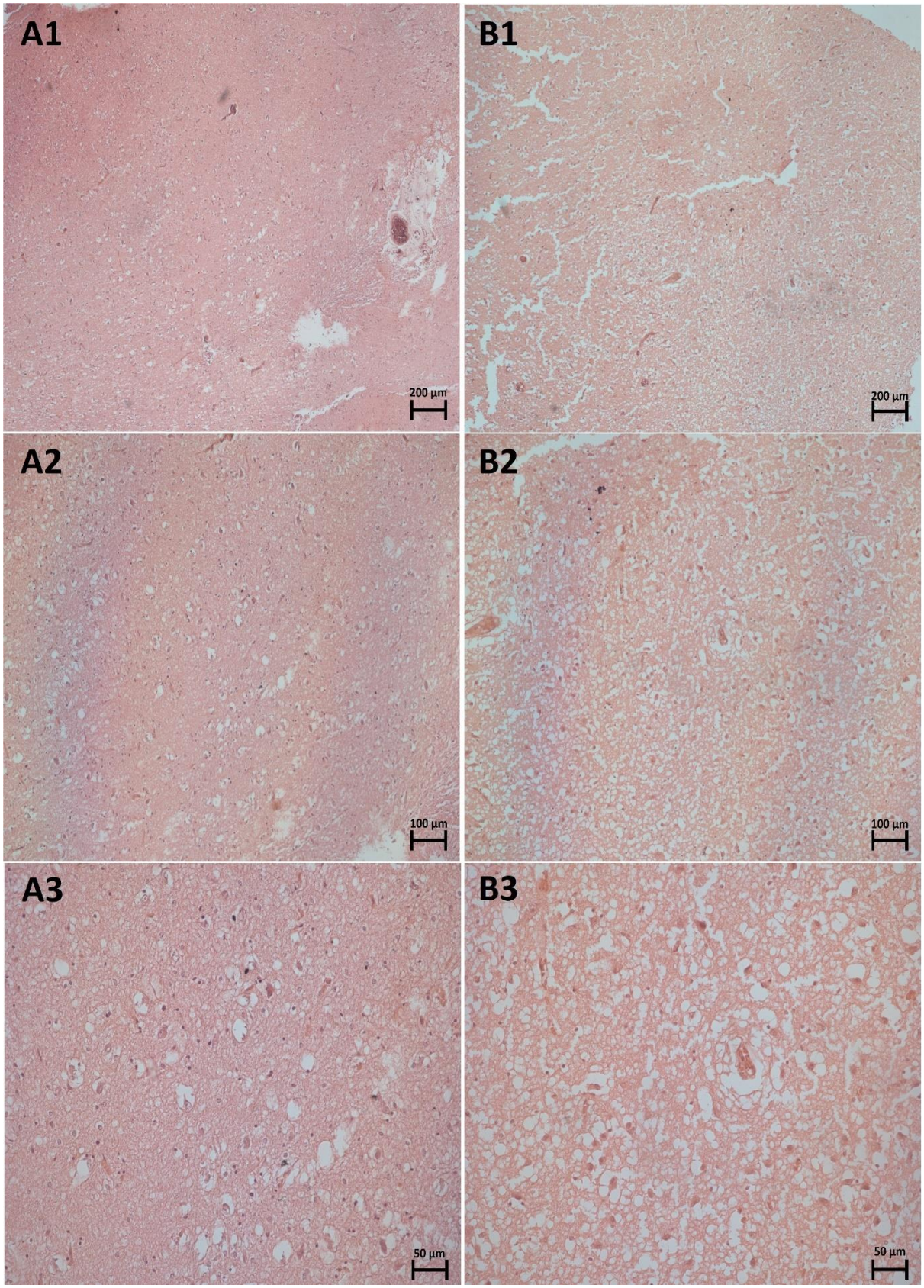

Figure 33 An H&E-stained sample of the IA (A) and PVR (B) at 5X (1), 10X (2), and 20X (3) magnifications.

In Figure 34, a comparison of the IA and PVR in the same sample with CV staining also seems to show a higher density of glial cells in the IA region. The neuronal cells appear to have a similar orientation, but no sophisticated structural organisation.

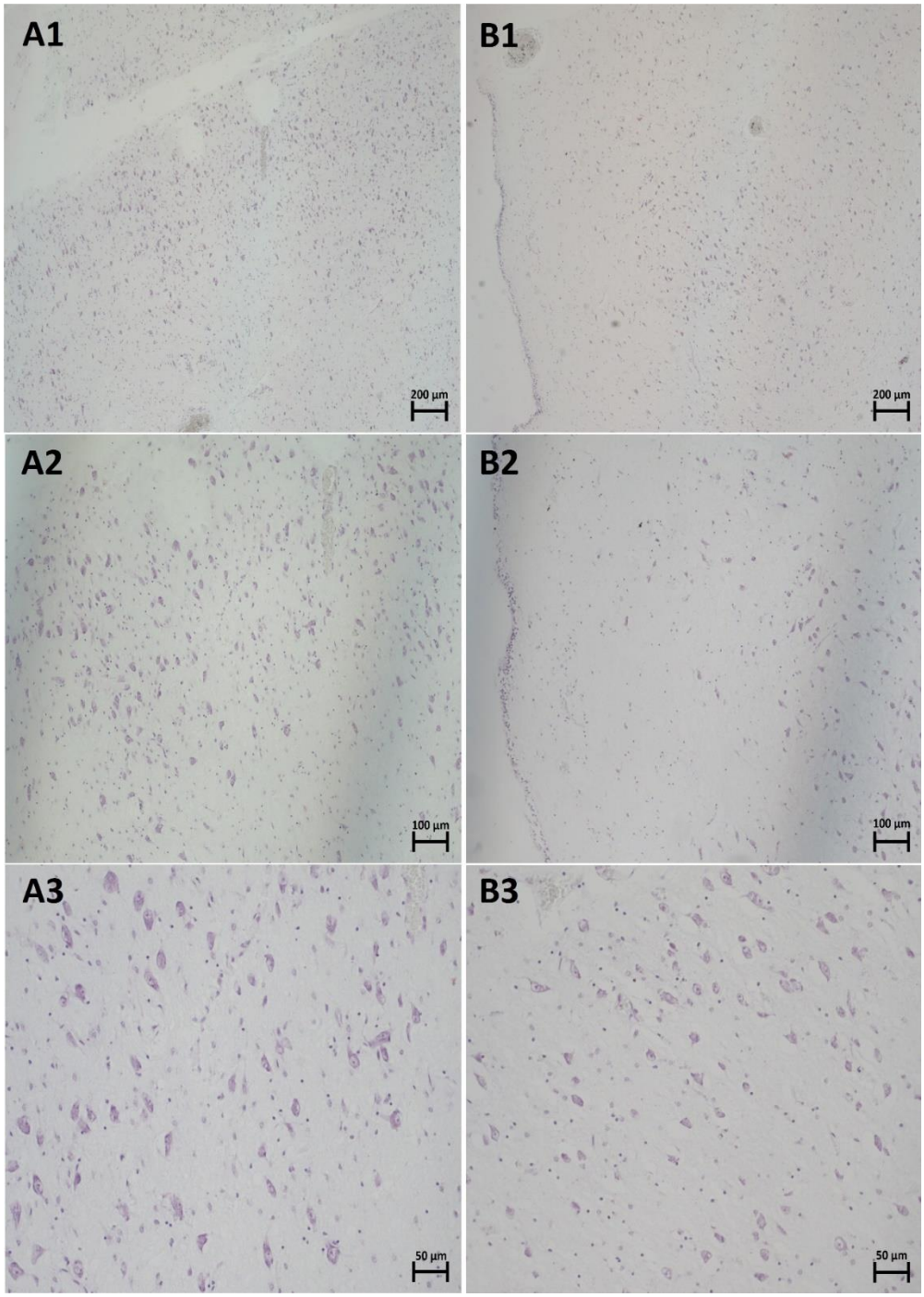

Figure 34 A CV-stained sample of the IA (A) and PVR (B) at 5X (1), 10X (2), and 20X (3) magnifications.

As shown in Figure 35 below, comparing the PVR in H&E stained specimens with and without an IA, there is a common presence of blood vessels within this region. Although differences between these specimens with and without an IA do not appear significant, there is a notable difference between the two specimens without an IA. In Figure 35B there is a much lower density of glial cells, and a portion of tissue in one specimen, Figure 35C, has a striated appearance.

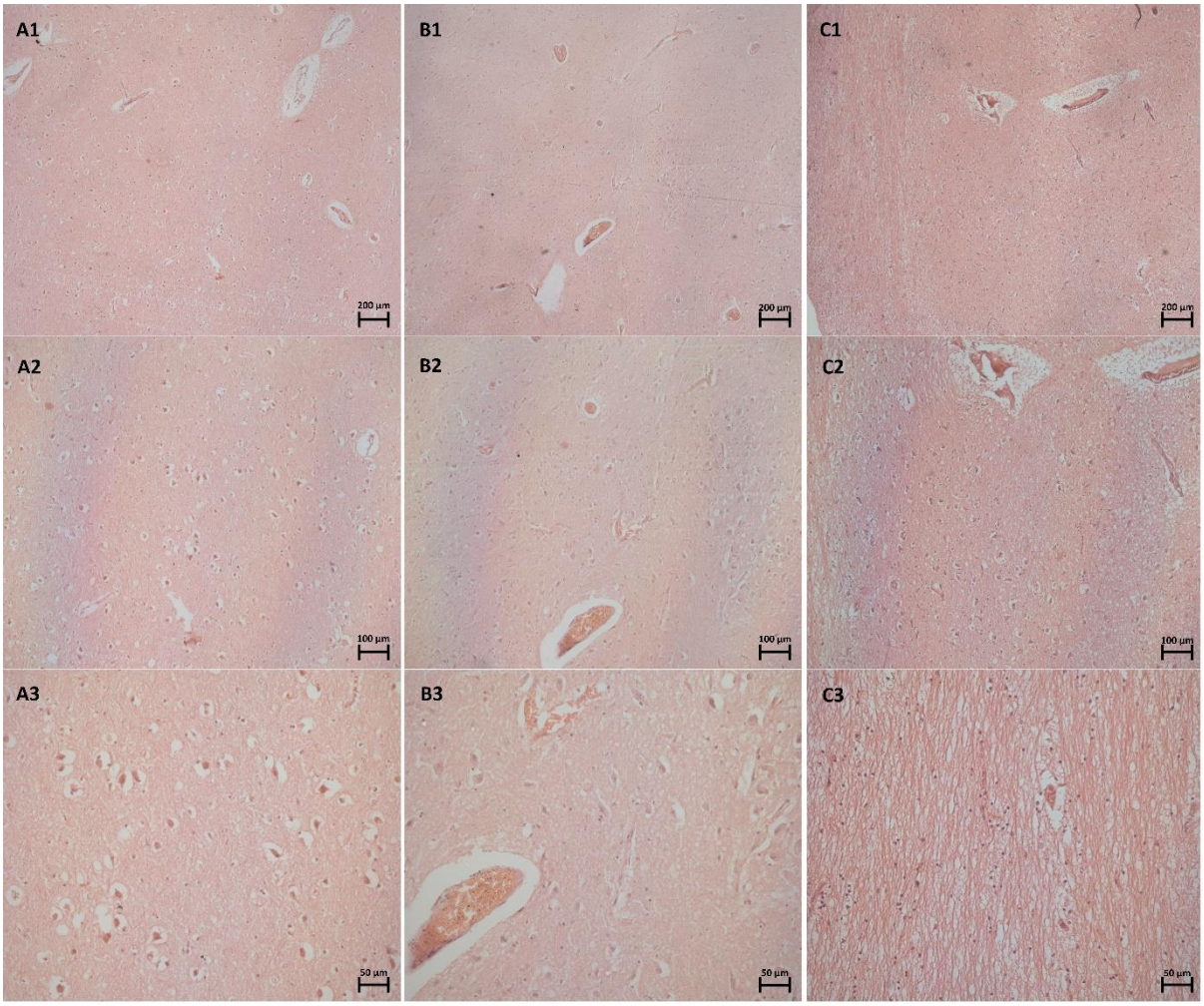

Figure 35 An H&E-stained sample of the PVR in a specimen with an IA (A) and PVR in specimens without an IA (B and C) at 5X (1), 10X (2), and 20X (3) magnifications.

As can be more clearly shown in Figure 36 below, comparing the PVR in CV stained specimens with and without an IA, there appears to be a difference in glial cell density. Although differences between these specimens with and without an IA do not appear significant, there is again a notable difference between the two specimens without an IA. In Figure 36C, this specimen shows a much higher glial cell density than in Figure 36A and 36B, in addition to the acute density of these cells that appear to form a cellular lining.

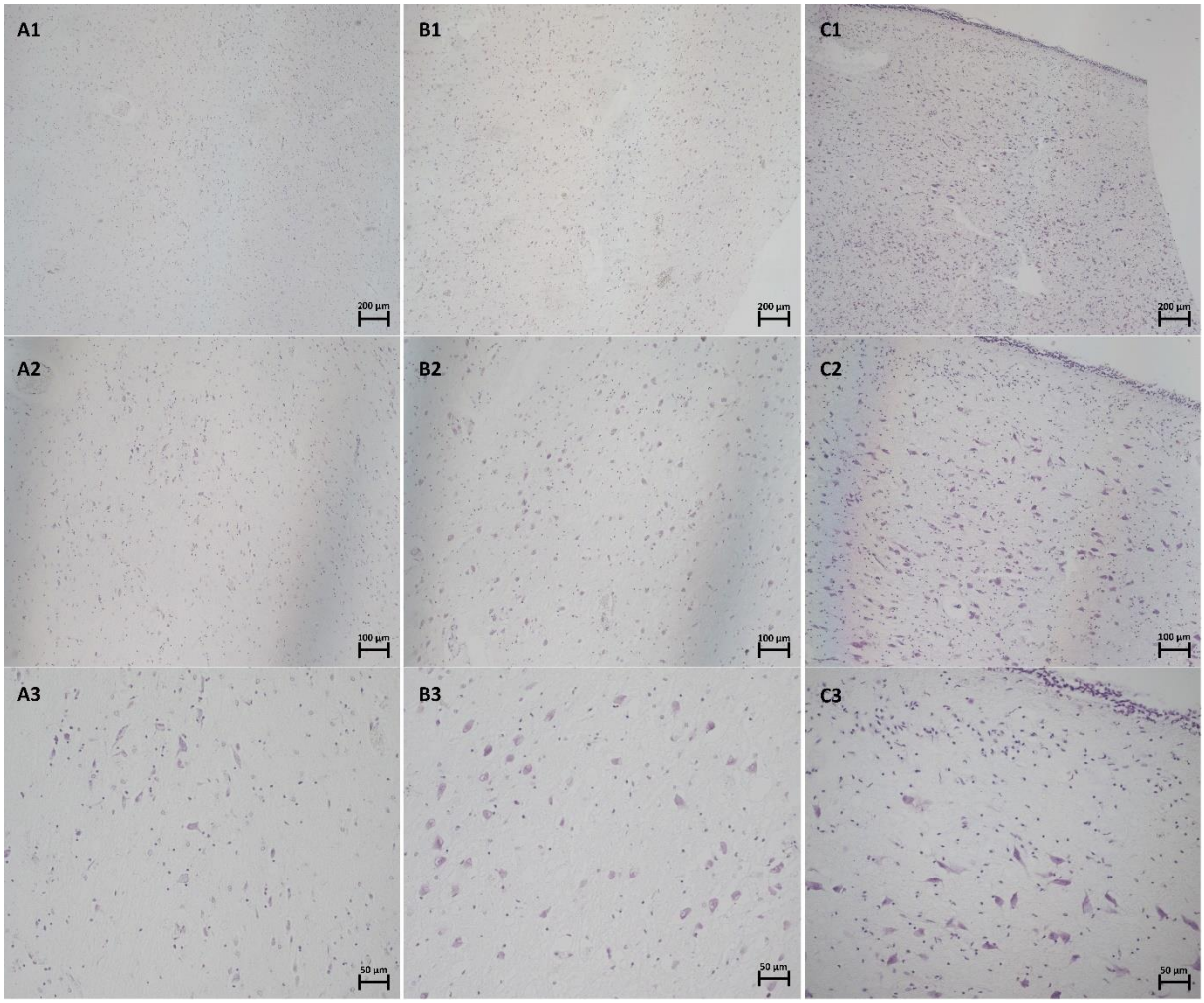

Figure 36 A CV-stained sample of the PVR in a specimen with an IA (A) and PVR in specimens without an IA (B and C) at 5X (1), 10X (2), and 20X (3) magnifications.

In Figure 37, these specimens were uniquely sectioned horizontally as opposed to the sagittal sectioning of the rest of the sample. Figure 37 with H&E staining can be easily compared to Figure 38 with CV staining. The horizontal sections can be seen compared to the sagittal sections in Figure 39, however no significant differences are observable with H&E staining of glial and neuronal cell density and structural organisation.

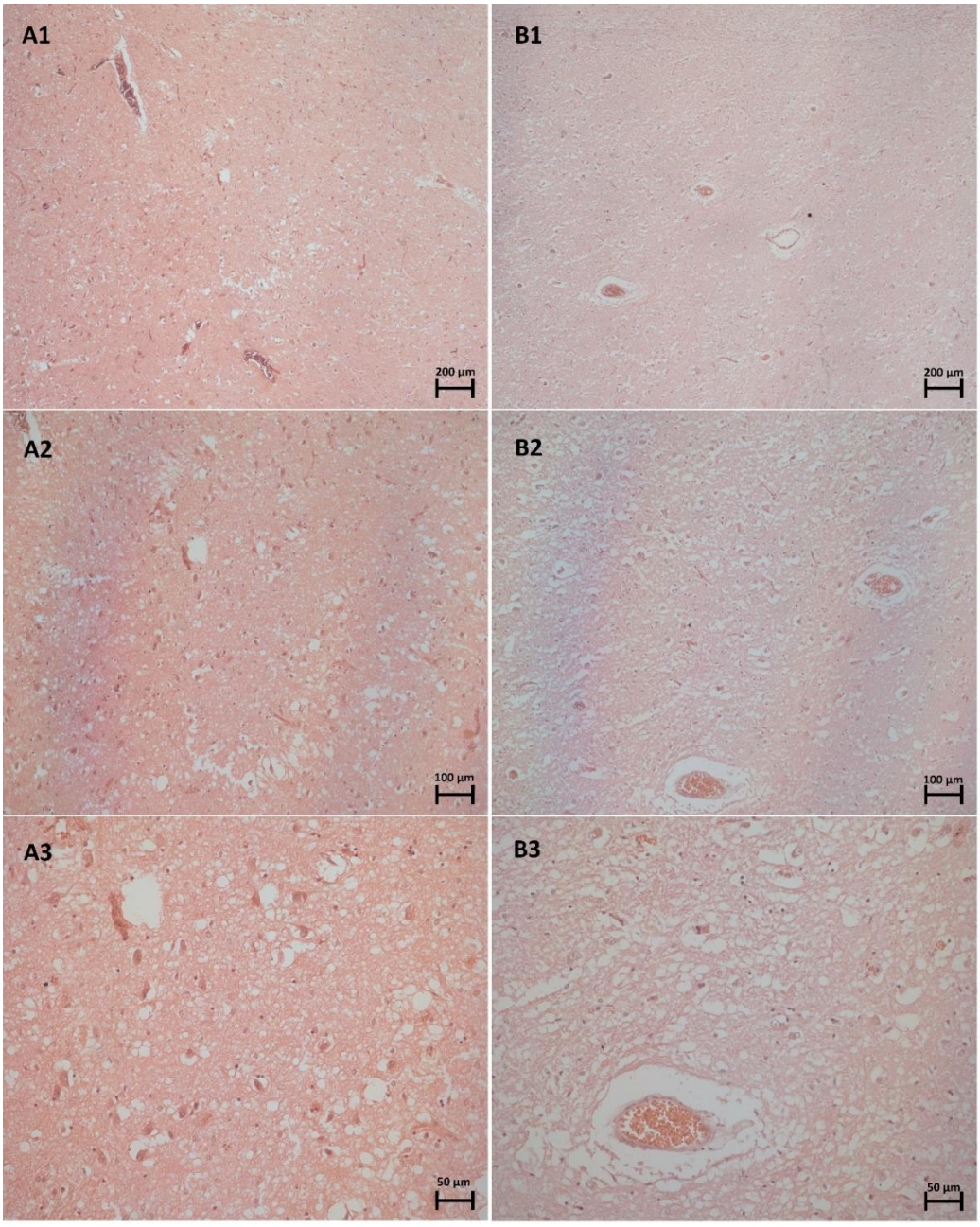

Figure 37 An H&E-stained image of a horizontal section in a specimen with an IA (A) and horizontal section in a specimen without an IA (B) at 5X (1), 10X (2), and 20X (3) magnifications.

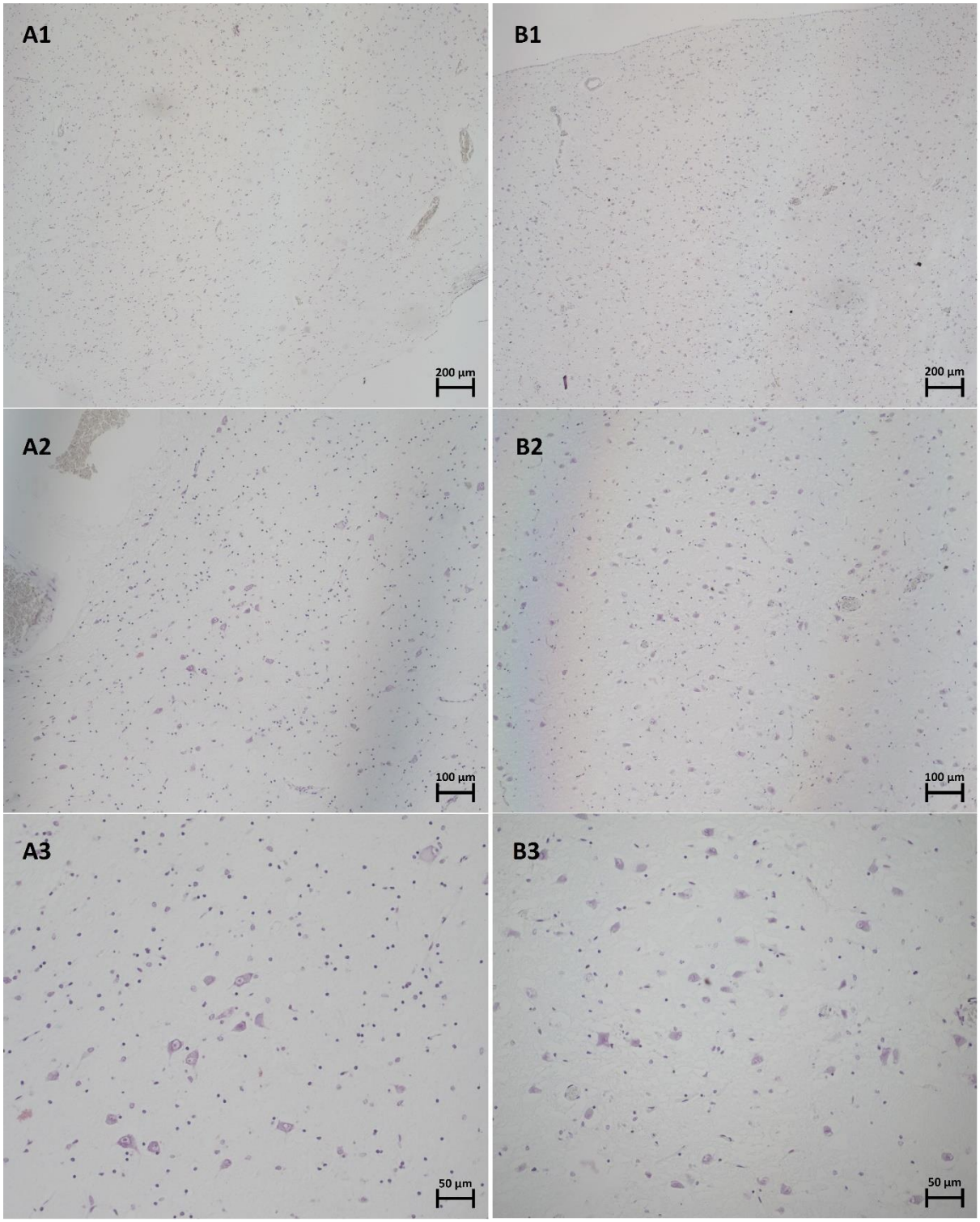

Figure 38 A CV-stained image of a horizontal section in a specimen with an IA (A) and horizontal section in a specimen without an IA (B) at 5X (1), 10X (2), and 20X (3) magnifications.

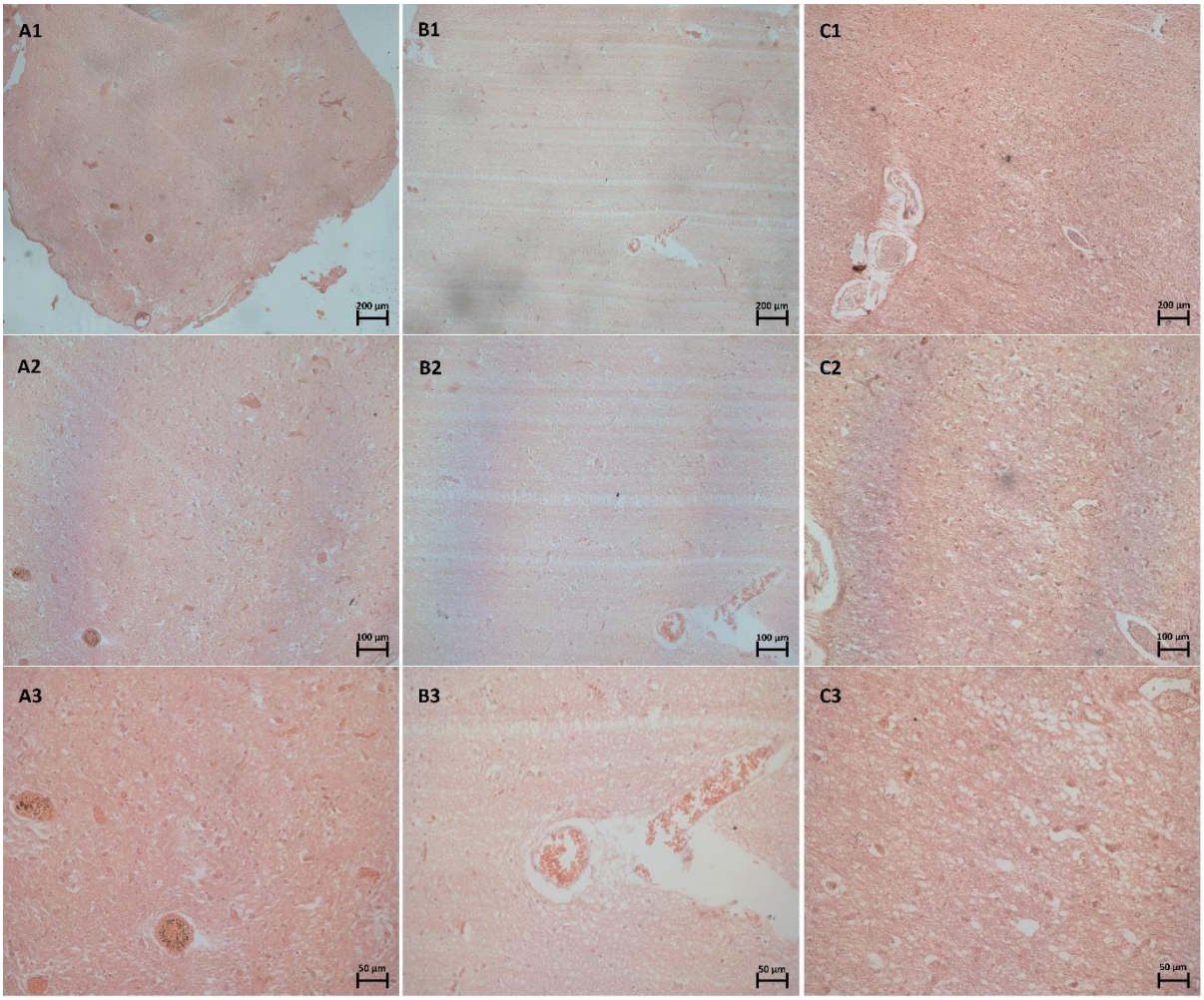

Figure 39 An H&E-stained image comparing sagittal sections of the IA (A) and PVR (B) to a horizontal section in the same specimen (C) at 5X (1), 10X (2), and 20X (3) magnifications.

In Figure 40, horizontal sections of the IA/PVR region appears less densely populated than the sagittal sections. This could mean that glial cell density may differ depending on the orientation of the cellular structure and at which level at which the section is made.

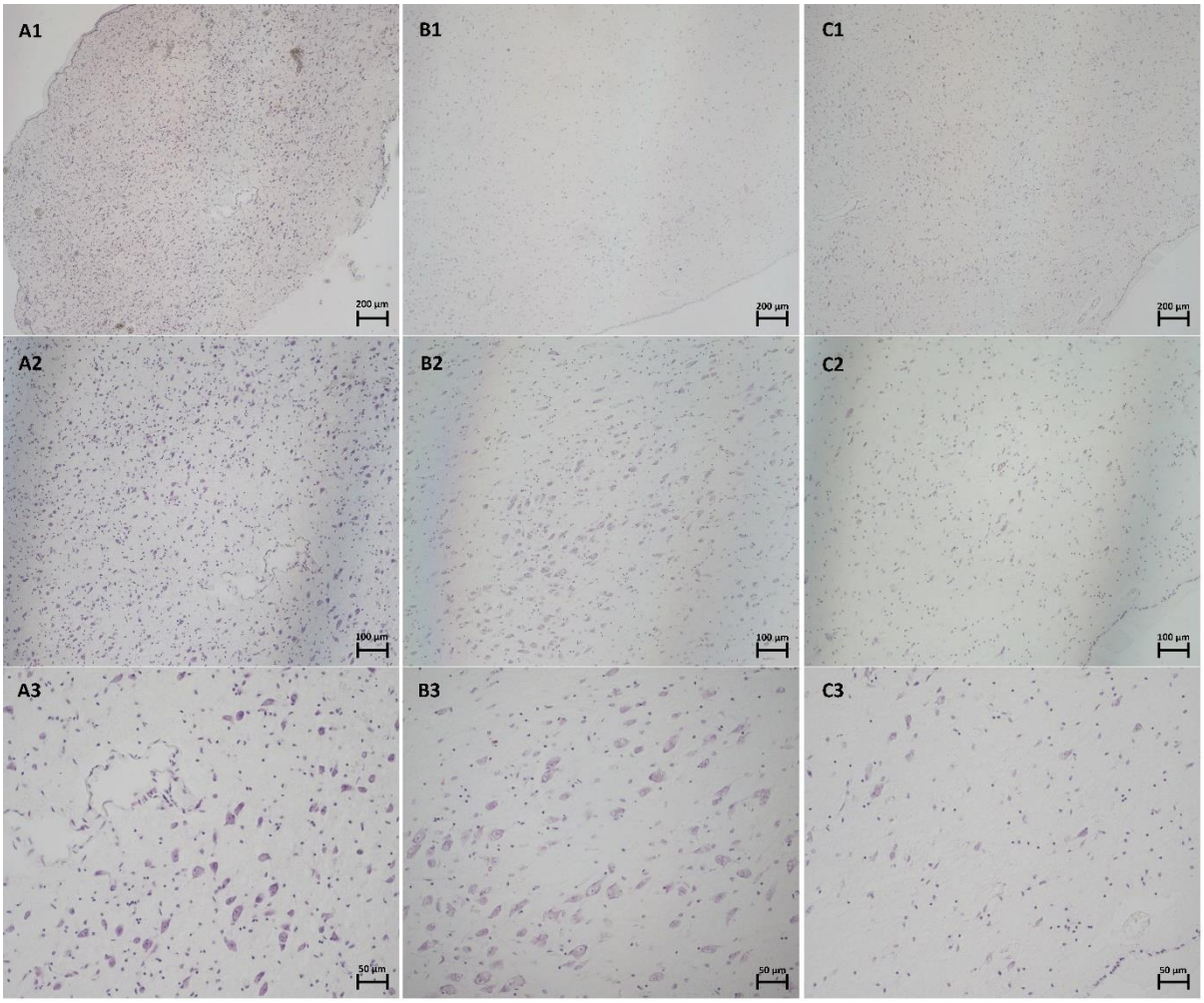

Figure 40 A CV-stained image comparing sagittal sections of the IA (A) and PVR (B) to a horizontal section in the same specimen (C) at 5X (1), 10X (2), and 20X (3) magnifications.

STUDY RELIABILITY AND REPEATABILITY

To conduct an ICC test to measure the reliability of this study, 10% of the sample was randomly selected and used to record the APL, SIL, SAIA and SAV measurements by an independent inter-observer and the primary investigator of the study at a later stage after the initial data collection. The shape and location of the IA were also recorded, however an ICC test could not be performed on nominal data with more than two categories (Chakraborty *et al.*, 2021).

A two-way random effect, absolute agreement, single-rater model was used. The ICC tests returned values greater than 0.9, indicating excellent reliability of results, for the APL, SIL, and SAIA measurements with values of 0.977, 0.978, and 0.968, respectively. The SAV measurement is considered moderately reliable as indicated by an ICC value of 0.737. However, when evaluating the SAV measurement using a mean-measurement model instead of a single-rater model the ICC value was 0.893, indicating a good reliability.

Due to the acceptable ICC values indicating reliability of this study the same methodology can be used in future investigations by other authors. However, in future investigations the SAV measurement should be reported as a mean of at least three measurements to improve the reliability of these results and their associated correlations.

DISCUSSION

The IA is prevalent in approximately 70-80% of typical human brains, with a higher prevalence in females than in males (Nopoulos *et al.*, 2001). It has been reported that the prevalence is significantly lower in patients with neurological disorders, such as schizophrenia (Takahashi *et al.*, 2008; Trzesniak *et al.*, 2011, 2016).

The 68.67% prevalence of the IA in this sample represents the lower end of general prevalence in a healthy population, but is similar to the prevalence in a sample of neuropathological subjects. For instance, Nopoulos and co-workers report a 68.42% prevalence of the IA in 114 patients with schizophrenia (Nopoulos *et al.*, 2001). A meta-review of IA studies conducted in 2011 showed a percentage of prevalence ranging from 77.7% to 97.7% in healthy subjects (Trzesniak *et al.*, 2011). However, prevalence has recently been shown to be higher in MRI studies, 89.7% of a total of 2208 subjects, than in anatomical macroscopic studies, 73.8% of a total of 389 subjects (Wong *et al.*, 2021). The percentage of prevalence in another recent study with a large sample of 1410 subjects obtained from MRI scans was 87.3% (Borghei *et al.*, 2021). These recent results raise the average percentage of prevalence of the IA in a population to 87%, which makes the 68.67% prevalence in this cadaveric sample of a South African population almost 20% lower than expected.

There is a higher incidence in females than in males in both MRI (prevalent in 90.6% of females and 83.0% of males) and cadaveric (prevalent in 68.5% of females and 66.2% of males) research samples of healthy subjects (Wong *et al.*, 2021). However, there was no significant degree of sexual dimorphism in the prevalence of the IA in this research study, where prevalence was 75.68% in females and 63.04% in males (p-value ≈ 0.217). Other literature that reported no significant relationship between sex and prevalence of the IA included a

study by Snyder and co-workers consisting of both healthy and neuropathological cohorts (Snyder *et al.*, 1998), as well as a recent study of a Serbian population, which showed a prevalence of 81.82% in females and 78.95% in males (Pavlović *et al.*, 2020).

The higher prevalence reported in MRI studies may be due to the possibility of type II errors (falsely declaring that the IA is absent when it is present) in cadaveric studies, due to the potential desiccation of brain tissue during the fixation process (Wong *et al.*, 2021). It is further hypothesised that this higher prevalence in MRI studies is due to a better representation of a population, accounted for by the larger sample size including a wider range of subject age capable of being attained in MRI studies as compared to cadaveric studies (Wong *et al.*, 2021), and the ability to observe prevalence without causing damage to the brain. The resolution of MRI scans allows for accurate visualisation of the IA but has also been noted to have trouble when identifying the IA in subjects with a narrow third ventricle, typical in younger subjects (Borghei *et al.*, 2021).

Incidence of a double IA is rare and has only been reported a few times in previous literature according to the authors' knowledge (Malobabić *et al.*, 1987; Tubbs *et al.*, 2004; Whitehead, 2015; Baydin *et al.*, 2016; Yasaka *et al.*, 2019; Pavlović *et al.*, 2020). In these reports three of the incidences were found in female patients, whereas the remaining three reports did not provide this information. In this study, one incidence of a double IA was observed in a 72-year-old male, where both IAs were the same oval shape but different sizes. Pavlović and co-workers as well as Whitehead also reported that the double IAs in their samples differed in size (Whitehead, 2015; Pavlović *et al.*, 2020). In our study, the secondary IA was slightly smaller than the primary IA and located in the posterior-superior quadrant, posteriorly to the primary IA located in the anterior-superior quadrant. The secondary IA had an APL of 6.07

mm, an SIL of 2.1 mm and an area of 11.17 mm^2, as opposed to the larger primary IA which had an APL of 6.99 mm, an SIL of 5.36 mm, and an area of 29.95 mm^2.

A recent MRI study of 205 patients by Tsutsumi and co-workers (2021) devised an original method to classify both the shape and location of the IA which was vastly different to what has been used in the known literature. The shape of the IA was more loosely/vaguely defined and based on its general size and incidence. The authors reported their results as a single, styloid IA with variable thickness in 68% of their sample, a broad IA in 18%, a bi-lobar IA, similar in shape to the semi-lunar / bean-shaped category in our study, in 3% and a unique tubular, multiple, and rudimental IA in three patients in their sample.

Interestingly, the remaining 33 individuals (10%) of their sample were reported to have a double IA with a higher frequency in patients over 60-years-old, and with at least one other instance of an individual with more than three IAs (Tsutsumi *et al.*, 2021). These findings are surprising due to the rarity of reports on double IAs in the known literature. Additionally, there has never been any other report on the incidence of multiple IAs (more than two) within a single individual.

Furthermore, to determine the location of the IA within the third ventricle, Tsutsumi and co-workers arbitrarily divided the third ventricle into nine areas and reported their results as thirds within the ventricle. In the anteroposterior dimension of the nine areas described, almost the entirety of the IA sample group, “184 of 205 (99%)”, was reported within the middle third area, followed by “13 (7%)” within the posterior third and “2 (1%)” within the anterior third (Tsutsumi *et al.*, 2021). In the superior-inferior dimension of the nine areas described, the IA was reportedly found in “176 (95%)” of the middle third, “64 (35%)” of the upper third, and “4 (2%)” of the lower third areas (Tsutsumi *et al.*, 2021). These percentages

do not add to make 100% in either of the two reported dimensions and are thus misleading. Therefore, the results of this study were limited by unreliable reporting and could not be discussed. However, we take note of dividing the third ventricle arbitrarily into nine sections instead of four as done in our study. We propose that the most informative arbitrary division of the third ventricle would be into six sections, three superiorly and three inferiorly. To keep this method standardised we suggest that researchers still make use of the horizontal plane along the ACPC line and dividing this line into three equal parts with perpendicular vertical lines. This proposed method is visualised in Figure 41 below.

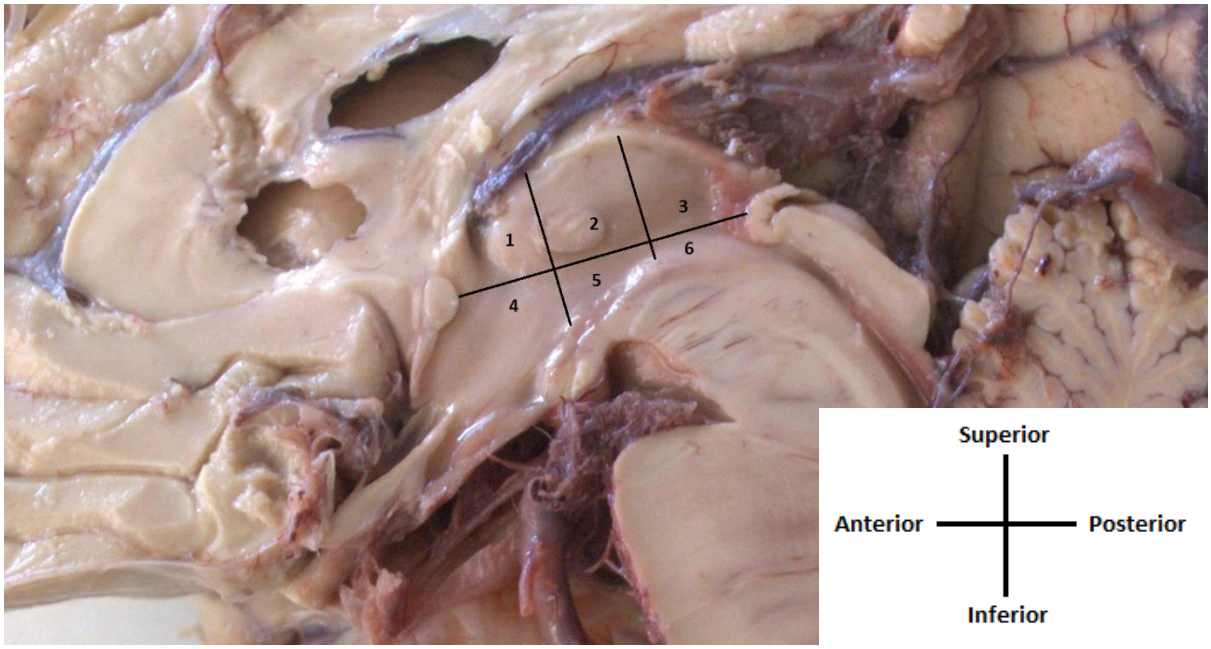

Figure 41 Proposed division of third ventricle into six sections.

We hope that the location of the IA would be more accurately reported with this classification method, as we often observed within our sample that the IA was found between the anterior-superior and posterior-superior quadrants whereby the location was determined based on

the quadrant in which most of the IA mass was predominantly located. We hypothesise that such cases would have been more reliably described as being in the middle-superior section of the third ventricle, or quadrant 2 in Figure 41.

This study by Tsutsumi and co-workers (2021) included a population presumably exclusively Japanese and may be worth comparing to other population groups. The authors also report a high prevalence of IA within their total sample (93%), with prevalence of 91 % in females and 89% in males. It would be interesting to repeat their study using the categories for size, shape and location standardised and described in our study to determine if the difference in their results are significant amongst population groups. Further investigation will be required to determine if there is a relationship between the morphology and prevalence, as well as high incidence of multiple IAs, and the development of neurological disorders.

When analysing the relationship between the IA morphology and sexual dimorphism and age of the individual our study results showed that size of the IA is not dependent on these factors.

In our study, we reported that the average values for the APL and SIL were 6.31 mm and 4.23 mm, respectively. Because most studies in the literature of the IA consist of MRI samples, the measurements used to record the size and length of the IA differ to the measurements used in this cadaveric study, and the few other cadaveric studies in the known literature. Sometimes, the literature does not define a measurement clearly. For example, length of the IA is stated without describing the plane of reference, orientation or formula (when using multiple MRI slices) used during measurement (Takahashi *et al.*, 2008; Takahashi, Yücel, *et al.*, 2009; Takahashi *et al.*, 2010; Trzesniak *et al.*, 2012). Thus, it is not certain that these measurements can then be compared reliably and accurately to the presumed equivalent measurement in this study.

Only one known MRI study makes mention of realigning the images to the ACPC plane, a plane that is used as a reference when measuring the APL of the IA in our study. This MRI study, by Trzesniak and co-workers, reports a median length of 13 mm in healthy subjects, where length in females was greater than in males (Trzesniak *et al.*, 2016). The anterior-posterior length in a midsagittal section was also shown to be greater in females (8.31 ± 3.09 mm) than in males (6.98 ± 2.88 mm) by Sen and co-workers (Sen *et al.*, 2005). However, no statistically significant sexual dimorphism for the APL was found in our sample.

The length of the IA has also been reported to be significantly less in patients with neurological disorders, including schizophrenia, bipolar disorder, and major depressive disorder (Takahashi et al., 2008a, 2008c, 2009a, 2009b, 2010; Trzesniak et al., 2011, 2012, 2016).

A study by Marjorie LeMay in 1984 regarding the aging brain focused on the relationship between a person's age and the widening of the third ventricle, associated with the deterioration of the IA. Pneumoencephalography showed regression of the IA's superior region from posterior to anterior in the later decades of life, although this regression was greater in males than in females (LeMay, 1984).

A more recent study in 2021, with a large retrospective sample of 1410 subjects, had concurrent findings with the aforementioned 1984 study. Borghei, Piracha and Sani reported statistically significant increases in the width of the third ventricle and declines in the size of the IA with age until the age of 70 from where their findings then showed an increase in IA size with age (Borghei *et al.*, 2021). The regression of the IA with age was significantly greater in males than in females. Although the IA slowly disappears with age, an absent IA is commonly attributed to being congenital. The authors mention that it was previously shown

that the absence of the IA was associated with a decreased performance during neuropsychological tests of attention (Borghei *et al.*, 2021), although this may be alluding to unpublished findings as an article of this nature by these authors could not be found.

The largest area of the IA within our study sample was found to be 113.23mm^2, where the average size viewed on the midsagittal plane was found to be only 25.68mm^2. Figure 42 below shows a comparison of the largest IA within our study sample to an IA similar to the average size (26.18 mm^2).

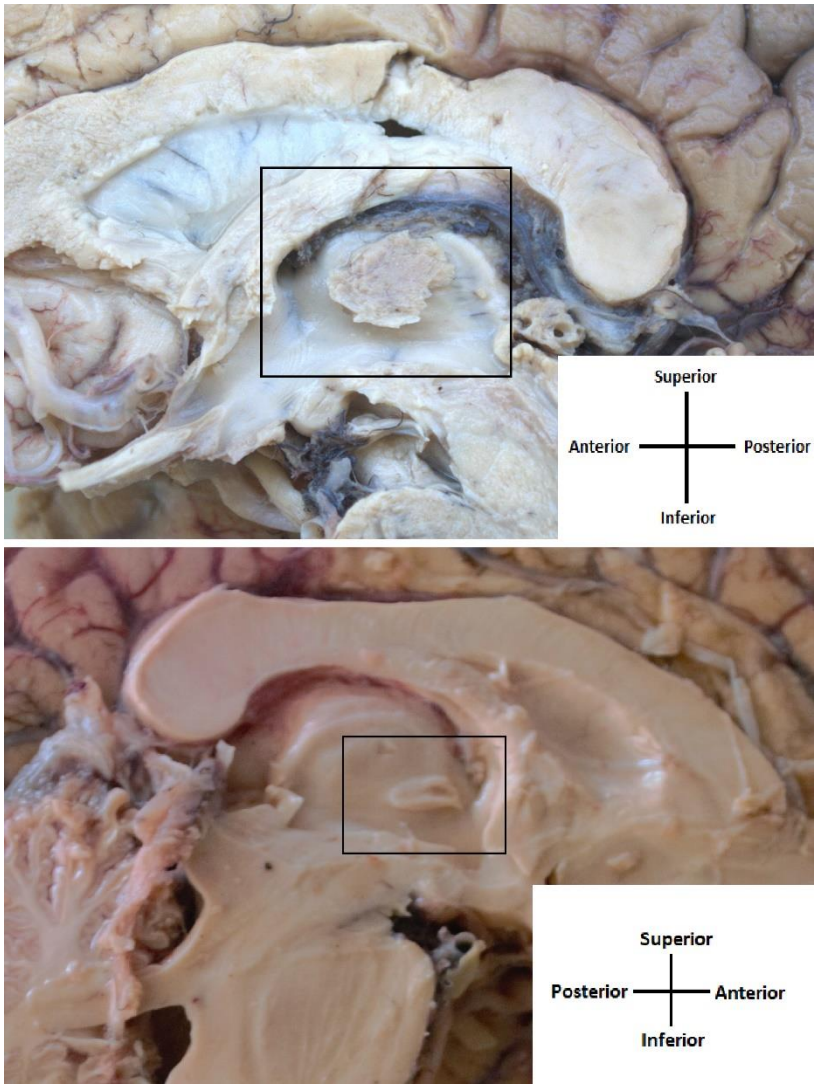

Figure 42 Comparison of large IA [top] to average-sized IA [bottom].

Few recent studies report on the area of the IA on the midsagittal plane as was done in our study, therefore there is limited literature in the past 15 years with which to compare this value to. In a 1987 cadaveric study by Malobabić and co-workers, the average midsagittal surface area of the IA in 39 subjects was 13.1 mm^2 (Malobabić *et al.*, 1987). In a more recent cadaveric study, Pavlović and co-workers report a slightly larger average cross-sectional area of 29.81 mm^2, significantly larger in females (average of 34.13 mm^2) than in males (average of 24.12 mm^2). The largest IA in their sample was significantly smaller than in ours, with a cross-sectional area of 56.50 mm^2 (Pavlović *et al.*, 2020). In an MRI study by Ceyhan and co-workers, the authors recorded the area of the IA on the midsagittal plane and reported an average area of 90 ± 55 mm^2 in the healthy control group, 58 ± 45 mm^2 in the schizophrenic group and 76 ± 53 mm^2 in the group consisting of subjects with bipolar disorder (Ceyhan *et al.*, 2008). These averages are significantly greater than in our sample, however it should be noted that the standard deviations for these averages are also quite large. A recent study, also from a sample consisting of MRI scans, reported an average surface area of 42.9 mm^2 in a healthy, control group and 44.2 mm^2 in a group with midline abnormalities (Whitehead and Najim, 2020).

Although the largest IA in our study is an outlier, it proves that awareness and morphological understanding of this structure is crucial during any neuropathological diagnosis or surgical procedure pertaining to the diencephalon, or the third ventricle specifically. An unusually large IA can be mistaken for a tumour or cause complications during neurosurgery (Nayak and Soumya, 2010). The surgeon should also be aware of the occurrence of a double IA, despite the rarity (Baydin *et al.*, 2016).

A study conducted in 2016 classified the IA as one of the four critical structures to be taken into consideration when planning the approach of surgical tumour removal within the third ventricle (Spina *et al.*, 2016). Subsequently, a study in 2017 further reiterated the importance of the IA as a critical structure noted in surgeries of the third ventricle (Zhang *et al.*, 2017). The authors noted an unreliable relation in the position of the pineal body to the IA. This is most likely due to the varying size and location of the IA within the third ventricle. Knowledge of the anatomy in the surgical region can be the deciding factor in the success or failure of a surgery, which can have dire implications for the patient's health and safety. In 2020, a study reported the interruption of a neuro-endoscopy due to the thickening of the IA, which obliterated the floor of the third ventricle (Furtado *et al.*, 2020). This made it impossible for the surgeons to continue the neuro-endoscopy to treat the patient and shows how the IA can influence clinical decisions and approaches.

The decrease in the size of the IA has also been reported to be significantly related to disorders such as schizophrenia (Takahashi *et al.*, 2008; Takahashi *et al.*, 2009; Trzesniak *et al.*, 2011, 2012, 2016). However, Yasaka and co-workers (2019) state that a small IA is not necessarily an explicit finding of a psychological disorder and cannot be used in isolation to infer from this relationship. The authors advise on considering the lateral diameter of the third ventricle as an additional variable linked to neurological disorders. The authors report that this measurement has a major impact on the size of the IA in terms of its long diameter and should even be considered more than the individual's age and sex (Yasaka *et al.*, 2019). Unfortunately, the lateral diameter of the third ventricle cannot be measured accurately in a cadaveric specimen, therefore we were not able to test this relationship in our study.

Review of the known literature regarding the IA shows few histological studies in this region. Literature on brain histology, specifically of the thalamic region, is also quite scarce. Our histological study was inspired by a study conducted by Puskas and co-workers in 2005. It was this study that introduced the concept of a circular arrangement of neurons in the cytoarchitecture of the IA and PVR regions from their findings in a sample of six human brains with an IA. The methods of visualisation of the histology of the cells that we decided was most optimal to use in our study differed to the method used by Puskas and co-workers. This may be due to the large time period between the two studies, in which histological methods have changed and improved, or merely based on preferred methods for histological observation. Our sample included both sagittal and horizontal sections that were 5 µm thick and stained with H&E and CV dyes, whereas Puskas and co-workers included only frontal sections that were 10 µm thick and stained using the Kluver-Barrera (KB) protocol. It was decided that sagittal sections would be used instead of frontal sections for our study due to the presumed course in which connections would run sagittally through the IA and that this would be more representative of any significant cytoarchitectural arrangements observed. The difference in staining protocols used between the two studies is of little importance in this regard. The KB staining is a double stain protocol which combines CV staining for Nissl bodies with luxol fast blue (LFB) staining for myelin (Dorathy *et al.*, 2012). The thalamus is a grey matter structure within the brain and CV staining was sufficient for the objectives of our study, which did not include identification of white matter within the IA and PVR regions. Therefore, we did not use an LFB staining protocol. Despite making use of the KB staining method in their study, Puskas and co-workers did not report any findings regarding white matter/myelin within the IA and PVR.

We did not observe any distinct neuronal structural arrangements in either the IA or PVR regions using light microscopy. Furthermore, it must be noted that we do not agree with the findings of Puskas and co-workers' 2005 study and their results could not be replicated in our study, or any study within the known literature since 2005. Only five images, all of which appear to be of the same 55-year-old male specimen, are available, of which only a single circular arrangement is depicted. However, we do not observe any distinct circular arrangement of the neurons, and this presumed pattern was not shown in the remaining five specimens of the sample for comparison in the article.

In contrast to both our results and that of Puskas and co-workers' study, recently published findings by Parra and co-workers (2022) allude to the possibility of glial cell bridges within the IA, but report no existence of neuronal cell bodies in the same region (Parra *et al.*, 2022). Therefore, they conclude that the IA is unlikely to be a grey commissure. However, this 2022 study's methodology included only H&E staining, which we have noted is not truly representative of the observation of neuronal cells within the tissue. This is also noted by Selcuk and Colakoglu (2020) when researching the most suitable staining method to distinguish between grey and white matter. The authors concluded that KB staining, which includes CV staining, is one of the best staining protocols to observe neuroglia and Nissl bodies, whereas H&E is one of the best staining protocols to observe ependymal cells instead (Selcuk and Colakoglu, 2020).

Our study's design for the histological component was purely observational, therefore no inferences can be made about the function and cytoarchitecture of the IA without further investigation. Although no specific organisation of the cells could be found, our study has

offered a novel inspection of the histology of the thalamus, specifically of the IA and PVR, in midsagittal sections.

Unfortunately, vacuolation and damage to the cells in our sample was visible, however this did not negatively impact on our observational findings. The cell integrity and quality can be influenced by the fixation quality which is dependent on a number of variables, including the fixation type, the PMI, the fixative solution and factors such as its constituents, temperature and osmolarity, as well as the fixative buffer used during the histological process (McFadden *et al.*, 2019). In addition, the tissue can be damaged during physical processes such as sectioning the tissues with a microtome or mishandling of the specimens during the histological processes.

A thalamic commissure is said to exist within the IA, with fibres connecting the various thalamic nuclei, namely the midline, dorsomedial, paraventricular, ventral posteromedial and intralaminar nuclei (Zawisch, 1952; Heick, 1996). Therefore, one would expect to find neurons within both the IA and PVR regions. However, no other mention of a “thalamic commissure” was known to the author in prior literature until very recently. A significant finding was made in a probabilistic tractography study by Borghei and co-workers in 2021. This study showed that the IA was vastly interconnected between the limbic, frontal and temporal lobes, insula, and pericalcarine cortices of the brain (Borghei *et al.*, 2021). The authors further reported that the IA formed a stronger bridge of connectivity in females than males. These findings may significantly alter the academic view of the IA in literature, lending it greater importance as a grey matter commissure, integral to some pathways within the brain, specifically to the amygdala, hippocampus and entorhinal cortex (Borghei *et al.*, 2021).

Another recent study by Chen and co-workers reported findings of a robust thalamocortical signal circuit in which the IA is involved that plays a role in cognitive function by means of perception and the transmission, processing and integration of information (Chen *et al.*, 2021).

It is evident that the future of IA studies should now move on from the anatomical investigation to focus on the functional investigation of this structure. This shift of focus in the literature is likely to reveal insights to questions that have gone unanswered in prior literature. For example, a study by Heick in 1996 makes mention of the unexplained failure of callosotomy (a medical procedure whereby the corpus callosum undergoes a sagittal surgical division to treat epilepsy) in some patients where it is a significant success in others. This study refers to a thalamic commissure within the IA, which they hypothesize to contribute in part to the failure of callosotomies, as its nature as a commissure allows continued interhemispheric communication in the brain attributing to the frequency and severity of epileptic seizures even after the division of the corpus callosum (Heick, 1996). Heick further hypothesizes the possible correlation between the diameter of the IA and the severity of the patient's epilepsy after callosotomy, however it is not known if further literature in this regard was published.

Although the function of the IA is not known, those without an IA do not appear to suffer any significant loss in neurological functions or significant difference from typical neurocognition. It is plausible that this is due to fibre pathways through other commissures compensating for when there is no IA (Borghei *et al.*, 2021).

A recent study in 2017 used fractional anisotropy and mean diffusivity in a retrospective MRI study of the IA and showed a statistically significant relationship between the size of the IA and the age and attention function in females (Damle *et al.*, 2017). To our knowledge, this

study by Damle and co-workers is one of the first to link the IA to any neuropsychological function in the known published literature.

CONCLUSION

The results from this study were able to confirm the value of using fixed human tissue in a sample for anatomical and histological investigation studies for research purposes. Despite a few disadvantages of using fixed human tissue (as mentioned in the following limitations section) it remains a valuable source of data for research.

Although prior literature does show significant relationships between the age, sex and morphology of the IA, no such relationships were found in this research study. However, this study has provided additional data to add to the limited knowledge regarding the anatomy of the IA, such as the prevalence (68.67%), most common location (anterior-superior quadrant of the third ventricle) and average midsagittal surface area (25.68 mm^2). Moreover, the rare occurrence of a double IA, in a male specimen, which is not commonly found, could be reported on.

This study further confirmed the existence of neurons within the IA, forming a bridge between the PVR of the thalami. No specific structural organisation of the neurons within the IA or PVR could be identified in this study, therefore a hypothetical link between the cytoarchitecture of the regions and their functions could not be analysed. Even though the histological findings from this study differ from the known literature this study was able to propose that the IA could serve as a potential bridge, or commissure, for neural pathways crossing over the midline of the brain.

With repetition of and addition to this study, contradictions in the known literature regarding the cytoarchitecture within the IA could be cleared and suggestions could be made regarding its function within neural pathways and implications in neurological disorders on a cellular level.

Further investigation of the function of the IA is crucial to understanding its role within the brain. Providing evidence of significant relationships between the IA and neuropsychological functions and behaviours will greatly influence the academic perception of this structure and the importance of brain commissures consisting of both white and grey matter fibre conduits.

Understanding the normal anatomy and variation of the IA within the third ventricle will better our understanding of its effect on the progress of diseases, such as hydrocephalus or schizophrenia, and the effect on the IA in return and how this can further influence brain function and morphology.

LIMITATIONS

The size of this sample is considered small, especially when other studies in the same subject area have much larger samples, often with at least over 100 individual specimens. This larger sample size is more likely in retrospective studies that include digital data collection (usually MRI scans only), whereas this study used cadavers only, thus limiting the procurement of specimens.

As would be predicted, using fixed post-mortem tissue has disadvantages over using fresh post-mortem tissue, even more so over living tissue. However, benefits of using post-mortem tissue, such as the low cost for data collection (if a donor collection is available) for example, still make post-mortem studies highly viable and convenient for research. Cadaver research is informative and beneficial. However, it is important to note that pre- and post-mortem processing of tissue can lead to alterations in anatomical structures, therefore deviating from the typical anatomy of a living human being. Alternatively, imaging studies using MRI scanning for example, can be more reliable for reporting on the natural structure and behaviour of

anatomy and physiology. This also prevents possible destruction of anatomical samples in the process of data collection. Furthermore, fixation of the brain could cause artefacts that alter the appearance of the post-mortem brain (LeMay, 1984). As seen with the histological component of this study, damage caused by long-term fixation is inevitable and more clearly shown on the cellular level than macroscopically.

Unfortunately, in this study, it was impossible to avoid destruction of / damage to the brain when retrieving the necessary data from a cadaveric specimen due to the nature of the brain needing to be sliced into midsagittal sections. Due to the typically small size of the IA, removal of this region for histological examination led to further destruction of the brain sample. Studies whose methodologies include scanning technology for data collection can avoid this destruction of sample tissue.

Studies on the structure and anatomy of a region are informative but limited when used alone to study the extent of related clinical implications and pathophysiologies (Ceyhan *et al.*, 2008). Anatomical studies such as this one would benefit from being researched in tandem with functional and clinical studies.

Certain methodologies make it possible to record results that are perhaps not possible to record when using other methods of data collection. In this study, the use of cadavers made it impossible to record the lateral diameter of the third ventricle, therefore it was not possible to analyse if this type of measurement would have had a significant relationship with the morphology of the IA or not. In this way, there could be other confounding variables not considered when using cadavers only as a sample.

The objectives for the histological section of this study were updated due to unforeseen limitations in the original methodology. Due to the lack of observable neuronal organisational

structures in the cytoarchitecture we could not report on data such as shape and appearance of organisational structures of neurons and the average size and frequency of neurons within a single organisational structure.

OUTSTANDING QUESTIONS

Below is a list of questions that could not be answered in this study, but will inform and guide future research of the IA.

1. What is the correlation of the anteroposterior length of the third ventricle in relation to the IA size?
2. Is there a significant difference in the SAV between specimens with an IA and specimens without an IA?
3. Is there a significant relationship between the size of the IA and other variables such as age and sex when the length of the IA is measured as the long diameter of the IA instead of the APL?
4. What is the frequency of the different morphological types of neurons within the IA? How does this frequency differ to the frequency of the same neuron types in surrounding regions such as the PVR?
5. Are there any white matter structures that can be visualised in the histology of the IA and PVR?
6. To what degree can we observe cortical expansion, change in neuron size, change in complexity of dendritic connections and increase in efficiency of neural transmissions via synapses in the IA and PVR when comparing the human IA to other species?

FUTURE INVESTIGATIONS

The aim of subsequent studies could focus primarily on investigating the functional anatomy of the IA using different imaging modalities, such as DTI. Other areas of interest also include the histological anatomy of the IA and the implications of the anatomy of the IA in neurological disorders, specifically in relation to the limbic system. The impact of the IA within the ventricular system, on CSF flow dynamics and in medical conditions like hydrocephalus will further enrich the literature pertaining to the IA in a clinical setting. These aforementioned research focuses and the outstanding questions in the previous section can all be considered for future investigations.

Mention of an interhypothalamic adhesion (IHA) was made in a 2019 study using endoscopic third ventriculotomy that identified four incidences of an IHA, with a double IHA in two patients (Phillips *et al.*, 2019). The authors noted that the IHA is "similar but distinct" to the IA. Investigation of the IHA alongside the IA may lead to similar findings in the IA and shed light on the occurrence of interhemispheric bridges of grey matter.

Anatomy of a structure provides valuable information with regard to determining the function of that structure. More detailed histological investigation of the IA region may inform the functional imaging studies that follow. Therefore, future investigations will benefit from including the study of the frequency of different morphological types of neurons within the IA. This study will require much more time and acute observation under a microscope for accurate and reliable results. Data from future imaging and histological studies can be correlated and superimposed into what is known as magnetic resonance microscopy, or MRM (Fatterpekar *et al.*, 2002). This will help visualise the relationship between the cytoarchitecture of a region and its functional pathways. The use of DTI alongside microscopic

analysis of the thalamus and IA specifically can reveal the orientation of white matter fibre tracts and provide insight into the role of the IA in thalamic pathways (Kumar *et al.*, 2016; Kochanski *et al.*, 2018). Furthermore, a comparison of different staining techniques in the human thalamic region and IA specifically will greatly enrich academic resources.

A future application can be developed, based on a standard of anatomy of the IA collected from results of the known academic literature. This data, along with findings in studies of the state of CSF flow dynamics, can be used to create a simulation of the third ventricle and ventricular system within the brain where the anatomical features of the IA, including prevalence, size, shape and location within the third ventricle, can be adjusted to test different hypothetical scenarios. For instance, to test the influence that the IA anatomy has on the flow of CSF within the ventricular system, and subsequently, the onset of conditions such as hydrocephalus.

This can further inform investigations of other regions of neuroanatomy, creating a simulation of neurological conditions influenced by the variation in anatomy and physiology within the brain.

PERSONAL REFLECTION

In every given situation in life there is something to learn, not necessarily pleasant but, more often than not, necessary. My master's journey has been subjectively difficult to complete and sometimes I thought I would never reach the end. There were indeed many times I wished to give up and forget that it was ever a path I started to tread.

I have stumbled - am still stumbling - but I believe I shall find my footing yet. Because I have been told that it is alright to take my own time and trusting in those words has become easier the further along I have come.

Certain circumstances did not make these past years any easier, like the unforeseen loss of friends and family, the outbreak of the Covid 19 pandemic and national lockdown, the disheartening decline in the state of the world, my dwindling mental health, the existential crises we all inevitably face, the underestimated demand of my time for work and the ever-frustrating disruption to any momentum I built up, load-shedding. Despite all this, I still wished that I could have given more to my master's. Upon reflection however, I know that I should not be so hard on myself.

Master's is not to be taken lightly. I respect all academics who have gone through it and still continue to further their careers. I look forward to the next steps in my own journey, whether they remain in academics or go beyond. There are still so many other opportunities in life that I'd like to explore.

I still have a lot to learn. I am not afraid of making more mistakes although I will thus endeavour to avoid making the same mistakes I have these past three years.

I am truly grateful, for the both the experience of this master's itself as well as knowing that it has come to an end at last.

REFERENCES

Alrafiah, A. and Alshali, R. (2019) 'The effect of prolonged formalin fixation on the staining characteristics of archival human brain tissue', *Folia Morphologica (Poland)*, 78(2), pp. 230–236. Available at: https://doi.org/10.5603/FM.a2018.0099.

Amunts, K. *et al.* (1999) 'Broca's Region Revisited: Cytoarchitecture and Intersubject Variability', *Journal of Comparative Neurology*, 412(2), pp. 319–341. Available at: https://doi.org/10.1002/(SICI)1096-9861(19990920)412:2<319::AID-CNE10>3.0.CO;2-7.

Baydin, S. *et al.* (2016) 'The double massa intermedia', *Surgical Neurology International*, 7(1). Available at: https://doi.org/10.4103/2152-7806.179383.

Black, D.W. and Grant, J.E. (2014) *DSM-5® Guidebook : The Essential Companion to the Diagnostic and Statistical Manual of Mental Disorders, Fifth Edition*. [Washington, DC]: American Psychiatric Association Publishing. Available at: https://search.ebscohost.com/login.aspx?direct=true&db=nlebk&AN=1610168&site=ehost-live&scope=site.

Blumenfeld, H. (2010) *Neuroanatomy through Clinical Cases*. 2nd edn. Sunderland, MA: Sinauer Associates Inc.

Borghei, A. *et al.* (2021) 'Structural connectivity of the human massa intermedia: A probabilistic tractography study', *Human Brain Mapping*, 42(6), pp. 1794–1804. Available at: https://doi.org/10.1002/hbm.25329.

Borghei, A., Piracha, A. and Sani, S. (2021) 'Prevalence and anatomical characteristics of the human massa intermedia', *Brain Structure and Function*, 226(2), pp. 471–480. Available at: https://doi.org/10.1007/s00429-020-02193-5.

Borsook, D. *et al.* (2016) 'Neuroscience and Biobehavioral Reviews Reward deficiency and anti-

reward in pain chronification', *Neuroscience and Biobehavioral Reviews*, 68, pp. 282–297. Available at: https://doi.org/10.1016/j.neubiorev.2016.05.033.

Ceyhan, M. *et al.* (2008) 'Absence and size of massa intermedia in patients with schizophrenia and bipolar disorder', *Acta Neuropsychiatrica*, 20(4), pp. 193–198. Available at: https://doi.org/10.1111/j.1601-5215.2008.00296.x.

Chakraborty, H., Solomon, N. and Anstrom, K.J. (2021) 'A method to estimate intra-cluster correlation for clustered categorical data', *Communications in Statistics - Theory and Methods*, 0(0), pp. 1–18. Available at: https://doi.org/10.1080/03610926.2021.1914660.

Chen, C. *et al.* (2021) 'Thalamocortical Functional Connectivity in Patients With White Matter Hyperintensities', *Frontiers in Aging Neuroscience*, 13(March), pp. 1–12. Available at: https://doi.org/10.3389/fnagi.2021.632237.

Cheng, S., Tan, K. and Bilston, L.E. (2010) 'The effects of the interthalamic adhesion position on cerebrospinal fluid dynamics in the cerebral ventricles', *Journal of Biomechanics*, 43(3), pp. 579–582. Available at: https://doi.org/10.1016/j.jbiomech.2009.10.002.

Damle, N.R. *et al.* (2017) 'Relationship among interthalamic adhesion size, thalamic anatomy and neuropsychological functions in healthy volunteers', *Brain Structure and Function*, 222(5), pp. 2183–2192. Available at: https://doi.org/10.1007/s00429-016-1334-6.

Davie, J. and Baldwin, M. (1967) 'Radiographic-anatomical study of the massa intermedia.', *Journal of neurosurgery*, 26(5), pp. 483–7. Available at: https://doi.org/10.3171/jns.1967.26.5.0483.

Dawe, R.J. *et al.* (2009) 'Postmortem MRI of Human Brain Hemispheres : T 2 Relaxation Times During Formaldehyde Fixation', *Magnetic Resonance in Medicine*, 61(4), pp. 810–818. Available at: https://doi.org/10.1002/mrm.21909.

DeFelipe, J. (2011) 'The evolution of the brain, the human nature of cortical circuits, and intellectual creativity', *Frontiers in Neuroanatomy*, 5(MAY), pp. 1–17. Available at:

https://doi.org/10.3389/fnana.2011.00029.

Dorathy, J.T.F. *et al.* (2012) 'A Simple Cost Effective Rapid Differential Staining Technique for Myelinated Fibres and Nerve Cells', 2(November), pp. 43–46.

Fatterpekar, G.M. *et al.* (2002) 'Cytoarchitecture of the human cerebral cortex: MR microscopy of excised specimens at 9.4 Tesla', *American Journal of Neuroradiology*, 23(8), pp. 1313–1321.

Felten, D.L., O'Banion, M.K. and Maida, M.S. (2016) '6 - Ventricles and the Cerebrospinal Fluid', in D.L. Felten, M.K. O'Banion, and M.S.B.T.-N.A. of N. (Third E. Maida (eds) *Netter's Atlas of Neuroscience*. Third. Philadelphia: Elsevier, pp. 85–91. Available at: https://doi.org/https://doi.org/10.1016/B978-0-323-26511-9.00006-0.

Furtado, L.M.F. *et al.* (2020) 'Endoscopic third ventriculostomy in patients with myelomeningocele after shunt failure', *Child's Nervous System*, 36(12), pp. 3047–3052. Available at: https://doi.org/10.1007/s00381-020-04596-5.

Galakhova, A.A. *et al.* (2022) 'Evolution of cortical neurons supporting human cognition', *Trends in Cognitive Sciences*, 26(11), pp. 909–922. Available at: https://doi.org/10.1016/j.tics.2022.08.012.

Garman, R.H. (2011) 'Histology of the Central Nervous System', *Toxicologic Pathology*, 39(1), pp. 22–35. Available at: https://doi.org/10.1177/0192623310389621.

Gold, P.W. and Kadriu, B. (2019) 'A major role for the lateral habenula in depressive illness: Physiologic and molecular mechanisms', *Frontiers in Psychiatry*, 10(MAY), pp. 1–7. Available at: https://doi.org/10.3389/fpsyt.2019.00320.

Graham, C.H., Storch, D. and Machac, A. (2018) 'Phylogenetic scale in ecology and evolution', *Global Ecology and Biogeography*, 27(2), pp. 175–187. Available at: https://doi.org/10.1111/geb.12686.

Grisan, E. *et al.* (2018) 'Resolving single cells in heavily clustered Nissl-stained images for the analysis of brain cytoarchitecture', in *2018 IEEE 15th International Symposium on Biomedical Imaging (ISBI*

2018), pp. 427–430. Available at: https://doi.org/10.1109/ISBI.2018.8363608.

Grow, W.A. (2018) 'Chapter 5 - Development of the Nervous System', in D.E. Haines and G.A.B.T.-F.N. for B. and C.A. (Fifth E. Mihailoff (eds) *Fundamental Neuroscience for Basic and Clinical Applications*. Fifth. Elsevier, pp. 72-90.e1. Available at: https://doi.org/https://doi.org/10.1016/B978-0-323-39632-5.00005-0.

Gupta, T. and Gauba, K. (2011) 'Cadaveric tissue histology: A viable alternative', *Journal of Clinical and Diagnostic Research*, 5(8), pp. 1505–1509.

Habbal, O. (2017) 'Anatomical Research: Misconceptions and opportunities', *Sultan Qaboos University Medical Journal*, 17(1), pp. 1–2. Available at: https://doi.org/10.4322/jms.090015.17.

Heick, A. (1996) 'The thalamic commissure in generalized epilepsy', *British Journal of Neurosurgery*, 10(3), pp. 309–311. Available at: https://doi.org/10.1080/02688699650040205.

IGAKUKEN Neuropathology Database (no date) *Histological methods for CNS - Nissl Staining*. Available at: https://pathologycenter.jp/method-e/nissl.html (Accessed: 11 July 2022).

IHC WORLD (no date) *Nissl Staining Method and Protocol on Paraffin Sections for Brain & Spinal Cord*. Available at: http://www.ihcworld.com/_protocols/special_stains/nissl.htm#:~:text=Description%3A This method is used,brain and spinal cord tissue. (Accessed: 11 July 2022).

Kalanjati, V.P., Dewi, A.K. and Santoso, M.W.A. (2017) 'Quantitative Study on Human Cerebellar Cortex from Anatomy Cadaver Preparations', *International Journal of Morphology*, 35(1), pp. 167–171. Available at: https://doi.org/10.4067/s0717-95022017000100027.

Katz, D.M. and Chandar, K. (2014) 'Thalamus', in M.J. Aminoff and R.B.B.T.-E. of the N.S. (Second E. Daroff (eds) *Encyclopedia of the Neurological Sciences*. Second. Oxford: Academic Press, pp. 425–430. Available at: https://doi.org/https://doi.org/10.1016/B978-0-12-385157-4.01181-7.

Khasawneh, A., Garling, R. and Harris, C. (2018) 'Cerebrospinal fluid circulation: What do we know and how do we know it?', *Brain Circulation*, 4(1), p. 14. Available at: https://doi.org/10.4103/bc.bc_3_18.

Kochanski, R.B. *et al.* (2018) 'Identification of Stria Medullaris Fibers in the Massa Intermedia Using Diffusion Tensor Imaging', *World Neurosurgery*, 112, pp. 497–504. Available at: https://doi.org/10.1016/j.wneu.2018.01.066.

Koo, T.K. and Li, M.Y. (2016) 'A Guideline of Selecting and Reporting Intraclass Correlation Coefficients for Reliability Research', *Journal of Chiropractic Medicine*, 15(2), pp. 155–163. Available at: https://doi.org/10.1016/j.jcm.2016.02.012.

Kumar, M. *et al.* (2016) 'Diffusion tensor imaging for assessing brain gray and white matter abnormalities in a feline model of α-Mannosidosis', *Journal of Neuropathology and Experimental Neurology*, 75(1), pp. 35–43. Available at: https://doi.org/10.1093/jnen/nlv007.

LeMay, M. (1984) 'Radiologic changes of the aging brain and skull.', *AJR. American journal of roentgenology*, 143(2), pp. 383–389. Available at: https://doi.org/10.2214/ajr.143.2.383.

Malobabić, S., Puskas, L. and Blagotić, M. (1987) 'Size and position of the human adhaesio interthalamica.', *Gegenbaurs morphologisches Jahrbuch*, 133(1), pp. 175–180.

McFadden, W.C. *et al.* (2019) 'Perfusion fixation in brain banking: a systematic review', *Acta neuropathologica communications*, 7(1), p. 146. Available at: https://doi.org/10.1186/s40478-019-0799-y.

Meisenzahl, E.M. *et al.* (2000) 'Adhesio interthalamica in male patients with schizophrenia', *American Journal of Psychiatry*, 157(5), pp. 823–825. Available at: https://doi.org/10.1176/appi.ajp.157.5.823.

Meunier, A., Sawamoto, K. and Spassky, N. (2020) 'Chapter 42 - Ependyma', in J. Rubenstein et al. (eds) *Patterning and Cell Type Specification in the Developing CNS and PNS*. Second. Academic Press,

pp. 1021–1036. Available at: https://doi.org/https://doi.org/10.1016/B978-0-12-814405-3.00042-4.

Mihailoff, G.A. and Haines, D E (2018) 'Chapter 15 - The Diencephalon', in Duane E Haines and G.A.B.T.-F.N. for B. and C.A. (Fifth E. Mihailoff (eds) *Fundamental Neuroscience for Basic and Clinical Applications*. Fifth. Elsevier, pp. 212-224.e1. Available at: https://doi.org/https://doi.org/10.1016/B978-0-323-39632-5.00015-3.

Milligan, M. and Chen, A. (2018) 'Study Designs', in *Principles of Clinical Cancer Research*. Springer International Publishing, pp. 161–178. Available at: https://doi.org/10.5005/jp/books/12430_3.

Morel, A., Magnin, M. and Jeanmonod, D. (1997) 'Multiarchitectonic and stereotactic atlas f the human thalamus', *Journal of Comparative Neurology*, 387(4), pp. 588–630. Available at: https://doi.org/10.1002/(SICI)1096-9861(19971103)387:4<588::AID-CNE8>3.0.CO;2-Z.

Naidoo, S.V.K. *et al.* (2019) 'Oral exposure to cadmium and mercury alone and in combination causes damage to the lung tissue of Sprague-Dawley rats', *Environmental Toxicology and Pharmacology*, 69(March 2019), pp. 86–94. Available at: https://doi.org/10.1016/j.etap.2019.03.021.

Nayak, S. and Soumya, K. (2010) 'Unusually large interthalamic adhesion and its clinical importance', *International Journal of Anatomical Variations*, 3, pp. 174–175.

Neubacher, U. (2022) *Re: Cresyl violet staining for neurons ?* Available at: www.researchgate.net/post/Cresyl_violet_staining_for_neurons/633bfe7e20e6680573075d6c/citation/download (Accessed: 12 July 2022).

Nlebedum, U. and Ekele, I. (2013) 'Effect of Embalming Fluid on Histological Appearance of Organs From Embalmed West African Dwarf Goat Cadavers', *HISTOLOGIC*, XLVI(May 2014), pp. 1–4.

Nopoulos, P.C. *et al.* (2001) 'Sex differences in the absence of massa intermedia in patients with schizophrenia versus healthy controls', *Schizophrenia Research*, 48(2–3), pp. 177–185. Available at: https://doi.org/10.1016/S0920-9964(00)00067-0.

Paradiso, B. *et al.* (2018) 'From fix to fit into the autoptic human brains', *European Journal of Histochemistry*, 62(3), pp. 257–265. Available at: https://doi.org/10.4081/ejh.2018.2944.

Park, K.A. *et al.* (1993) 'A morphologic study of interthalamic adhesions in Korean brains', *Clinical Anatomy*, 6(1), pp. 33–36. Available at: https://doi.org/10.1002/ca.980060106.

Parra, J.E.D., Ripoll, Á.P. and García, J.F.V. (2022) 'Interthalamic adhesion in humans: a gray commissure?', *Anatomy and Cell Biology*, 55(1), pp. 109–112. Available at: https://doi.org/10.5115/acb.21.164.

Pavlović, M.N. *et al.* (2020) 'Position and size of massa intermedia in Serbian brains', *Folia Morphologica (Poland)*, 79(1), pp. 21–27. Available at: https://doi.org/10.5603/FM.a2019.0046.

Pegg, D.E. (2010) 'Cryobiology The relevance of ice crystal formation for the cryopreservation of tissues and organs', *Cryobiology*, 60(3), pp. S36–S44. Available at: https://doi.org/10.1016/j.cryobiol.2010.02.003.

Phillips, D. *et al.* (2019) 'Interhypothalamic adhesions in endoscopic third ventriculostomy', *Child's Nervous System*, 35(9), pp. 1565–1570. Available at: https://doi.org/10.1007/s00381-019-04231-y.

Puškaš, L. *et al.* (2005) 'Specific circular organization of the neurons of human interthalamic adhesion and of periventricular thalamic region', *International Journal of Neuroscience*, 115(5), pp. 669–679. Available at: https://doi.org/10.1080/00207450590524340.

Puškaš, L. *et al.* (2014) 'Imunolokalizacija različitih neuropeptida u intertalamičkoj adheziji čoveka ukazuje na njenu funkcionalnost', *Vojnosanitetski Pregled*, 71(7), pp. 646–650. Available at: https://doi.org/10.2298/VSP1407646P.

Roddy, D.W. *et al.* (2018) 'Awakening neuropsychiatric research into the stria medullaris: Development of a diffusion-weighted imaging tractography protocol of this key limbic structure', *Frontiers in Neuroanatomy*, 12(May), pp. 1–17. Available at: https://doi.org/10.3389/fnana.2018.00039.

Selcuk, M.L. and Colakoglu, F. (2020) 'Distinction of gray and white matter for some histological staining methods in New Zealand rabbit's brain', *International Journal of Current Research and Review*, 12(11), pp. 11–17. Available at: https://doi.org/10.31782/IJCRR.2020.12112.

Sen, F. *et al.* (2005) 'Morphometric measurements of the thalamus and interthalamic adhesion by MR imaging', *Neuroanatomy*, 4, pp. 10–12.

Severino, M. *et al.* (2016) 'Expanding the spectrum of congenital anomalies of the diencephalic–mesencephalic junction', *Neuroradiology*, 58(1), pp. 33–44. Available at: https://doi.org/10.1007/s00234-015-1601-x.

Shiurba, R.A. *et al.* (1998) 'Immunocytochemistry of formalin-fixed human brain tissues: Microwave irradiation of free-floating sections', *Brain Research Protocols*, 2(2), pp. 109–119. Available at: https://doi.org/10.1016/S1385-299X(97)00029-9.

Snyder, P.J. *et al.* (1998) 'Absence of the adhesio interthalamica as a marker of early developmental neuropathology in schizophrenia: An MRI and postmortem histologic study', *Journal of Neuroimaging*, 8(3), pp. 159–163. Available at: https://doi.org/10.1111/jon199883159.

Spina, A. *et al.* (2016) 'Comparative Anatomical Study on Operability in Surgical Approaches to the Anterior Part of the Third Ventricle', *World Neurosurgery*, 95, pp. 457–463. Available at: https://doi.org/10.1016/j.wneu.2016.08.073.

Srikanth, D. (2013) 'Overview of Study Designs', *International Journal of Pharmacy and Pharmaceutical Sciences*, 5(3), pp. 1011–1015. Available at: https://doi.org/10.1093/med/9780195314465.003.0005.

Takahashi, T., Yücel, M., *et al.* (2008) 'Adhesio interthalamica in individuals at high-risk for developing psychosis and patients with psychotic disorders', *Progress in Neuro-Psychopharmacology and Biological Psychiatry*, 32(7), pp. 1708–1714. Available at: https://doi.org/10.1016/j.pnpbp.2008.07.007.

Takahashi, T., Suzuki, M., Nakamura, K., *et al.* (2008) 'Association between absence of the adhesio interthalamica and amygdala volume in schizophrenia', *Psychiatry Research - Neuroimaging*, 162(2), pp. 101–111. Available at: https://doi.org/10.1016/j.pscychresns.2007.04.005.

Takahashi, T., Suzuki, M., Zhou, S.Y., *et al.* (2008) 'Prevalence and length of the adhesio interthalamica in schizophrenia spectrum disorders', *Psychiatry Research - Neuroimaging*, 164(1), pp. 90–94. Available at: https://doi.org/10.1016/j.pscychresns.2008.03.001.

Takahashi, T., Yücel, M., *et al.* (2009) 'Midline brain structures in patients with current and remitted major depression', *Progress in Neuro-Psychopharmacology and Biological Psychiatry*, 33(6), pp. 1058–1063. Available at: https://doi.org/10.1016/j.pnpbp.2009.05.020.

Takahashi, T., Chanen, A.M., *et al.* (2009) 'Midline brain structures in teenagers with first-presentation borderline personality disorder', *Progress in Neuropsychopharmacology & Biological Psychiatry*, 33(5), pp. 842–846. Available at: https://doi.org/10.1016/j.pnpbp.2009.03.035.

Takahashi, T. *et al.* (2010) 'Midline brain abnormalities in established bipolar affective disorder', *Journal of Affective Disorders*, 122(3), pp. 301–305. Available at: https://doi.org/10.1016/j.jad.2009.09.003.

Terminology, F.C. on A. (1998) *Terminologia anatomica: international anatomical terminology*. Stuttgart, SE: Thieme.

The University of Queensland (no date) *Nissl Staining Method and Protocol on Paraffin Sections for Brain & Spinal Cord*. Available at: https://biomedical-sciences.uq.edu.au/files/57/Nissl Staining Method brain.docx (Accessed: 12 July 2022).

Trzesniak, C. *et al.* (2011) 'Adhesio interthalamica alterations in schizophrenia spectrum disorders: A systematic review and meta-analysis', *Progress in Neuro-Psychopharmacology and Biological Psychiatry*, 35(4), pp. 877–886. Available at: https://doi.org/10.1016/j.pnpbp.2010.12.024.

Trzesniak, C. *et al.* (2012) 'Longitudinal follow-up of cavum septum pellucidum and adhesio

interthalamica alterations in first-episode psychosis: A population-based MRI study', *Psychological Medicine*, 42(12), pp. 2523–2534. Available at: https://doi.org/10.1017/S0033291712000839.

Trzesniak, C. *et al.* (2016) 'Adhesio interthalamica and cavum septum pellucidum in mesial temporal lobe epilepsy', *Brain Imaging and Behavior*, 10(3), pp. 849–856. Available at: https://doi.org/10.1007/s11682-015-9461-x.

Tsutsumi, S., Ono, H. and Ishii, H. (2021) 'Massa intermedia of the thalamus: an anatomical study using magnetic resonance imaging', *Surgical and Radiologic Anatomy*, 43(12), pp. 1927–1932. Available at: https://doi.org/10.1007/s00276-021-02788-5.

Tubbs, R.S. *et al.* (2004) 'Duplication of the massa intermedia in a child', *Pediatric Neurosurgery*, 40(1), pp. 42–43. Available at: https://doi.org/10.1159/000076578.

Vorstenbosch, M.A.T.M. *et al.* (2015) 'An Investigation of Anatomical Competence in Junior Medical Doctors', *Anatomical Sciences Education*, 9(1). Available at: https://doi.org/10.1002/ase.1513.

Whitehead, M.T. (2015) 'Thalamic massa intermedia duplication in a dysmorphic 14 month-old toddler', *Journal of Radiology Case Reports*, 9(6), pp. 1–5. Available at: https://doi.org/10.3941/jrcr.v9i6.2297.

Whitehead, M.T., Nagaraj, U.D. and Pearl, P.L. (2015) 'Neuroimaging features of Cornelia de Lange syndrome', *Pediatric Radiology*, 45(8), pp. 1198–1205. Available at: https://doi.org/10.1007/s00247-015-3300-5.

Whitehead, M.T. and Najim, N. (2020) 'Thalamic massa intermedia in children with and without midline brain malformations', *American Journal of Neuroradiology*, 41(4), pp. 729–735. Available at: https://doi.org/10.3174/AJNR.A6446.

Wong, A.K. *et al.* (2021) 'Prevalence of the interthalamic adhesion in the human brain: a review of literature', *Brain Structure and Function*, 226(8), pp. 2481–2487. Available at: https://doi.org/10.1007/s00429-021-02287-8.

Yasaka, K. *et al.* (2019) 'Factors associated with the size of the adhesio interthalamica based on 3.0-T magnetic resonance images', *Acta Radiologica*, 60(1), pp. 113–119. Available at: https://doi.org/10.1177/0284185118774952.

Zawisch, C. (1952) 'Kommissuren und andere Fasersysteme in einer Massa intermedia Thalami des Menschen.', *Wien Z Nervenheük*, 4, pp. 74–93.

Zhang, H. *et al.* (2017) 'Three-Dimensional Imaging Anatomic Study and Clinical Application of the Third Ventricle Transcallosal-Transforniceal Approach', *Journal of Craniofacial Surgery*, 28(6), pp. e587–e591. Available at: https://doi.org/10.1097/SCS.0000000000003918.

APPENDICES

APPENDIX A: Ethical Consent Documents

The protocol for this study was submitted in 2020, therefore ethical consent was only requested in 2021 for the duration of one year and renewed in 2022 for the duration of one year to complete data collection.

Ethical Consent 2021

UNIVERSITEIT VAN PRETORIA
UNIVERSITY OF PRETORIA
YUNIBESITHI YA PRETORIA

Faculty of Health Sciences

Institution: The Research Ethics Committee, Faculty Health Sciences, University of Pretoria complies with ICH-GCP guidelines and has US Federal wide Assurance.

- FWA 00002567, Approved dd 22 May 2002 and Expires 03/20/2022.
- IORG #: IORG0001762 OMB No. 0990-0279 Approved for use through February 28, 2022 and Expires: 03/04/2023.

12 April 2021

Approval Certificate
New Application

Ethics Reference No.: 3/2021
Title: Anatomical investigation of the interthalamic adhesion

Dear Miss N van Heerden

The **New Application** as supported by documents received between 2021-01-04 and 2021-03-31 for your research, was approved by the Faculty of Health Sciences Research Ethics Committee on 2021-03-31 as resolved by its quorate meeting.

Please note the following about your ethics approval:

- Ethics Approval is valid for 1 year and needs to be renewed annually by 2022-04-12.
- Please remember to use your protocol number (3/2021) on any documents or correspondence with the Research Ethics Committee regarding your research.
- Please note that the Research Ethics Committee may ask further questions, seek additional information, require further modification, monitor the conduct of your research, or suspend or withdraw ethics approval.

Ethics approval is subject to the following:

- The ethics approval is conditional on the research being conducted as stipulated by the details of all documents submitted to the Committee. In the event that a further need arises to change who the investigators are, the methods or any other aspect, such changes must be submitted as an Amendment for approval by the Committee.

We wish you the best with your research.

Yours sincerely

Professor Werdie (CW) Van Staden
MBChB MMed(Psych) MD FCPsych(SA) FTCL UPLM
***Chairperson**: Faculty of Health Sciences Research Ethics Committee*

The Faculty of Health Sciences Research Ethics Committee complies with the SA National Act 61 of 2003 as it pertains to health research and the United States Code of Federal Regulations Title 45 and 46. This committee abides by the ethical norms and principles for research, established by the Declaration of Helsinki, the South African Medical Research Council Guidelines as well as the Guidelines for Ethical Research: Principles Structures and Processes, Second Edition 2015 (Department of Health)

Research Ethics Committee
Room 4-60, Level 4, Tswelopele Building
University of Pretoria, Private Bag x323
Gezina 0031, South Africa
Tel +27 (0)12 356 3084
Email: deepeka.behari@up.ac.za
www.up.ac.za

Fakulteit Gesondheidswetenskappe
Lefapha la Disaense tša Maphelo

Ethical Consent 2022

UNIVERSITEIT VAN PRETORIA
UNIVERSITY OF PRETORIA
YUNIBESITHI YA PRETORIA

Faculty of Health Sciences

Institution: The Research Ethics Committee, Faculty Health Sciences, University of Pretoria complies with ICH-GCP guidelines and has US Federal wide Assurance.

- FWA 00002567, Approved dd 18 March 2022 and Expires 18 March 2027.
- IORG #: IORG0001762 OMB No. 0990-0278 Approved for use through August 31, 2023.

Faculty of Health Sciences **Research Ethics Committee**

14 April 2022

Approval Certificate
Annual Renewal

Dear Miss N van Heerden,

Ethics Reference No.: 3/2021 – Line 1
Title: Anatomical investigation of the interthalamic adhesion

The **Annual Renewal** as supported by documents received between 2022-03-16 and 2022-04-13 for your research, was approved by the Faculty of Health Sciences Research Ethics Committee on 2022-04-13 as resolved by its quorate meeting.

Please note the following about your ethics approval:

- Renewal of ethics approval is valid for 1 year, subsequent annual renewal will become due on 2023-04-14.
- Please remember to use your protocol number (3/2021) on any documents or correspondence with the Research Ethics Committee regarding your research.
- Please note that the Research Ethics Committee may ask further questions, seek additional information, require further modification, monitor the conduct of your research, or suspend or withdraw ethics approval.

Ethics approval is subject to the following:

- The ethics approval is conditional on the research being conducted as stipulated by the details of all documents submitted to the Committee. In the event that a further need arises to change who the investigators are, the methods or any other aspect, such changes must be submitted as an Amendment for approval by the Committee.

We wish you the best with your research.

Yours sincerely

On behalf of the FHS REC, Dr R Sommers
MBChB, MMed (Int), MPharmMed, PhD
Deputy Chairperson *of the Faculty of Health Sciences Research Ethics Committee, University of Pretoria*

The Faculty of Health Sciences Research Ethics Committee complies with the SA National Act 61 of 2003 as it pertains to health research and the United States Code of Federal Regulations Title 45 and 46. This committee abides by the ethical norms and principles for research, established by the Declaration of Helsinki, the South African Medical Research Council Guidelines as well as the Guidelines for Ethical Research: Principles Structures and Processes, Second Edition 2015 (Department of Health)

Research Ethics Committee
Room 4-60, Level 4, Tswelopele Building
University of Pretoria, Private Bag x323
Gezina 0031, South Africa
Tel +27 (0)12 356 3084
Email: deepeka.behari@up.ac.za
www.up.ac.za

Fakulteit Gesondheidswetenskappe
Lefapha la Disaense tša Maphelo

APPENDIX B: Raw Data / Data Collection Sheets for Objective 1 and 2

Key	
APL	Anterior-posterior length
Avg	Average
C#	Cadaver number
F	Female
L	Location within third ventricle
M	Male
Max	Maximum
Min	Minimum
P	Prevalence
S#	Sample number
S	Shape
SAIA	Surface area of interthalamic adhesion
SAV	Surface area of third ventricle
SIL	Superior-inferior length
T#	Table number

All raw images used for objectives 1 and 2 can be found in the Google Drive accessed via the following link: https://drive.google.com/drive/folders/1Ju0HXikMGT2Qc3-KPE_Mo7BBieXAuiQG?usp=share_link

Sample specimens

S#	T#	C#	Sex 0 = F 1 = M	Age	P 0 = absent 1 = present
1	303	7633	1	74	0
2	305	7628	1	55	1
3	306	7647	0	67	0
4	308	7638	0	84	1
5	309	7632	1	84	1
6	310	7653	0	86	1
7	101	7602	1	59	0
8	104	7624	0	71	1
9	105	7620	1	68	1
10	106	7589	0	43	1
11	107	7627	1	89	1
12	109	7609	1	78	1
13	110	7615	0	39	1
14	111	7618	1	57	1
15	112	7625	0	99	1
16	118	7622	0	94	1
17	119	7619	1	72	1
18	120	7631	0	85	1
19	122	7593	0	63	0

S#	T#	C#	Sex 0 = F 1 = M	Age	P 0 = absent 1 = present
20	201	7543	1	40	0
21	202	7565	0	67	1
22	205	7575	1	78	0
23	206	7581	0	96	1
24	209	7564	1	76	1
25	210	7606	0	86	1
26	212	7577	0	84	1
27	213	7576	1	83	1
28	214	7585	0	71	1
29	215	7583	1	39	0
30	217	7568	1	77	1
31	218	7572	0	93	1
32	219	7574	1	84	0
33	220	7578	0	76	1
34	222	7588	0	86	0
35	223	7584	1	83	1
36	303	7595	1	80	0
37	304	7612	0	82	0
38	305	7592	1	70	0
39	306	7603	1	78	1

S#	T#	C#	Sex 0 = F 1 = M	Age	P 0 = absent 1 = present
40	308	7613	0	95	1
41	309	7591	1	65	0
42	310	7605	1	74	1
43	311	7626	1	56	1
44	312	7614	0	80	1
45	101	7716	1	72	0
46	109	7718	1	77	1
47	117	7719	1	80	1
48	118	7724	0	88	1
49	202	7701	0	62	0
50	204	7713	0	65	1
51	213	7714	1	56	0
52	219	7706	1	75	1
53	101	7636	1	71	1
54	103	7674	1	74	1
55	106	6589	0	43	1
56	109	7637	1	67	1
57	110	7670	0	83	1
58	113	7691	1	95	1
59	114	7689	0	90	1

S#	T#	C#	Sex 0 = F 1 = M	Age	P 0 = absent 1 = present
60	119	7677	1	74	0
61	121	7685	1	82	1
62	201	7642	1	72	0
63	202	7649	0	102	1
64	203	7676	1	74	0
65	205	7682	1	43	1
66	206	7686	0	65	0
67	209	7643	1	63	0
68	210	7585	0	71	0
69	211	7587/7687	1	43	1
70	212	7644	0	91	1
71	213	7683	1	56	1
72	214	7693	0	68	1
73	217	7645	1	70	1
74	218	7672	0	27	0
75	219	7678	1	30	1
76	221	7684	1	70	0
77	222	7696	0	46	0
78	305	7654	1	72	1
79	308	7666	0	65	1

S#	T#	C#	Sex 0 = F 1 = M	Age	P 0 = absent 1 = present
80	309	7660	1	52	1
81	310	7661	0	67	1
82	311	7673	1	85	0
83	312	7668	0	87	1

Excluded specimens

T#	C#	Sex	Age	P	Reason for exclusion
102	7611	F	51	?	Excessive damage
204	7573	F	66	?	Bad midsagittal cut
307	7601	M	?	0	Age unknown
312	7639	F	92	?	Excessive damage
306	7659	F	60	?	Excessive damage
204	7679	F	72	1	Excessive damage
220	7664	F	58	1	Excessive damage
203	7703	M	74	1	Region of interest indistinguishable

Specimens with an IA

T#	C#	Sex	Age	S	L	APL	SIL	SAIA	SAV
104	7624	0	71	1	1	5,339	3,391	17,349	390,952

T#	C#	Sex	Age	S	L	APL	SIL	SAIA	SAV
105	7620	1	68	4	1	4,811	3,549	13,206	503,596
106	7589	0	43	1	1	6,05	3,727	17,637	517,2
107	7627	1	89	1	1	5,526	3,626	16,234	360,918
109	7609	1	78	1	1	5,523	2,624	12,585	448,237
110	7615	0	39	4	1	9,437	3,331	26,177	409,629
111	7618	1	57	3	1	8,932	4,929	35,617	591,327
112	7625	0	99	3	1	4,307	2,177	6,248	630,808
118	7622	0	94	1	1	5,63	4,563	23,301	524,429
119	7619	1	72	1	1	6,986	5,259	29,948	535,339
119	7619	1	72	1	2	6,072	2,104	11,173	535,339
120	7631	0	85	3	1	3,787	1,776	5,193	482,762
202	7565	0	67	1	1	6,625	5,356	31,177	708,517
206	7581	0	96	3	1	6,259	3,905	17,116	540,524
209	7564	1	76	1	1	6,781	3,304	17,541	648,782
210	7606	0	86	5	1	10,642	10,251	89,992	548,647
212	7577	0	84	1	1	5,201	3,805	16,445	553,046
213	7576	1	83	1	1	9,899	7,155	59,623	749,524
214	7585	0	71	1	2	2,799	1,595	3,44	599,609
218	7572	0	93	1	1	5,998	4,138	21,016	703,433
220	7578	0	76	3	1	7,258	3,02	19,205	508,206
223	7584	1	83	1	1	7,555	4,203	27,61	569,765
305	7628	1	55	2	1	4,373	3,057	11,872	562,979

T#	C#	Sex	Age	S	L	APL	SIL	SAIA	SAV
306	7603	1	78	2	2	8,799	8,169	65,97	529,139
308	7613	0	95	5	1	6,259	3,943	25,975	630,939
308	7638	0	84	4	1	6,541	8,709	53,783	726,254
309	7632	1	84	1	1	7,961	2,747	18,342	754,615
310	7605	1	74	1	1	4,836	1,731	6,969	777,661
310	7653	0	86	4	1	8,255	6,102	34,354	669,614
311	7626	1	56	1	3	10,689	2,591	24,611	672,562
312	7614	0	80	2	1	3,203	5,123	11,64	539,872
217	7568	1	77	4	1	1,027	1,251	1,208	541,34
109	7718	1	77	1	1	6,684	3,827	21,936	644,905
117	7719	1	80	4	1	7,243	6,887	47,141	588,178
118	7724	0	88	4	1	7,682	6,296	37,239	292,453
204	7713	0	65	1	1	6,554	3,881	31,096	490,841
219	7706	1	75	3	1	4,823	3,509	14,579	504,769
101	7636	1	71	1	1	6,797	3,2	18,107	422,202
103	7674	1	74	1	2	6,363	3,907	23,177	510,342
106	6589	0	43	2	1	9,229	8,06	61,854	488,399
109	7637	1	67	1	1	6,457	3,567	18,746	443,213
110	7670	0	83	3	1	6,313	3,924	20,734	440,935
113	7691	1	95	3	1	1,996	2,052	4,011	634,873
114	7689	0	90	5	1	6,934	3,076	19,295	410,228
121	7685	1	82	1	1	7,556	2,821	18,743	681,969

T#	C#	Sex	Age	S	L	APL	SIL	SAIA	SAV
202	7649	0	102	4	1	5,433	2,695	13,817	390,852
205	7682	1	43	4	2	5,296	5,887	24,901	528,445
211	7587	1	43	4	1	1,759	1,138	1,836	578,647
212	7644	0	91	1	1	6,361	6,465	36,114	452,972
213	7683	1	56	5	1	5,669	2,057	8,057	782,257
214	7693	0	68	5	2	12,626	11,715	113,233	571,372
217	7645	1	70	3	1	1,363	0,885	1,806	381,764
219	7678	1	30	1	1	9,528	5,028	40,867	562,203
305	7654	1	72	1	1	6,032	4,214	22,975	743,388
308	7666	0	65	2	1	10,569	8,198	72,353	367,937
309	7660	1	52	4	1	2,832	3,406	8,398	499,748
310	7661	0	67	1	1	3,603	3,093	11,344	535,544
312	7668	0	87	1	1	6,751	4,212	24,233	422,434

Inter-observer data

T#	C#	S	L	APL	SIL	SAIA	SAV
104	7624	1	1	5,633	3,511	15,391	410,993
105	7620	4	1	4,932	3,423	13,474	466,188
106	7589	1	1	6,429	4,027	19,359	506,59
109	7609	1	1	5,521	3,255	13,278	463,114
110	7615	1	1	9,808	3,435	26,787	370,556

T#	C#	S	L	APL	SIL	SAIA	SAV
111	7618	1	1	9,573	5,284	36,381	601,375
109	7718	1	1	6,28	3,621	18,426	490,516
117	7719	4	1	6,793	6,513	36,906	396,518
118	7724	1	1	7,812	6,265	39,5	306,862
204	7713	1	1	5,506	3,818	33,264	486,512
219	7706	1	1	4,939	4,05	15,803	481,665

Intra-observer data

T#	C#	S	L	APL	SIL	SAIA	SAV
104	7624	1	1	5,527	3,488	16,791	413,299
105	7620	4	1	4,912	3,331	13,778	565,395
106	7589	1	1	5,968	3,758	19,195	523,881
109	7609	1	1	5,129	2,513	12,288	450,329
110	7615	4	1	9,576	3,495	23,952	445,168
111	7618	1	1	9,519	4,837	35,506	582,155
109	7718	1	1	6,384	3,813	20,442	512,509
117	7719	4	1	7,044	6,657	44,046	529,348
118	7724	1	1	7,651	6,267	37,322	322,806
204	7713	1	1	6,012	3,868	31,631	451,35
219	7706	3	1	4,713	3,76	18,046	488,492

APPENDIX C: Raw Results for Statistical Analyses Tests

Normality tests

Tests of Normality						
	Kolmogorov-Smirnov[a]			Shapiro-Wilk		
	Statistic	df	Sig.	Statistic	df	Sig.
APL	0,095	58	,200*	0,979	58	0,414
SAIA	0,198	58	0,000	0,811	58	0,000
SAV	0,078	58	,200*	0,980	58	0,439
SIL	0,192	58	0,000	0,903	58	0,000
*. This is a lower bound of the true significance.						
a. Lilliefors Significance Correction						

Descriptive statistics

Statistics					
		Sex	Age	S	L
N	Valid	58	58	58	58
	Missing	0	0	0	0
Mean		0,5172	73,9138	2,3103	1,1379
Mode		1,00	43,00	1,00	1,00
Minimum		0,00	30,00	1,00	1,00
Maximum		1,00	102,00	5,00	3,00

Frequency tables

Sex					
		Frequency	Percent	Valid Percent	Cumulative Percent
Valid	,00	28	48,3	48,3	48,3
	1,00	30	51,7	51,7	100,0
	Total	58	100,0	100,0	

Age					
		Frequency	Percent	Valid Percent	Cumulative Percent
Valid	30,00	1	1,7	1,7	1,7
	39,00	1	1,7	1,7	3,4
	43,00	4	6,9	6,9	10,3
	52,00	1	1,7	1,7	12,1
	55,00	1	1,7	1,7	13,8
	56,00	2	3,4	3,4	17,2
	57,00	1	1,7	1,7	19,0
	65,00	2	3,4	3,4	22,4
	67,00	3	5,2	5,2	27,6
	68,00	2	3,4	3,4	31,0
	70,00	1	1,7	1,7	32,8
	71,00	3	5,2	5,2	37,9

	72,00	3	5,2	5,2	43,1
	74,00	2	3,4	3,4	46,6
	75,00	1	1,7	1,7	48,3
	76,00	2	3,4	3,4	51,7
	77,00	2	3,4	3,4	55,2
	78,00	2	3,4	3,4	58,6
	80,00	2	3,4	3,4	62,1
	82,00	1	1,7	1,7	63,8
	83,00	3	5,2	5,2	69,0
	84,00	3	5,2	5,2	74,1
	85,00	1	1,7	1,7	75,9
	86,00	2	3,4	3,4	79,3
	87,00	1	1,7	1,7	81,0
	88,00	1	1,7	1,7	82,8
	89,00	1	1,7	1,7	84,5
	90,00	1	1,7	1,7	86,2
	91,00	1	1,7	1,7	87,9
	93,00	1	1,7	1,7	89,7
	94,00	1	1,7	1,7	91,4
	95,00	2	3,4	3,4	94,8
	96,00	1	1,7	1,7	96,6
	99,00	1	1,7	1,7	98,3
	102,00	1	1,7	1,7	100,0

	Total	58	100,0	100,0	

S					
		Frequency	Percent	Valid Percent	Cumulative Percent
Valid	1,00	28	48,3	48,3	48,3
	2,00	5	8,6	8,6	56,9
	3,00	9	15,5	15,5	72,4
	4,00	11	19,0	19,0	91,4
	5,00	5	8,6	8,6	100,0
	Total	58	100,0	100,0	

L					
		Frequency	Percent	Valid Percent	Cumulative Percent
Valid	1,00	51	87,9	87,9	87,9
	2,00	6	10,3	10,3	98,3
	3,00	1	1,7	1,7	100,0
	Total	58	100,0	100,0	

Location correlation with measurements

Tests of Homogeneity of Variances					
		Levene Statistic	df1	df2	Sig.
APL	Based on Mean	1,602	1	55	0,211
	Based on Median	0,842	1	55	0,363
	Based on Median and with adjusted df	0,842	1	46,913	0,363
	Based on trimmed mean	1,495	1	55	0,227
SIL	Based on Mean	6,767	1	55	0,012
	Based on Median	6,217	1	55	0,016
	Based on Median and with adjusted df	6,217	1	50,031	0,016
	Based on trimmed mean	6,705	1	55	0,012
SAIA	Based on Mean	11,459	1	55	0,001
	Based on Median	4,421	1	55	0,040
	Based on Median and with adjusted df	4,421	1	29,817	0,044
	Based on trimmed mean	10,178	1	55	0,002
SAV	Based on Mean	5,669	1	55	0,021
	Based on Median	5,898	1	55	0,018
	Based on Median and with adjusted df	5,898	1	51,211	0,019
	Based on trimmed mean	5,687	1	55	0,021

ANOVA						
		Sum of Squares	df	Mean Square	F	Sig.
APL	Between Groups	23,434	2	11,717	2,130	0,129
	Within Groups	302,537	55	5,501		
	Total	325,971	57			
SIL	Between Groups	14,170	2	7,085	1,438	0,246
	Within Groups	270,904	55	4,926		
	Total	285,074	57			
SAIA	Between Groups	1434,892	2	717,446	1,561	0,219
	Within Groups	25282,898	55	459,689		
	Total	26717,791	57			
SAV	Between Groups	15566,633	2	7783,316	0,581	0,563
	Within Groups	736831,179	55	13396,931		
	Total	752397,812	57			

Age correlations with measurements

Descriptive Statistics			
	Mean	Std. Deviation	N
Age	73,9138	16,24406	58
APL	6,3071	2,39140	58
SIL	4,2278	2,23636	58
SAIA	25,6750	21,65025	58

SAV	548,9040	114,89109	58

Correlations						
		Age	APL	SIL	SAIA	SAV
Age	Pearson Correlation	1	-0,115	0,003	-0,053	0,017
	Sig. (2-tailed)		0,388	0,980	0,695	0,900
	N	58	58	58	58	58
APL	Pearson Correlation	-0,115	1	,692**	,805**	0,061
	Sig. (2-tailed)	0,388		0,000	0,000	0,648
	N	58	58	58	58	58
SIL	Pearson Correlation	0,003	,692**	1	,945**	-0,008
	Sig. (2-tailed)	0,980	0,000		0,000	0,951
	N	58	58	58	58	58
SAIA	Pearson Correlation	-0,053	,805**	,945**	1	0,005
	Sig. (2-tailed)	0,695	0,000	0,000		0,968
	N	58	58	58	58	58
SAV	Pearson Correlation	0,017	0,061	-0,008	0,005	1
	Sig. (2-tailed)	0,900	0,648	0,951	0,968	
	N	58	58	58	58	58
**. Correlation is significant at the 0.01 level (2-tailed).						

Nonparametric Correlations							
			Age	APL	SIL	SAIA	SAV
Spearman's rho	Age	Correlation Coefficient	1,000	-0,061	0,069	-0,013	0,034
		Sig. (2-tailed)		0,649	0,608	0,921	0,798
		N	58	58	58	58	58
	APL	Correlation Coefficient	-0,061	1,000	,586**	,851**	0,074
		Sig. (2-tailed)	0,649		0,000	0,000	0,580
		N	58	58	58	58	58
	SIL	Correlation Coefficient	0,069	,586**	1,000	,878**	-0,006
		Sig. (2-tailed)	0,608	0,000		0,000	0,965
		N	58	58	58	58	58
	SAIA	Correlation Coefficient	-0,013	,851**	,878**	1,000	0,023
		Sig. (2-tailed)	0,921	0,000	0,000		0,867
		N	58	58	58	58	58
	SAV	Correlation Coefficient	0,034	0,074	-0,006	0,023	1,000
		Sig. (2-tailed)	0,798	0,580	0,965	0,867	
		N	58	58	58	58	58
**. Correlation is significant at the 0.01 level (2-tailed).							

Sex correlation with shape

Crosstab							
Count							
		S					Total
		1,00	2,00	3,00	4,00	5,00	
Sex	,00	11	3	5	5	4	28
	1,00	17	2	4	6	1	30
Total		28	5	9	11	5	58

Chi-Square Tests			
	Value	df	Asymptotic Significance (2-sided)
Pearson Chi-Square	3,423[a]	4	0,490
Likelihood Ratio	3,558	4	0,469
Linear-by-Linear Association	1,747	1	0,186
N of Valid Cases	58		
a. 6 cells (60,0%) have expected count less than 5. The minimum expected count is 2,41.			

Sex correlation with location

Crosstab					
Count					
		L			Total
		1,00	2,00	3,00	

Sex	,00	26	2	0	28
	1,00	25	4	1	30
Total		51	6	1	58

Chi-Square Tests			
	Value	df	Asymptotic Significance (2-sided)
Pearson Chi-Square	1,619[a]	2	0,445
Likelihood Ratio	2,017	2	0,365
Linear-by-Linear Association	1,534	1	0,216
N of Valid Cases	58		
a. 4 cells (66,7%) have expected count less than 5. The minimum expected count is ,48.			

Age correlation with shape

Crosstab							
Count							
		S					Total
		1,00	2,00	3,00	4,00	5,00	
Age	30,00	1	0	0	0	0	1
	39,00	0	0	0	1	0	1
	43,00	1	1	0	2	0	4
	52,00	0	0	0	1	0	1
	55,00	0	1	0	0	0	1

	56,00	1	0	0	0	1	2
	57,00	0	0	1	0	0	1
	65,00	1	1	0	0	0	2
	67,00	3	0	0	0	0	3
	68,00	0	0	0	1	1	2
	70,00	0	0	1	0	0	1
	71,00	3	0	0	0	0	3
	72,00	3	0	0	0	0	3
	74,00	2	0	0	0	0	2
	75,00	0	0	1	0	0	1
	76,00	1	0	1	0	0	2
	77,00	1	0	0	1	0	2
	78,00	1	1	0	0	0	2
	80,00	0	1	0	1	0	2
	82,00	1	0	0	0	0	1
	83,00	2	0	1	0	0	3
	84,00	2	0	0	1	0	3
	85,00	0	0	1	0	0	1
	86,00	0	0	0	1	1	2
	87,00	1	0	0	0	0	1
	88,00	0	0	0	1	0	1
	89,00	1	0	0	0	0	1
	90,00	0	0	0	0	1	1

	91,00	1	0	0	0	0	1
	93,00	1	0	0	0	0	1
	94,00	1	0	0	0	0	1
	95,00	0	0	1	0	1	2
	96,00	0	0	1	0	0	1
	99,00	0	0	1	0	0	1
	102,00	0	0	0	1	0	1
Total		28	5	9	11	5	58

Chi-Square Tests			
	Value	df	Asymptotic Significance (2-sided)
Pearson Chi-Square	143,132[a]	136	0,321
Likelihood Ratio	119,006	136	0,850
Linear-by-Linear Association	0,054	1	0,816
N of Valid Cases	58		
a. 175 cells (100,0%) have expected count less than 5. The minimum expected count is ,09.			

Age correlation with location

Count					
		L			Total
		1,00	2,00	3,00	
Age	30,00	1	0	0	1

	39,00	1	0	0	1
	43,00	3	1	0	4
	52,00	1	0	0	1
	55,00	1	0	0	1
	56,00	1	0	1	2
	57,00	1	0	0	1
	65,00	2	0	0	2
	67,00	3	0	0	3
	68,00	1	1	0	2
	70,00	1	0	0	1
	71,00	2	1	0	3
	72,00	2	1	0	3
	74,00	1	1	0	2
	75,00	1	0	0	1
	76,00	2	0	0	2
	77,00	2	0	0	2
	78,00	1	1	0	2
	80,00	2	0	0	2
	82,00	1	0	0	1
	83,00	3	0	0	3
	84,00	3	0	0	3
	85,00	1	0	0	1
	86,00	2	0	0	2

	87,00	1	0	0	1
	88,00	1	0	0	1
	89,00	1	0	0	1
	90,00	1	0	0	1
	91,00	1	0	0	1
	93,00	1	0	0	1
	94,00	1	0	0	1
	95,00	2	0	0	2
	96,00	1	0	0	1
	99,00	1	0	0	1
	102,00	1	0	0	1
Total		51	6	1	58

Chi-Square Tests			
	Value	df	Asymptotic Significance (2-sided)
Pearson Chi-Square	47,717[a]	68	0,971
Likelihood Ratio	25,237	68	1,000
Linear-by-Linear Association	2,289	1	0,130
N of Valid Cases	58		
a. 105 cells (100,0%) have expected count less than 5. The minimum expected count is ,02.			

Inter- and intra-class correlations

APL				
ANOVA table				
	Sum of sqrs	**df**	**Mean square**	**F**
Between raters:	0,032153	2	0,016076	0,2387
Between cases:	81,8864	10	8,18864	121,6
Within cases:	1,37895	22	0,06268	
Residual:	1,3468	20	0,06734	
Total:	83,2653	32		
				95% confidence
Model 1	Individual	ICC(1,1)	0,9774	[0,9405, 0,9933]
	Mean	ICC(1,k)	0,9923	[0,9793, 0,9977]
Model 2	Individual	ICC(2,1)	0,9774	[0,9395, 0,9933]
	Mean	ICC(2,k)	0,9923	[0,979, 0,9978]
Model 3	Individual	ICC(3,1)	0,9757	[0,9346, 0,9928]
	Mean	ICC(3,k)	0,9918	[0,9772, 0,9976]

SIL				
ANOVA table				
	Sum of sqrs	**df**	**Mean square**	**F**
Between raters:	0,108913	2	0,054456	1,625
Between cases:	46,47	10	4,647	138,7

Within cases:	0,779138	22	0,035415	
Residual:	0,670225	20	0,033511	
Total:	47,2491	32		
				95% confidence
Model 1	Individual	ICC(1,1)	0,9775	[0,9407, 0,9933]
	Mean	ICC(1,k)	0,9924	[0,9794, 0,9978]
Model 2	Individual	ICC(2,1)	0,9775	[0,9403, 0,9933]
	Mean	ICC(2,k)	0,9924	[0,9793, 0,9978]
Model 3	Individual	ICC(3,1)	0,9787	[0,9423, 0,9937]
	Mean	ICC(3,k)	0,9928	[0,98, 0,9979]

SAIA				
ANOVA table				
	Sum of sqrs	**df**	**Mean square**	**F**
Between raters:	1,75674	2	0,878371	0,2169
Between cases:	3433,11	10	343,311	84,76
Within cases:	82,7605	22	3,76184	
Residual:	81,0038	20	4,05019	
Total:	3515,87	32		
				95% confidence
Model 1	Individual	ICC(1,1)	0,9678	[0,9162, 0,9904]
	Mean	ICC(1,k)	0,989	[0,9704, 0,9968]
Model 2	Individual	ICC(2,1)	0,9678	[0,9147, 0,9904]

	Mean	ICC(2,k)	0,989	[0,9699, 0,9968]
Model 3	Individual	ICC(3,1)	0,9654	[0,9079, 0,9897]
	Mean	ICC(3,k)	0,9882	[0,9673, 0,9965]

SAV				
ANOVA table				
	Sum of sqrs	**df**	**Mean square**	**F**
Between raters:	7962,38	2	3981,19	2,242
Between cases:	183469	10	18346,9	10,33
Within cases:	43484,4	22	1976,56	
Residual:	35522	20	1776,1	
Total:	226953	32		
				95% confidence
Model 1	Individual	ICC(1,1)	0,7341	[0,4483, 0,9104]
	Mean	ICC(1,k)	0,8923	[0,7091, 0,9682]
Model 2	Individual	ICC(2,1)	0,7365	[0,4523, 0,9111]
	Mean	ICC(2,k)	0,8934	[0,7125, 0,9685]
Model 3	Individual	ICC(3,1)	0,7567	[0,4759, 0,9196]
	Mean	ICC(3,k)	0,9032	[0,7315, 0,9717]